Title
Wildfire Effects on the Ecohydrology of a Sierra Nevada Watershed

Author
Boisrame, Gabrielle Boisrame

Publication Date
2016

Peer reviewed|Thesis/dissertation

Wildfire Effects on the Ecohydrology of a Sierra Nevada Watershed

by

Gabrielle Fernande Simone Boisramé

A dissertation submitted in partial satisfaction of the
requirements for the degree of
Doctor of Philosophy

in

Engineering - Civil and Environmental Engineering

in the

Graduate Division

of the

University of California, Berkeley

Committee in charge:

Professor Sally E. Thompson, Chair
Professor Scott Stephens
Professor Mark Stacey
Professor Naomi Tague

Fall 2016

Wildfire Effects on the Ecohydrology of a Sierra Nevada Watershed

Abstract

Wildfire Effects on the Ecohydrology of a Sierra Nevada Watershed

by

Gabrielle Fernande Simone Boisramé

Doctor of Philosophy in Engineering - Civil and Environmental Engineering

University of California, Berkeley

Professor Sally E. Thompson, Chair

The mountain watersheds of the Sierra Nevada supply the majority of California's water, but this supply has always been highly variable. The 2012-2016 drought in California has demonstrated that this water supply is also highly vulnerable to increasing temperatures and/or reduced precipitation. Not only did the 2012-2016 drought reduce water supply for human use, but it also led to unprecedented forest mortality and fire damage. Unfortunately, the fire suppression strategy that was nearly uniformly applied to mountain forests during the 20^{th} century may have exacerbated the effects of drought by increasing vegetation density and thus increasing evapotranspiration and precipitation interception. Could restoring fire regimes to their pre-European settlement condition increase water yield from these forested catchments? Such a policy would also have the potential to restore the ecological function of landscapes and reduce the risk of catastrophic fires (such as the 2013 Rim Fire) by reducing fuel loads.

This dissertation studies the hydrological and landscape-level ecological effects of restoring a frequent, mixed severity fire regime to the Illilouette Creek Basin in Yosemite National Park. A combination of field measurements, historical data analysis, remote sensing, and modeling approaches are employed to strengthen the argument by providing multiple lines of evidence. There is limited data available for Illilouette Creek Basin during much of the four decades in which the new fire regime became established, inhibiting direct evaluation of the fire regime's effects. Nevertheless, a variety of different metrics and analyses indicate a number of important changes that can be attributed to the restored fire regime: increased landscape diversity (including reduced forest cover), increased soil moisture and streamflow (both according to measurements and hydrological modeling), and decreased drought stress (both according to observations and from hydrological modeling).

Contents

List of Figures

List of Tables

Acknowledgments

I thank Yosemite National Park for permitting us to conduct research in wilderness areas.

Special thanks to Kate Wilkin for her field expertise, and to all of this project's field crew members and volunteers: Miguel Naranjo, Andy Wong, Perth Silvers, Jeremy Balch, Seth Bergeson, Amanda Atkinson, Tom Bruton, Diane Taylor, Madeleine Jensen, Isabel Schroeter, Katy Abbott, Bryce King, Zubair Dar, Katherine Eve, Sally McConchie, James Hart, Caroline Delaire, Louis Alexandre-Couston, Catherine Fong, Melissa Thaw, Anthony Everhart, Skye Niles, Lena Nitsan, Chris Phillips, Anthony Ambrose, Wendy Baxter, Jens Stevens, Stacey Sargent Frederick, and Kirt Siders (in order of appearance).

I received a wonderful amount of support in many forms (including some fieldwork) from my parents, Karen Klonsky and Yves Boisramé.

The vegetation maps were created with the help of GIS technicians Julia Cavalli, Miguel Naranjo, and Melissa Ferriter, with guidance from Professor Maggi Kelly.

The MOPEX weather and phenological data used in this paper can be downloaded from $ftp://hydrology.nws.noaa.gov/pub/gcip/mopex/US\_Data/$ free of charge. Special thanks to Matej Durcik for providing us with terrain variables for the MOPEX watersheds.

This dissertation also makes use of data analysis and imagery analysis performed by Ian McGregor, Kelly Archer, Shahad Jawad, Jingxuan Xiao, and Frank He.

RHESSys help was provided by Professor Noami Tague, Janet Choate, and Tyler Brandt.

I received important guidance and suggestions from Sally Thompson, Scott Stephens, Brandon Collins, Maggi Kelly, John Battles, Iryna Dronova, James Roche, and many others.

This work was made possible thanks to financial support from Joint Fire Science grant # 14-1-06-22, NSF EAR # 1013339, Sigma Xi Grants in Aid of Research, the UC Berkeley SMART program, Hellman Fellows Program, and the UC Berkeley Philomathia Graduate Fellowship in Environmental Sciences.

The RHESSys modeling portion of this research used the Savio computational cluster resource provided by the Berkeley Research Computing program at the University of California, Berkeley (supported by the UC Berkeley Chancellor, Vice Chancellor for Research, and Chief Information Officer).

This project also used software resources provided by the UC Berkeley Geospatial Innovation Facility (gif.berkeley.edu).

Chapter 1

Introduction

1.1 Motivation

California's historic 2012-2016 drought demonstrates the dire need for watershed management techniques that maximize water yield and enhance ecosystem drought resilience (http://earthobservatory.nasa.gov). Unfortunately, the fire suppression strategy that has been nearly uniformly applied to mountain forests for the last century may actually be *reducing* water yield and groundwater stores by increasing vegetation density and thus increasing evapotranspiration and interception of precipitation (Ursino and Rulli, 2011). This suggests that restoring fire regimes to their pre-European settlement condition could increase the water yield from the forested catchments that supply the majority of California's water (www.sierranevadaalliance.org). Such a policy could also help restore the ecological function of landscapes and reduce the risk of catastrophic events such as the 2013 Rim Fire by reducing fuel loads (http://abclocal.go.com/kgo).

A "fire regime" is defined as the combination of fire frequency and severity that is characteristic of a given area. It is distinct from the occurrence of any individual fire, but represents the combined effects of topography, fuels, climate, and ignition sources. Land management changes fire regimes by altering fuel loads (which affect severity) and suppressing fires (which reduces fire frequency) (Miller et al., 2012b). The majority of research literature about watershed-scale responses to fire describes severe, infrequent burning events, rather than evaluating the effects of fire regimes over time (e.g. Helvey (1980); Moody and Martin (2001)). Understanding of the impact of natural fire regimes on hydrological dynamics and long-term ecosystem dynamics in the Western U.S. (and similar fire-adapted regions with mediterranean climates) is limited to theoretical proposals and modeling studies. These studies suggest that increased fire frequency could increase average soil moisture (Ursino and Rulli, 2011) and that it could restore landscape structure in fire-suppressed landscapes within 50-75 years (Baker, 1994; Peterson, 2002). A major contribution of this dissertation is to address some of the knowledge gaps surrounding fire regime and hydrology by providing the first field-based analysis of the effects of a restored natural fire regime on the ecohydrology

of a Western U.S. watershed following at least 90 years of fire suppression.

The main focus of the research presented in this dissertation is to test a broad hypothesis that restoring a fire-suppressed watershed's fire regime causes changes in vegetation structures that enhance water storage within the basin and water yield from the basin. My work addresses this hypothesis within the Illilouette Creek Basin (ICB) in Yosemite National Park, CA, the only monitored watershed in the Western U.S. that has been allowed to revert to an unsuppressed fire regime, incorporating high fire frequency and mixed severity fires, and thus provides the only setting in which to effectively test this hypothesis.

1.2 Important Vocabulary

The following terms are used frequently within this dissertation:

- Evapotranspiration (ET): The flux of water from land surface to the atmosphere in the form of water vapor through either evaporation from water, soil, or plant surfaces or transpiration through the leaves of plants. ET is equivalent to the latent heat flux, if measured in energetic (rather than water mass) terms. *Potential evapotranspiration (PET)* is the maximum ET flux under conditions of unlimited water availability. PET is controlled by a combination of temperature, wind speed, solar radiation, humidity, and resistance to air or water vapor flow (primarily controlled by leaf-level - stomatal - and canopy level features) (Fisher et al., 2005). When there is sufficient water available, ET is equal to PET.

- Fire Frequency: The number of times that fires occur in a given area over a given period of time (e.g. twice per decade or once per century).

- Fire Regime: the combination of fire frequency and severity that is characteristic of a given area. For example, high altitude forests with fire-tolerant species have fire regimes characterized by high frequency of fire but low severity. In contrast, dense shrublands in areas with few ignition sources often have fire regimes consisting of infrequent fires that burn at high severity. Fire regime is determined by a combination of factors including vegetation type, weather, topography, and ignition sources, as well as human activity (both igniting and suppressing fires) (Keane et al., 2004).

- Fire Severity: The effect of fire on an ecosystem, generally measured as a propotion of vegetation that is killed. A high severity fire is a stand replacing event resulting in high or complete vegetation mortality, while a low severity fire consumes surface fuels but leaves the majority of the canopy intact, and moderate severity fires exhibit a mixture of canopy changes ranging from low to high mortality (Miller and Thode, 2007).

- Interception: This is the term for when rain or snow covers the leaves and/or branches of plants rather than falling directly to the ground. Water that is intercepted can

either subsequently fall to the ground (this flux is termed "throughfall" in the case of intercepted rain) or return to the atmosphere via evaporation or sublimation.

- Landscape Diversity: A measure of whether a landscape contains a range of land cover types in relatively even proportions (high diversity) rather than being dominated by a small number of land cover types (low diversity).

- Paired Catchment Study: A method of determining the effect of disturbance on a watershed by comparing streamflow in an altered basin to a similar, unaltered basin both before and after the disturbance. If the relationship between the two basins is different in the before and after periods, then that difference is attributed to the disturbance. This method allows researchers to estimate the magnitude of the effect of a known landscape change while accounting for climatic variability. (Brown et al., 2005)

- Resilience: The ability of a system to absorb impacts before a threshold is reached where the system changes into a different state (Gunderson, 2000). For example, a landscape with low drought resilience might experience a permanent shift in dominant vegetation species following an extended drought period, whereas a resilient landscape would quickly recover from the same drought conditions with much the same species composition as before.

- Sublimation: The process of frozen water transforming directly into water vapor rather than melting. Sublimation is the snow equivalent of evaporation.

- Water Balance: Conservation of mass requires that watersheds be described by the following formula: $\Delta S = P - ET - Q$, where S is water storage, P is precipitation, ET is evapotranspiration, and Q is outflow. In this work, I refer to each component of this equation as part of the water balance, so-called because a change in any one component must necessarily accompany a compensatory change in at least one other component.

1.3 Background - Fire Effects on the Landscape

The landscape-scale changes explored in this dissertation are based on a relatively simple premise: wildfires have the ability to reduce vegetation cover and/or change the dominant vegetation type over large scales, and these fire-induced vegetation changes affect the water balance. This is true both at the scale of individual fires and at long time scales involving multiple fires over the same landscape. Beyond this basic statement, however, the extent, nature, magnitude and principle mechanistic drivers of such alterations are unknown. This is because fire can have many gradations of impact on vegetation, and because vegetation

changes impact multiple components of the land surface water balance, with potentially confounding effects. The net changes in ecology and hydrology experienced by a landscape due to a change in fire regime thus arise from the interaction of changes in multiple mechanisms.

The dominant plant species and forest structure in fire-affected areas are typically influenced by the fire regime. For example, frequent fires can lead to more even-aged stands with less understory and more shade-intolerant species (Scheller et al., 2005). Mixed severity fires create a mosaic of land cover types and forest structures, providing diverse habitat and seed sources, rather than altering landscapes uniformly (Baker, 1994; Kane et al., 2013). Thus, more frequent fire helps to increase landscape diversity and heterogeneity relative to fire suppressed forests (Collins et al., 2016; Romme, 1982).

Fire regime and landscape pattern impose a two-way feedback upon each other (Collins and Stephens, 2010; Pausas, 2006). Patches with low fuel loads, either due to a recent burn or because of the local land cover type, can limit the spread of subsequent fires (Collins et al., 2009; Parks et al., 2014; van Wagtendonk et al., 2012). Increasing fire occurrence can lead to changes in the dominant species. For example, the proportion of early successional species such as shrubs can increase with increasing fire frequency (Pausas and Lloret, 2007). Vegetation cover, in turn, can affect fire severity and the sizes of high severity patches - for example, shrubs also often promote high-severity fires (Collins and Stephens, 2010; Silva et al., 2011).

Just as fire is important in shaping landscapes, so is the lack of fire; the effects of fire suppression on the landscape can be clearly observed. For example, fire-suppressed forest stands have more than doubled in density since the early 1900s (Collins et al., 2011). Fire suppression has also increased the density of small trees and ground fuels in fire-adapted forests, as well as altered species dominance in many forests (e.g. by decreasing reproductive rates of giant sequoia or promoting increased growth of shade-tolerant firs) (Parsons and DeBenedetti, 1979). Model results have shown that prescribed fires and mechanical thinning may not be able to reconstruct historical forest structure as well as wildfires can (Baker, 1994; North et al., 2007), although mechanical treatments as well as prescribed fire can reduce the likelihood of high severity fires (Stephens et al., 2009). Managed wildfire may provide the only tool that can truly return a forest to its pre-suppression condition without a prohibitively large investment of time and money. Few studies exist on long-term changes in landscape structure following the restoration of a natural fire regime.

1.4 Background - Vegetation and water

Vegetation change can have profound impacts on watershed hydrology due to the role of plants in regulating soil structure, transpiration, interception, and shade (Brown et al., 2005). Altering vegetation will therefore likely affect regional water balance, but how these multiple changes will product a net, watershed scale, impact remains generally hard to predict. Developing such predictive knowledge provides water managers with the ability

to develop management strategies that improve the resilience of watersheds to change and increase their water yield.

Globally, annual transpiration represents approximately 40% of annual precipitation (Schlesinger and Jasechko, 2014). Transpiration depletes soil moisture until the moisture is low enough to limit further transpiration by causing plants to shut their stomata and halt gas exchange (Katul et al., 2012). Interception of precipitation also accounts for a significant portion of the water balance; the importance of interception varies depending on canopy storage capacity and potential evaporation (Rutter et al., 1972, 1975). In conifer forests, interception losses (water evaporated off of plant surfaces) account for ≈20 to 40% of annual rainfall (Zinke, 1967). The roles of vegetation structure (e.g. interception) and function (e.g. transpiration) on water balance can be separated through experimental treatment or design (see Chapter 2). For example, He et al. (2013) girdled trees to kill them, without disturbing the soil or (initially) removing the intercepting layer. They found that soil moisture at multiple depths was higher in study plots where trees had been girdled compared to undisturbed plots, likely due to reduced rain interception and reduced transpiration during growing seasons following the girdling operation. These changes were enough to counteract increased soil evaporation in the plots with girdled trees. Surface soil moisture was more spatially variable in disturbed plots, and was generally wetter than in undisturbed plots, despite the fact that most water loss in the disturbed plots was concentrated in the shallow soil layers (He et al., 2013).

Vegetation also has measurable and meaningful effects on streamflow. Paired catchment studies, in which streamflow in an altered basin is compared to a similar, unaltered basin both before and after the disturbance in order to control for the effect of weather variability, show that annual water yield generally increases with decreasing forest cover and vice versa (from a review of 94 paired catchment studies, Brown et al., 2005). Following deforestation, at least in the short term, baseflow from a catchment increases as long as infiltration rates have not been affected (such as from machinery compacting the soil and lowering potential infiltration, or from the soil developing hydrophobic properties) (Brown et al., 2005). Paired catchment studies show that the greatest changes in streamflow distributions following deforestation in deciduous forests occur during the site's growing season, an effect attributed to transpiration changes (Brown et al., 2005). Other work on the seasonal effects of vegetation on streamflow show that streamflow recession constants - the amount of time between peak flow following a storm and return to baseflow - in deciduous Eastern U.S. forests are shorter during the growing season, presumably due to vegetation interception and transpiration (Czikowsky and Fitzjarrald, 2004; Federer, 1973). Conversely, Weisman (1977) found a negative correlation between recession constants and pan evaporation, suggesting that potential evapotranspiration (PET) was the strongest driver of recession constant. Different attributions for the same observation illustrate the difficulty of separating effects of temperature from those of canopy cover.

Despite the usefulness of paired catchment studies in quantifying the effects of vegetation on streamflow while controlling for climatic conditions, this method does have limitations. Most notably, the dramatic changes in vegetation cover usually incorporated into paired

catchment studies - such as clear-felling, mechanized planting or burning - can significantly alter soil properties and thus increase surface runoff (Brown et al., 2005), making the unambiguous identification of vegetation-driven effects challenging. Furthermore, many conclusions regarding the impact of vegetation are either limited to correlation (e.g. (Czikowsky and Fitzjarrald, 2004)) or treatment of a single watershed or pair of watersheds (e.g. (Federer, 1973)). Computer models overcome some of these issues by determining whether a given conceptual model of hydrologic processes is able to account for observed behaviors (Sivapalan et al., 2003; Ye et al., 2012; Zegre et al., 2010). Another challenge is that the effects of changes in vegetation cover can be highly dependent on the specific climate, topography, and geology of a catchment, and thus it can be difficult to generalize quantitative results from one study to other sites (Brown et al., 2005).

Initial study of vegetation change and streamflow

The issue of being able to generalize results and the difficulties in model selection has led to interest in "large-n hydrology," a strategy that involves testing a model on a large number of datasets, rather than focusing on detailed description of processes at one study site. This approach offers increased statistical power, and the opportunity to explore commonalities in hydrological response across gradients in climate, physiography and other watershed properties (Gupta et al., 2013). Before beginning my work on fire regimes, I used the large-n hydrology approach on a more general study of streamflow response to vegetation change. I studied patterns in streamflow recession using the nation-wide Model Parameter Estimation Experiment (MOPEX) dataset, which contains standardized information on streamflow, precipitation, temperature, potential evapotranspiration (PET), and vegetation activity as measured by greenness fraction (GF) for 438 watersheds within the United States. Details of this study are given in Chapter 2.

The main streamflow metric used in the MOPEX study is the recession constant (RC), a measure of how many days it takes for flow peaks to return to a pre-storm condition. This flow parameter has been shown to vary seasonally (Czikowsky and Fitzjarrald, 2004; Federer, 1973; Weisman, 1977). Recession constants can be linked directly to precipitation drivers, and are also indicative of catchment scale groundwater storage (Tallaksen, 1995) as well as evapotranspiration rates, making them a useful metric in exploring streamflow generation. The premise of my MOPEX study was that every spring a large-scale natural experiment is performed in temperate watersheds, as longer days and warmer weather increase the growth and water uptake of vegetation. By comparing catchment hydrology during the growing and dormant seasons, I was able to gain information similar to that of a paired catchment study without dealing with geologic differences between sites or alteration of soil properties.

I found a significant seasonal change in RC for most of the study watersheds. The effect of vegetation on RC was most prominent for smaller storms (when rainfall was in the lower 50^{th} percentile), and high rainfall tended to drown out signals of vegetation impact on streamflow. In the northeastern United States, in years when spring arrived earlier than usual (based on

flower bloom dates), mean June-August RC decreased by 13% compared to normal years ($p < 0.02$).

I also used lumped hydrological models to simulate streamflow from all of the MOPEX watersheds. These models demonstrated that vegetation interactions alone are capable of affecting streamflow generation processes in many watersheds, independent of temperature or humidity effects. Vegetation phenology had a measurable effect on recession constant, though the effect of seasonality in PET was generally stronger (Table 2.2).

For some watersheds, recession constants were reduced by multiple days due to vegetation cover. The 13% observed decrease in recession constants for years with early spring onsets in the Northeast is suggestive of climate change effects on streamflow generation. Theoretically, this observed decrease means that the total volume of quickflow from a rainstorm with a given magnitude will be 13% lower during an early spring than in spring of an average year. This finding demonstrates the value of incorporating seasonal variations in streamflow generation properties into predictions of runoff responses to future climate changes.

Snow-dominated Western watersheds also experienced hydrologic changes that correlated with vegetation activity, but their annual pattern of recession constants was reversed compared to rain-dominated watersheds: recession constants were longer during the growing season than the dormant season in snow dominated watersheds, because snowmelt during the peak growing period was the main driver of streamflow recession (Figure 2.3).

Studying the interplay between geologic, vegetative, and climatic drivers of runoff regimes through the MOPEX project was a valuable introduction to data analysis and modeling in ecohydrology, as well as an important lesson in the interplay between snowmelt and vegetation activity in Western watersheds. It also allowed me to explore the interplay between vegetation and weather in affecting streamflow, as well as the effects of climate change on seasonal behavior. The MOPEX project also provides a good demonstration of the diversity in streamflow generation processes between watersheds. Even though the same basic processes are at work everywhere on Earth (canopy interception, evaporation, transpiration, infiltration, etc.), not all watersheds respond to these drivers in the same way. The water balance depends on many factors including soil type, subsurface flow paths, land cover, and topography, which vary from catchment to catchment. Even within the same watershed, streamflow generation may behave differently in different years depending on the weather (for example, if rainfall is too low to saturate areas that would contribute to streamflow in wet years, temperatures cause abnormal amounts of evapotranspiration, or if precipitation is so high that it overwhelms the effects of interception in places where it is usually important). On the other hand, while working on the MOPEX project I also found that sites with similar geographic location, climate variables, and topographic variables generally behaved similarly (Figure 2.4), suggesting a basis for extending knowledge from one watershed to others as long as this extension is done carefully.

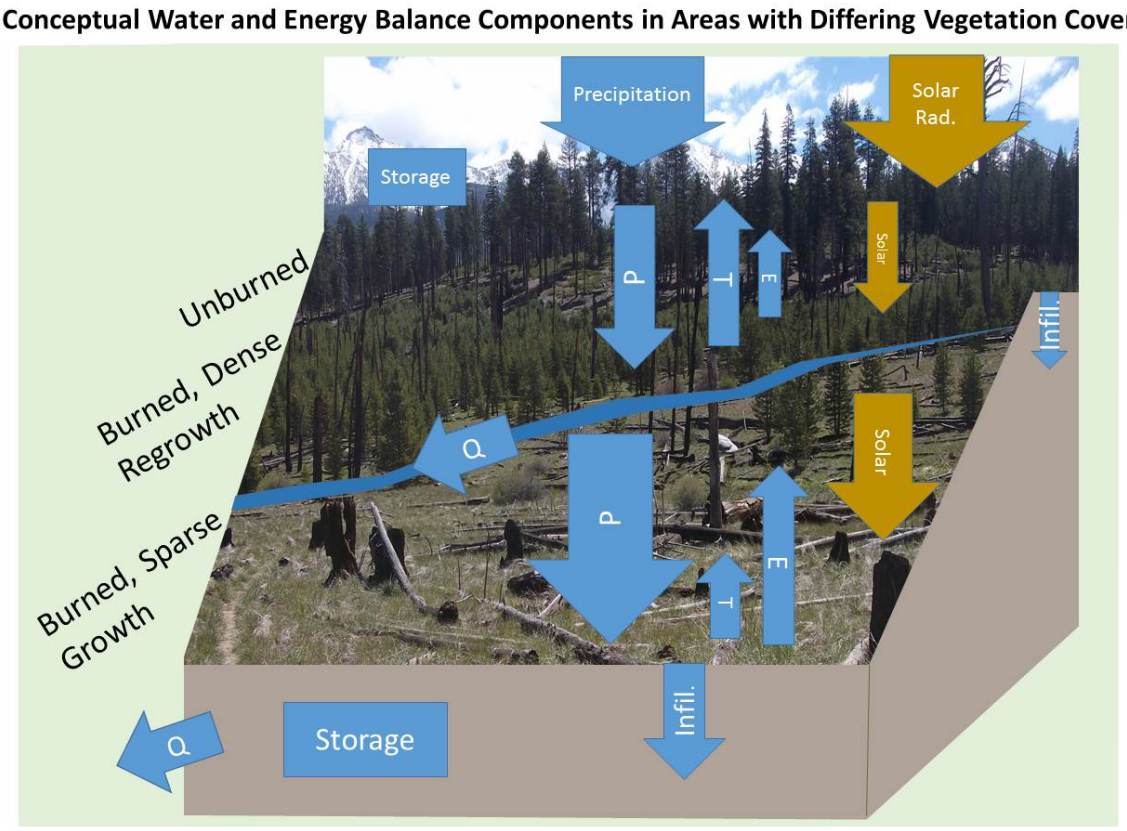

Figure 1.1: Conceptual diagram of how water (blue arrows) and energy balances (orange arrows) might differ in the burned and unburned portions of a watershed. The width of each arrow is proportional to the magnitude of the flux. In this conceptual water balance, less precipitation (P) reaches the ground in unburned or densely vegetated areas due to high interception rates, and more water leaves as transpiration (T). However, more water leaves the sparsely vegetated area via evaporation from the soil (E) because of increased solar radiation reaching the ground. The net effect of these fluxes of water will alter the amount available for streamflow (Q) or infiltration to groundwater storage. Storage of water in the snowpack as well as below ground supplies landscape with water even when there is no precipitation.

1.5 Background - Fire and Water

Watersheds have multiple ways in which they can respond to fire, making it challenging to a priori predict fire-specific shifts in water storage and fluxes (Lane et al., 2010; Ursino and Rulli, 2011). Because of decreased transpiration, a reduction in vegetation following fire can initially increase soil moisture (Helvey, 1980), while increasing forest density due to fire suppression has been shown to decrease soil moisture (Tague and Dugger, 2010). However, vegetation regrowth following a fire can lead to a high water demand by dense, fast-growing vegetation which can decrease soil moisture below pre-fire conditions (Lane et al., 2010; Neary et al., 2005), especially if the new growth cannot regulate transpiration as well as old growth forests (Perry and Jones, 2016). This juxtaposition between short term and long term trends in water storage suggests that a short fire return interval could maintain beneficial increases in soil moisture and baseflow by keeping vegetation density low, but this return interval might have to be less than ten years (Brown et al., 2005). Figure 1.1 illustrates mechanistically how vegetation in a burned landscape can affect the water balance. A landscape which includes many different types of land cover would impact energy and water in many different ways at different scales. Such diversification of the landscape also means a diversification in the types of water retention mechanisms throughout the landscape (e.g. low soil evaporation from shrub fields and forests, deep peak snowpacks in burned open areas, and low transpiration demands from sparsely vegetated areas).

Soil permeability affects soil water storage by controlling the amount of rain (or snowmelt) that can infiltrate into the soil. Fire-induced water repellency of shallow soil decreases its permeability, and thus can increase overland flow and reduce the amount of precipitation stored as soil moisture (Mayor et al., 2007; Neary et al., 2005; Vieira et al., 2015). Overland flow is also increased by reduction in litter cover after fire, since litter impedes overland flow and promotes percolation into the soil (Helvey, 1980; Neary et al., 2005). Soil erosion also often increases post-fire, largely due to these increases in overland flow, as well as loss of vegetation cover that increases soil cohesion (Vieira et al., 2015). All of these effects can reduce or negate any increases in soil moisture due to reduced transpiration and interception post-fire.

Vegetation cover also provides contrasting effects on snow accumulation: sublimation of intercepted snow reduces snowpack, but shading helps preserve snow on the ground from melting or sublimating (Andreadis et al., 2009; Tague and Dugger, 2010). Experiments in the Sierra Nevada have shown microclimate changes due to prescribed burning which could affect snowpack (Ma et al., 2010). Blackened trees and other surfaces heat up more than unburned forests from solar radiation, inducing an earlier snowmelt (Helvey, 1980; Neary et al., 2005). Canopy gap size regulates the balance between interception and shading, and can strongly affect the timing of snowmelt (Lundquist et al., 2013). Large open areas follwing fire can lead to deeper peak snowpack, but earlier and faster spring snowmelt (Seibert et al., 2010). In contrast, in areas that are snow-dominated but have relatively warm winters, dense canopies can increase longwave radiation enough to cause snow to melt earlier than in adjacent open areas, negating the canopy's shading effect and leading to a shorter period

that snow contributes to soil moisture stores and streamflow (Lundquist et al., 2013). Any change in the timing and magnitude of snowmelt will affect streamflow regimes in snow-dominated systems. Work in Glacier National Park suggested that annual runoff increases following fire may not be as large as in rainfall-dominated systems since snowmelt usually coincides with low ET (Mast and Clow, 2008), though a study in the Oregon Cascades found that a post-disturbance riparian species shift was followed by a 25% reduction in summer baseflow despite this area being snow-dominated (Hicks et al., 1991).

Changes from fire can impact the timing and volume of peak flow, leading to increased numbers of flash floods (Neary et al., 2005). High precipitation intensity in severely burned watersheds can cause disproportionately high peak flows (Moody and Martin, 2001). Such floods can also be accompanied by high sediment loads (Helvey, 1980). Post-fire changes in peak discharge are often larger than post-fire changes in total annual streamflow (Moody and Martin, 2001). Large flows after storms can cause damage both to the ecological integrity of a system and to human life and property.

Increases in low flow after a fire can be extremely beneficial to ecosystems and anthropogenic water demands (particularly in seasonally dry climates). There are "a number of anecdotal reports of springs beginning to flow after years of being dry," as well as measured increases in duration of flow in seasonal rivers following fire, suggesting a rise in water tables once dense vegetation is removed (Neary et al., 2005). Baseflow can also be decreased, however, if reduced infiltration lowers the water table (Neary et al., 2005). Increased baseflow after wildfire has been observed in multiple studies (Helvey, 1980; Neary et al., 2005). The elimination of diurnal fluctuations of flow following fire-caused mortality of riparian vegetation specifically demonstrates that transpiration reductions following fire can cause measurable changes in flow (Helvey, 1980; Neary et al., 2005).

Fire can be beneficial to the maintenance of wetland ecosystems. Reconstruction of fire histories using ash and charcoal deposits in wetland soils indicate that fire has long been a part of wetland ecology, and "light, frequent fires maintain the herbaceous vegetation in emergent meadows such as tidal marshes and sedge meadows" in the Southeastern U.S. (Neary et al., 2005). The relationship between fire and wetlands demonstrates how fires can serve as functional mechanisms in ecosystems, and not simply as sources of disturbance.

The intensity and location of a fire often determine the extent to which the fire will affect a watershed. Low severity fires, for example, rarely adversely affect watershed condition (Neary et al., 2005). Large burn areas with steep terrain are most at risk for negatively influencing water quality (Neary et al., 2005). Although large burned areas have a risk of generating high peakflows, specific discharge (normalized by watershed area) following wildfires is often greatest in small watersheds ($<1\text{km}^2$) (Neary et al., 2005). Weather can also affect post-fire hydrologic responses. For example, drought can limit the regrowth of vegetation after fire and thus prolong the period when the watershed is affected by clearing, while unusually heavy rainfall can magnify the effects of post-fire erosion and overland flow (Mayor et al., 2007).

Fire impacts on one watershed are not always transferable to others, or even different fires in the same watershed. This variation in responses between watersheds motivates the

desire to understand specific mechanisms that control hydrologic response to changes in land cover, rather than simply characterizing the responses. Variability in watershed response to wildfire also motivates the need for understanding how multiple overlapping fires might affect a landscape. The vast majority of the research discussed above is about individual fires, rather than the long term effect of a change in fire regime. This focus on individual fires is largely due to the fact that there are many watersheds available for study that have experienced isolated fires, but very few watersheds which have experienced a change in fire regime at time scales that can be observed by researchers.

1.6 Background - Climate and Hydrology in the Sierra Nevada

This dissertation focuses on the Sierra Nevada, a region with highly variable streamflow and weather. The Sierra Nevada has a mediterranean climate with wet winters and long, dry summers; the Pacific high-pressure area moves south in the winter, allowing Pacific storms to reach the Sierras, and moves north in the summer, deflecting storms from the Pacific further north (Curry, 1969; Dettinger et al., 2011). Most precipitation falls as snow, and peak snow depths are highly variable, but average about 2.5m in the south and 3.5m in the north at the elevations of maximum accumulation (Curry, 1969).

Peak snowpack (typically measured on April 1) contains an average of about 13km^3 of water in areas draining into Sacramento and San Joaquin rivers. For comparison, the largest man-made reservoir in California is Lake Shasta, with a volume of 5.5km^3 (Maurer et al., 2007). Earlier melting of the Sierran snowpack therefore reduces the amount of stored water available to California in the summer. Observational records show streamflow occurring earlier in the year, a change largely attributed to increasing temperature and earlier snowmelt (Department of Water Resources, 2008). A 1°C increase in temperature at certain elevations could lead to changes of up to 12 days in streamflow center of mass timing (the date at which half of annual flow volume has passed), while a 5°C increase could lead to changes up to about 45 days (Maurer et al., 2007). For areas south of 39.5°N (including the Tuolumne, which provides San Francisco's drinking water), the greatest change in streamflow timing is predicted to occur in the same elevations which currently store the greatest amount of snow in early spring (2000m-3200m, parts of the Illilouette Basin fall in this range) (Maurer et al., 2007). Sierra snowpack has been decreasing over the past century, and is projected to experience a 25 to 40 percent reduction from its historic average by 2050 (Department of Water Resources, 2008). These changes in timing and volume could lead to challenges for reservoir managers needing to balance between flood control and water supply (Maurer et al., 2007).

The Sierra Nevada is likely to be strongly affected by climate change: Dettinger et al. (2004) predict warmer temperatures, earlier snowmelt, and a slight rise in precipitation in the Merced watershed (within Yosemite National Park) by the end of this century. The

proportion of precipitation falling as rain in the Sierra Nevada has been increasing since 1949 (Cuthbertson et al., 2014). Streamflow from the Sierra Nevada is highly dependent on snowpack, and increased rain fraction leads to increased flooding as well as less water available downstream during the dry summer months (Department of Water Resources, 2008). Annual discharges from Sierra Nevada rivers are correlated since they originate from the same snowpack, though this correlation is weakened by a north-south trend (Benson et al., 2002). This means that information about one watershed in the Sierras gives a good measure of trends in other watersheds.

Fossilized timberlines suggest a downward shift in timberline since 3500 years b.p. (Curry, 1969). Curry (1969) finds that "all of the climatic variations thought to have occureed in the the Sierra Nevada during the last 10,000 years could have been the result of changes in mean climatic parameters that are within the range of known variation in the extremes of those parameters during the last 100 years", suggesting that it does not take unusually large changes in precipitation or temperature to create large changes in features such as treelines or glacial extent.

Graumlich (1993) found long term (centennial scale) trends in temperature which correspond with trends in average atmospheric volcanic aerosol loading, while variation of the solar constant on a decadal scale does not appear to be an important factor in temperature variation in the Sierra Nevadas. Trends in precipitation were found to be most important at a frequency of over 14.5 years.

Sustained droughts occurred in North America in the late 16th century and between 900-1300AD; both appear to have exceeded the duration and magnitude of any recorded droughts prior to 2010 (Woodhouse et al., 2010). Isotopic analysis of lake sediments suggest that California has experienced multiple droughts lasting decades at a time (Benson et al., 2002). In 1940, Los Angeles began diverting water from Mono Lake, exposing relic tree stumps from previous times when the lake level was lower due to drought. Dating these stumps using ^{14}C revealed that the Sierra Nevada experienced a two century drought before AD 1112 and for over 140 years before AD 1350 (this second drought corresponds to the widely observed Medieval Warm Epoch) which lowered the lake level to 15.5m and 11m, respectively, below the current natural level (Stine et al., 1994). One of the Sierra Nevada's most severe droughts occurred from 1915-1934 (the 20 year average precipitation only dropped lower during the Medieval Warm Epoch), while a long period of above average precipitation occurred from 1937-1986 (50 yr mean exceeded only twice in the last 1000 years) (Graumlich, 1993). Considering long-term reconstructions of California climate, long and severe droughts are not uncommon, leaving agricultural, industrial, and urban systems that are dependent on water resources vulnerable to water shortages (Graumlich, 1993).

Woodhouse et al. (2010) predicted that "Twenty-First Century droughts will occur under warmer temperatures, with greater rates of evapotranspiration than occurred during the major droughts of the 20^{th} Century... Thus, warm droughts of the prehistoric past might provide evidence useful in understanding the current climatological changes, and for providing scenarios for worst-case droughts of the future and evidence of hydroclimatic responses in the Southwest to warmer climatic conditions" (Woodhouse et al., 2010). Although the

2012-2016 California drought was not necessarily unusual in terms of length or precipitation, by 2014 it was the most extreme drought in 1200 years in terms of the Palmer Drought Severity Index (PDSI) which accounts for both precipitation and temperature (Griffin and Anchukaitis, 2014). The winter of 2015 was the warmest on record, meaning that very little of the precipitation that year (which was already below average) was actually stored as snowpack (Dettinger and Anderson, 2015).

Sierra Nevada precipitation and temperature are highly variable both spatially and temporally. This variability makes it difficult to identify meaningful changes in streamflow or forest health, since there is so much variability even when the system is unaltered. In my studies of the Illilouette Basin, I address this complication using models and with the paired catchment method. A major and important caveat on the results presented in this dissertation is that field data collection occurred entirely during a drought period, and therefore do not cover the range of hydrologic conditions possible within the watershed. Winter 2016 precipitation was close to the long-term average, however, which did allow field comparisons between summer 2014, 2015 and 2016 to shed some light on the effects of the drought on the study area.

1.7 Background - History of Fire in the Sierra Nevada

Historically, fire has played an important role in the Sierra Nevada: lightning and human caused fires have shaped Sierra Nevada ecosystems since prehistory. Starting in the early 20^{th} century, a blanket policy of fire exclusion drastically altered fire regimes in California, but from the beginning there were concerns about the impact that fire suppression would have on fuel buildup and forest ecology (Sugihara et al., 2006). From 1950-1999, forested areas in California burned at approximately 23,000 ha/yr, compared to over 1,000,000 ha of forest burning annually in California prior to European settlement (Stephens et al., 2007). California's forests are thus currently experiencing a fire deficit, with consequences for fuel loads and forest ecology. Although fire suppression has reduced the frequency of wildfires, it has led to an increase in the proportion of fires that burn at high severity, because of higher fuel loads (Miller et al., 2012b).

Swetnam and Baisan (2003) used dendrochronology to date fire scars in multiple locations in Arizona, New Mexico, and the west slope of the Sierra Nevada to determine fire frequency and extent from the mid 15^{th} century to the present. They found that fire frequency in the Southwest averaged about 1 fire per 7.5 years from 1700-1900. There was a sharp decrease in fires around 1900, especially after 1904, mainly due to the introduction of intensive livestock grazing. Organized fire fighting was severely limited until the 1930s or 1940s. A large fire year in 1970 was primarily attributed to an ambitious prescribed burning program undertaken that year in Sequoia National Park. While some researchers attribute pre-European fire regimes mainly to Native Americans, Swetnam and Baisan believe that indigenous influence on fires was very time- and place-specific, and cannot explain the widespread fire patterns observed in fire scar records. Some fires seem to have been very widespread, which

is consistent with 19^{th} century newspapers reporting wildfires burning for long periods of time (weeks to months) and sometimes exceeding 500,000 ha; some synchronous fires (or synchronous lack of fire) in the historical record are interpreted as responding to climate, especially when such synchronicity occurs across spatial scales that are too great to possibly be due to the same fire (Swetnam and Baisan, 2003). Years with many fires in the Western U.S. historically tended to be drought years, while years with little to no fire tended to be wet. At the decade-century timescales there was no correlation between fire occurrence and precipitation, though occurrence was correlated with growing season temperature. (Swetnam and Baisan, 2003)

Fire, landscape, and climate in the southwestern USA have thus all been affecting each other in multiple ways, both with and without human interference, for centuries (and probably much longer). Very few locations exist in which we can study how frequent, mixed severity, lightning-caused wildfires shape a landscape and alter watershed-scale hydrology, relative to the fire-suppressed conditions that now prevail almost universally across the southwestern USA. This dissertation studies one of these rare locations: Yosemite National Park's Illilouette Creek Basin.

1.8 Study Site: The Illilouette Creek Basin

The Illilouette Creek Basin (ICB) provides a unique opportunity to study the effect of natural fire regimes, and their associated land cover change, at watershed scales. Since the early 1900's, fire suppression has been a common practice throughout U.S. forests (Collins and Stephens, 2007). Thanks to its remote location within Yosemite National Park (YNP) and rocky boundaries that limit fire spread, in 1972 the ICB was chosen as the site of a long-term experiment in which lightning fires would be allowed to burn, thus replacing the fire suppression policy with a managed wildfire policy (Collins and Stephens, 2007). The ICB is one of only two areas in California that have been allowed to revert to a natural burning regime in this way, and the only one with long-term hydrological records (1915-present). During earlier work in this watershed, fire ecologists at UC Berkeley noticed that burned forest areas sometimes were being replaced by facultative or obligate wetland vegetation that would not usually grow in soil dry enough to support conifer forests (e.g. Figure 1.2), which led to a desire to study whether the area's frequent fires were increasing water availability.

The ICB is a 150 km^2 basin within the Upper Merced Watershed in Yosemite National Park, California, USA (Figure 1.3). It spans an 1800 m to ≈3000 m elevation range in the central Sierra Nevada mountain range. This area experiences a mediterranean climate. Based on observations from Remote Automated Weather Stations near ICB, average January daily minimum temperatures ranged from -5°C to 1°C, while average July daily maximum temperatures ranged from 24°C to 25°C (2000-2015; http://www.wrcc.dri.edu/; stations: White Wolf, Crane Flat). Average annual precipitation (Oct-Sep) ranged from 47 to 60 cm at these stations (for years 2000-2015), and is dominated by winter snow. The basin is covered by coniferous forests (dominated by Jeffrey pine, *Pinus jeffreyi*, red fir, *Abies*

Figure 1.2: Dense shade-intolerant and drought-intolerant understory growing in a burned area that was once densely forested, adjacent to an intact mature forest.

magnifica, white fir, *Abies concolor*, and lodgepole pine, *Pinus contorta*), rocks, meadows and shrublands (dominated by whitethorn ceanothus, *Ceanothus cordulatus*) (Collins et al., 2007). This area has never experienced timber harvesting and likely had minimal impacts from livestock grazing (Collins and Stephens, 2007).

Fire suppression began in ICB in the late 19th century (Collins and Stephens, 2007) and continued until 1972, when Yosemite National Park began its managed wildfire program (then called "natural fire management") (van Wagtendonk, 2007). The duration of the managed wildfire program at ICB and the large total proportion of the basin area that has burned since 1972 (52% of the total area and ≈75% of the vegetated area) make it an ideal place to study the landscape effects of managing wildfire rather than focusing on suppression. Although ICB was impacted by approximately 100 years of fire suppression (only 8 ha are known to have burned between 1880 and 1973), fire frequency and extent since the onset of the managed wildfire program in 1972 is similar to that in the non-fire suppressed historical period: Tree ring analysis shows that the current mean fire return interval of 6.8 years closely matches the 6.3 year mean interval for 1700-1900 AD (Collins and Stephens, 2007), suggesting a dynamic equilibrium between vegetation cover and fire has already been reached. Since ending fire suppression in 1972 there have been 30 fires exceeding 100 acres extent in the ICB (Figure 1.3). Burned patches form a mosaic of vegetation change, with high severity burn patches intermixed with intact older forests (Figure 1.2), and a large range in the time-since-last-fire and vegetation condition.

Collins and Stephens (2007) used tree ring records to compare historical fire patterns to modern ones in both the Illilouette Creek and Sugarloaf Creek watersheds of the Sierra

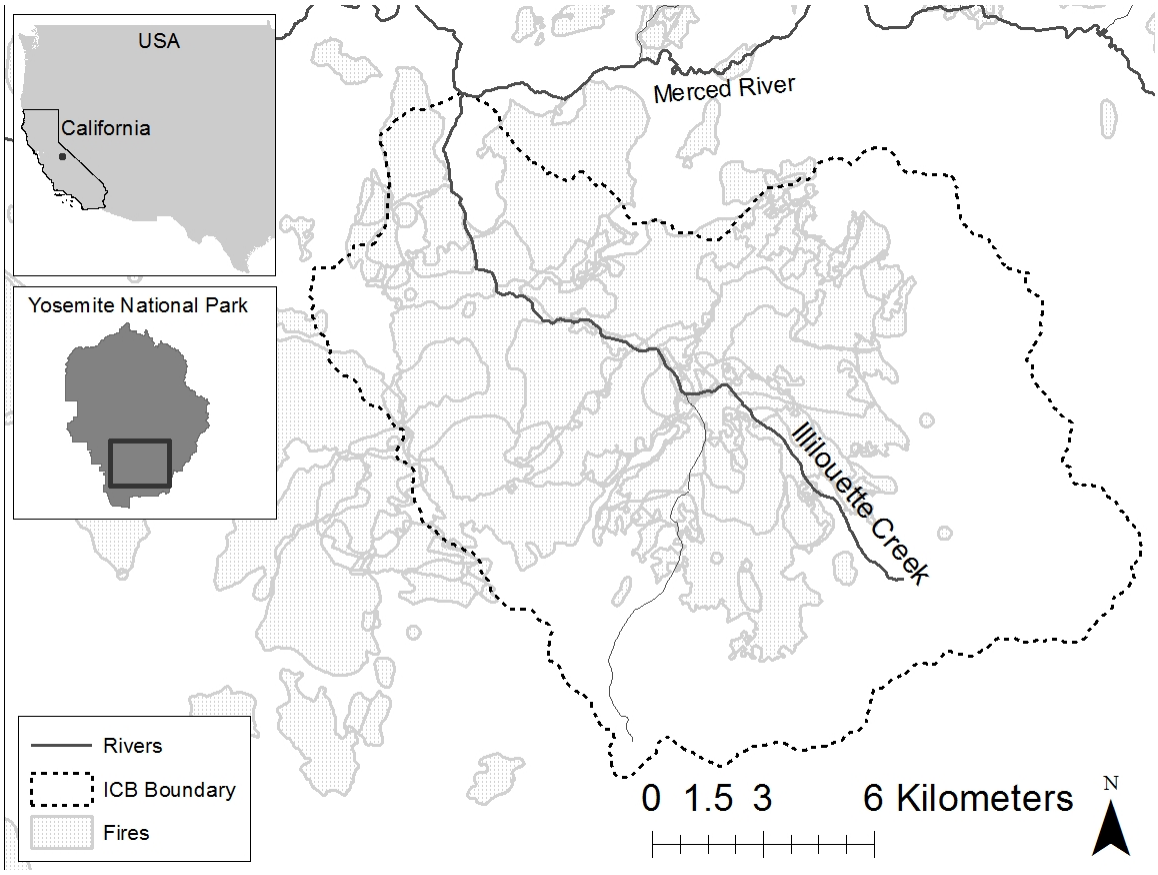

Figure 1.3: Location of Illilouette Creek Basin and its fires.

Nevada. They found that fires in the 200 years prior to fire suppression likely burned under low to moderate intensities in most cases.

The nearest stream gage downstream of the outlet of the ICB is the Happy Isles Gage in Yosemite Valley. This gage measures drainage from the Upper Merced Watershed (UMW), of which the ICB accounts for approximately 32% of the area. Studies have shown that removal of approximately 20% of a watershed's vegetation cover is required before a significant change in streamflow will be observed (Brown et al., 2005). While the UMW has experienced a number of relatively small fires over the years (mostly within the ICB) rather than a single tree-killing event, over 20% of the UMW's vegetated area has burned at some point in the last 40 years (CA Dpt. of Forestry and Fire Protection GIS data). Approximately 100 years of flow and weather data are available from the Happy Isles Gage and Yosemite Headquarters weather station, respectively.

One suggestive observation within this basin is that burned lodgepole pine (*Pinus contorta*) stands (locally common and typically associated with dry soils) have been replaced by wetland-adapted vegetation such as willows (*Salix spp.*). Wetland vegetation requires saturated soil at least part of the year, and its presence suggests that water tables in the

basin may be rising - an inference that is consistent with observations of rising water tables and increased streamflow in other thinned forests (Brown et al., 2005).

Previous work using the Regional Hydro-Ecological Simulation System (RHESSys) model on the UMW (which includes the ICB) suggests that the model may be able to capture fire-induced increases in streamflow: The model over-predicted flow by 20% prior to 1973, but only by 13% after 1973 (Naomi Tague, personal communication). These over-predictions could be due to the fact that the model was parameterized using a 1997 vegetation map (Christensen et al., 2008), meaning vegetation cover (and thus transpiration) was under-predicted for the majority of the modeled time period.

1.9 Challenges

Although the ICB provides the best dataset that we know of for studying the hydrological impacts of fire regimes in the Western U.S., there are multiple challenges to consider during this project. The ICB only makes up 32% of the monitored watershed. While the Illilouette Creek is the largest tributary to the Merced River within this watershed, we expect fire effects on Merced River streamflow to be muted by the influence of the extensive unburned areas of the UMW, inhibiting our ability to identify such changes. This lack of a long-term gage on Illilouette Creek is a major motivation for employing detailed hydrological modeling of the ICB.

Secondly, the variations in slope, aspect, and elevation in the Sierra Nevadas means that interpolating meteorological data between weather stations is subject to high levels of uncertainty. Previous work (Christensen et al., 2008) provides a peer-reviewed method for providing the best possible estimates of basin-wide precipitation and energy inputs. Short-term deployments of temperature sensors in the Upper Merced watershed allow for updating previous estimates of basin-wide temperature (Lundquist and Cayan, 2007).

With the exception of field data collected during this and related projects (e.g. Collins et al., 2016; Wilkin, 2016), and field observations used to validate the 1997 Yosemite National Park vegetation map, the only available information about vegetation cover is derived from remote sensing. Remotely sensed datasets necessarily contain some uncertainty that must be accounted for in subsequent statistical analyses. Morever, the classification of vegetation from remote sensing is also necessarily coarse, meaning that, for example, species level differences in drought tolerance (known to occur in willow species amongst others) cannot be discerned. This lack of resolution amongst plant cover types complicates the inference of hydrologic change from vegetation cover.

Finally, field measurements in the basin are constrained by time, funding for equipment, and the wilderness status of the ICB. Research in wilderness areas requires an in-depth approval and permitting process, and proscribes against use of, e.g., motorized equipment, permanent structures, and extensive ground disturbance. Total hours spent within the basin and the number of people present are also limited by this permitting process. As a consequence, the investigations detailed in this dissertation adopt a wide range of approaches

to infer processes and mechanisms driving hydrological change in the basin, such as remote sensing and modelling.

1.10 Scope of this Dissertation

Due to the inherent variability and complexity of hydrologic systems, it is important to approach hypothesis-testing from multiple angles. This dissertation combines analysis of historical data, field measurements, remote sensing, statistical modeling, and distributed hydrological modeling.

Because fires' effects on hydrology are largely driven by the effects of fire on vegetation, I began with a detailed study of how fire has altered the landscape in ICB: Using historic aerial imagery, I mapped vegetation cover from the fire-suppressed period through year 2012 and quantified the changes introduced by fire (Chapter 3). Next, I combined these maps of land cover change with field measurements relating soil moisture to land cover and other spatial variables in order to estimate fire-related changes in soil moisture basin-wide (Chapter 4). The timing of this project offered me the opportunity to study the effect of wildfires on the drought resilience of the ICB (Chapter 5). I also used historical records of streamflow and weather to explore whether reintroducing fire to the landscape had created measurable changes in water yield in ICB compared to control watersheds (Chapter 5). Field observations and historical records provide circumstancial evidence relating hydrologic change to fire history. Following these observational studies, I explored potential mechanisms of change using a distributed eco-hydrological model to reconstruct the history of vegetation, fire and hydrologic change in the ICB since 1970, and to compare this to a hypothetical situation in which fire suppression continued through to the present day (Chapter 6).

Broadly, this dissertation tested the hypothesis that restoring a fire regime can increase streamflow and soil moisture storage compared to fire-suppressed conditions. This theme is broken up into the following specific hypotheses:

1. Runoff ratio (Ratio of annual streamflow to annual precipitation) has increased significantly in the watershed containing the ICB since ending fire suppression in 1972, but not in nearby unburned watersheds (Chapter 5).

2. Vegetation and moisture changes are positively correlated, and thus satellite observations of vegetation can be used to map areas throughout the basin with high soil moisture storage. Specifically, I hypothesize that the presence of dense meadow vegetation is indicative of higher summer soil moisture levels compared to other vegetation types (Chapters 4 and 5).

3. Remote sensing will show that forest cover has significantly declined, while percent cover of grasslands, meadows, and wetlands has increased, since the reintroduction of wildfire to the ICB (Chapter 3).

4. Remote sensing data of drought-related tree mortality will show that the ICB has lower incidence of such mortality compared to nearby, unburned watersheds (Chapter 5).

5. A distributed hydrologic model of the ICB will demonstrate:

    a. A closer match to observed streamflow when parameterized with observed changes in vegetation cover compared to simulations in which vegetation is not altered (Chapter 6).

    b. Increases in soil moisture, decreases in evapotranspiration, and earlier snowmelt in burned areas, as well as at the watershed scale when compared with an unburned control (Chapter 6).

Chapter 2

MOPEX Watershed Study

2.1 Introduction

In Chapter 1, I discussed a project using the MOPEX watershed dataset which demonstrated the influence of vegetation on streamflow generation. This chapter provides additional information on the methods and results of that project in order to better explain the preliminary work that provided much of the process-based understanding which informed this dissertation. I do not go into the full details of the project here, because they are not central to the main hypothesis of this thesis. These results do, however, provide useful insights into how vegetation, temperature, and precipitation interact to affect watershed-scale water balances.

2.2 Methods

Data Sources

The National Oceanic and Atmospheric Administration (NOAA) Model Parameter Estimation Experiment (MOPEX) dataset provides historical daily values for streamflow and maximum and minimum temperature for 438 watersheds in the United States. The MOPEX dataset includes potential evapotranspiration (PET) and vegetation cover (parameterized as greenness fraction, or GF) as monthly means averaged over all years, as well as climate indices such as the proportion of annual precipitation to annual PET. The watershed areas range from dozens of square kilometers to over 10,000 km^2 (www.nws.noaa.gov/oh/mopex/mo_datasets.htm). The raw data used by MOPEX include: USGS streamgauge data, meteorological forcing data derived from data sets developed by the Dennis Lettenmaier lab at the University of Washington, PET based on the NOAA Pan Evaporation Atlas, and vegetation cover from NOAA AVHRR data (Duan et al., 2006; Gutman and Ignatov, 2010). Data for all watersheds cover roughly the same time span (1948-2002), and meet minimum data requirements with respect to the spatial density of rain gauges and the availability of daily streamflow data. The slope, elevation, and soil depth of each MOPEX watershed were

calculated by collaborators at the University of Arizona (Voepel et al., 2011) using topographic data from the Shuttle Radar Topography Mission (Farr et al., 2007) and geologic and soils information from the State Soil Geographic Database (Miller and White, 1998).

Recession Constant Calculation Methods

The recession constant (RC) provides a measure of the time period over which a watershed's response to rainfall declines and a flow returns to a baseflow-dominated condition. There are many alternative definitions of the recession constant available (Sujono et al., 2004). Here, rather than aiming to attach a strong physical interpretation to the recession constant, the approach follows Tallaksen (1995) in using a fast and objective method that (i) is feasible to compute over large datasets and (ii) is easily compared between different watersheds. Thus, the recession constant is defined in this study as the number of days required after peak flow for the flow rate to decline to $1/e$ of the peak flow (Figure 2.1b). Recession constants were automatically generated via a search algorithm for all storms unless the flow failed to monotonically decrease to at most $1/e$ of the storm's last flow peak before the next streamflow increase occurred.

To provide a simple indicator of the change in recession values throughout the year, a *recession constant seasonality* was computed using:

$$SeasRC = \frac{RC_{dorm} - RC_{grow}}{RC_{max}}; -1 \leq SeasRC \leq 1$$

where RC_{dorm} and RC_{grow} are the mean recession constant during the dormant and growing season, respectively, and RC_{max} is the highest monthly mean recession constant for the watershed. These values are applied across all years, as very few individual years contain enough clean streamflow recessions to allow for a reliable calculation of RC seasonality on an annual scale. On average, only 4.4 RCs were calculated per year per watershed, and these were concentrated in the watersheds' wet seasons.

Analysis of hydrological and phenological indices

For each watershed, I compared the histograms of the RCs for storms in the growing and dormant seasons. Because these data were non-normal, the differences in these groups were analyzed using a nonparametric two-sample Wilcoxon rank sum test.

I also compared the probability distributions of mean RCs for each season at regional scales by combining data across large numbers MOPEX watersheds. To control for the effect of storm intensity, all storms and their associated recessions were first subdivided into rainfall intensity quartiles, and the mean RC was computed for each watershed, in each season, for each rainfall quartile. I then created separate histograms of these mean RC values for each season and each rainfall quartile, and used these histograms to describe the distribution of mean RC for a given group of MOPEX watersheds.

Based on a qualitative exploration of the data, different geographic regions displayed different trends in RC with changing GF. Regions that behaved differently were analyzed separately to avoid confounding effects. Furthermore, stations with fewer than five measured recessions in each season were removed from the analysis.

Attribution of Seasonal Drivers

Although the correlations between streamflow metrics and phenology can be empirically characterized based on observed data, the attribution of the changes in hydrology to vegetation and climate effects requires further analysis. Decreases in recession constant can be induced by multiple phenomena, including increased evaporation (which in turn may be driven by temperature, humidity or insolation changes), increased plant water uptake due to growth, and increased interception due to expanding leaf area. During the growing season in temperate climates, changes in relevant climate and vegetation drivers occur synchronously and are likely to have similar impacts on the recession constants. Because these effects are not separable using data alone, a simple hydrological model was employed to attribute the observed changes in recession constant to climate and vegetation forcings (Sivapalan et al., 2003; Ye et al., 2012).

To provide a simple indicator of the change in plant activity throughout the year, we again compute a seasonality index, this time the *greenness seasonality*, using the maximum and minimum monthly GF values at each station:

$$SeasGF = GF_{max} - GF_{min} \; ; \; 0 \leq SeasGF \leq 100$$

Description of lumped watershed model

The watershed model used is a minor elaboration on the two-bucket model described in Ye et al. (2012) and previously used to describe flow duration curves across the MOPEX dataset (Figure 2.1a). I made two modifications to the model to ensure that vegetation drivers to the water balance could be explicitly represented. Firstly, I incorporated the Rutter et al. (1975) interception model, parameterized as a function of LAI, to account for evaporative losses due to interception. Secondly, I scaled the potential evaporation with LAI to capture the dependence of transpiration on leaf surface area. Although additional processes could potentially be added to this model to improve the representation of streamflow recession, in order to facilitate comparison between watersheds and avoid overparameterization, I restricted the model to the simplest form that still captured the processes of interest.

Model Experiment Methods

Once the full model was calibrated for each station, I used a hierarchical approach to explore potential drivers of observed RC seasonality. I successively "turned off" sources of seasonality present in the full model: interception, transpiration, and PET. When a source of seasonal

	Model 1	Model 2	Model 3	Model 4	Model 5	Model 6
Daily Precipitation	X	X	X	X	X	X
Daily Temperature	X	X	X	X	X	X
Monthly PET	X	X	X	X		
Interception capacity (C_{wet})	X			X	X	
Throughfall proportion (p)	X			X	X	
Potential transpiration from veg.	X	X			X	

Table 2.1: Table of values allowed to vary in time for each model. In model 1, the values in each row vary seasonally. Models 2 and 4 separately remove seasonality in interception and transpiration, respectively. Model 3 hold both interception and transpiration constant, thus measuring the total effect of vegetation. Model 5 isolates the effect of weather by holding only PET constant. In model 6, everything except precipitation and temperature is held fixed throughout the year.

variation was turned off I simply replaced the time varying values of the relevant parameters with their temporal means. By assessing how much the loss of different sources of variation impacted the model performance, I determined the significance of the seasonal drivers' impact on the observed changes in streamflow recession, similar to performing a sensitivity analysis. Eliminating the different drivers of seasonality resulted in six versions of the model, described in Table 2.1.

Calibration of vegetation and climate parameters was performed using only the complete model, as per Tian et al. (2012), and these calibrated values were used across all model versions. This approach reflects the fact that the goal of this analysis is to evaluate the effect of the forcing variables, rather than the model calibration. Re-calibrating parameters related to the physical properties of the watershed would remove the ability to directly compare the model runs. For example, in at least one case re-calibration enabled a selection of physical watershed properties (such as the root zone storage capacity) to compensate for lack of variation in PET and provide an equally good fit to observed recession constants - however it would be fallacious to conclude that this means that PET has no effect on streamflow.

The model performance in terms of RC was evaluated using three metrics:

- Nash-Sutcliffe Efficiency (NSE): This measure of fit is given by

$$NSE = 1 - \frac{\sum_{m=1}^{12} (RC_{obs}(m) - RC_{sim}(m))^2}{\sum_{m=1}^{12} (RC_{obs}(m) - RC_{mean})^2}$$

  where $RC_{obs}(m)$ and $RC_{sim}(m)$ are the monthly mean observed and simulated recession constant, respectively (for each month m), and RC_{mean} is the mean of all RC_{obs} values.

An NSE of 1 gives a perfect fit, and a value below 0 means that the model performs less well than using the mean of the observed values (Legates and McCabe, 1999).

- Seasonality: Our second measure of model fit is the proportion of observed RC seasonality captured by the model: $SeasRC_{sim}/SeasRC_{obs}$.
- Timing of the maximum recession constant: Difference (in months) between the simulated and observed months with the maximum monthly mean RC.

I used these three measures of model fit to quantify the effect that vegetation and climate each have on annual RC patterns. Although the number of sources of variability is different between model versions, the total number of parameters remains the same for all. For this reason, I did not use goodness of fit metrics such as Akaike Information Criterion (AIC) which account for the total number of parameters.

Using principal component analysis (PCA), I identified sources of variation in the watersheds and grouped watersheds with similar features, focusing on physiographic and ecological watershed properties related to streamflow recession. All potential covariates for the PCA were selected by first checking for non-zero correlation with recession constant seasonality. When pairs of covariates were highly correlated with each other, I kept only the member of the pair which led to a higher variability for the first principal component (PC) of the PCA. Factors include mean soil depth, geographical location (latitude and longitude), percent cover of deciduous forests and/or croplands, mean hillslope, aridity(P/PE), amount of precipitation occurring in winter, amount of PE occurring in winter, $SeasGF$, and annual precipitation.

Once principal components were identified, I applied k-means clustering to the watersheds within the PCA space in order to classify similar groups. Different numbers of clusters (k) were explored qualitatively for their ability to capture differences in recession constant seasonality; k=3 provided the most consistent division between clusters.

2.3 Results and Discussion

Streamflow recession constants could be computed during both growing and dormant seasons for 424 of the 483 MOPEX stations. The remaining 14 had insufficient flow during the dry season. Figure 2.2a shows the difference in RC between dormant and growing seasons at each watershed. The RC decreased during the growing season for approximately 60% of the 424 watersheds, primarily in the Midwest and East of the United States. This decrease was $> 10\%$ in approximately 2/3 of these watersheds. Many of the watersheds with significantly longer mean RC during the dormant season are concentrated in the Midwestern region (Figure 2.2a, blue watersheds).

The recession constants in 40% of the 424 watersheds, conversely, increased during the growing season. The RC increased by $> 10\%$ in approximately half of these watersheds. As shown in Figure 2.2a, most watersheds in the western United States have longer RC in

the growing season. We will differentiate between these two types of seasonality as G_{long} when growing season RC is larger than in the dormant season by at least 10% and D_{long} for dormant season RC being larger by at least 10%.

The geographic differences shown in Figure 2.2a primarily identify locations where the trends in GF are in phase with peak precipitation and snowmelt (this primarily occurs in the western, more arid watersheds, and results in an increase in RC throughout the early growing season) in contrast to locations where GF and snowmelt are out of phase (this primarily occurs in mesic, energy-limited watersheds in the northern and eastern locations in the USA). Because of the phase differences and their effects on recession seasonality, results are presented separately for watersheds east and west of 110° West.

Figure 2.3c-e shows the empirical distribution of mean growing and dormant season RCs. These distributions are significantly different for the two lower quartiles of rainfall in eastern watersheds ($p < 0.005$), but not for higher rainfall. In western watersheds, there is a significant difference between seasons for all precipitation levels. For both eastern and western sites, as precipitation increases a smaller proportion of sites display a significant seasonal change in RC, and the means in each season get closer together. This suggests that the effects of vegetation on streamflow generation may only be measurable when the watershed is somewhat water limited.

Using PCA, we reduced the dimensionality of our dataset of watershed properties from ten to five (Five PCs captured over 90% of the dataset's variance). Figure 2.4 shows the results of using k-means clustering to divide the first five principal components into three groups. These clusters captured spatial patterns of RC seasonality, despite the fact that streamflow metrics were not included in the PC calculations (Figure 2.4). One cluster contains the nearly uniformly D_{long} watersheds in the Midwest, the second contains Eastern watersheds that do not follow the D_{long} pattern as strongly, and the westernmost cluster contains mainly G_{long} type watersheds.

Because of the large differences in behavior between eastern and western watersheds, further analysis is restricted to a principal component space calculated using only watersheds east of 110° West. There is a significant correlation between the first PC and RC seasonality for the eastern watersheds. There is a division around the 0 point of the first principal component. The group with positive values in the first PC generally have more positive seasonality ($RC_{dorm} > RC_{grow}$) than those with negative values in PC space. This is the same as the division between the first two clusters in Figure 2.4. The first PC captures 53% of observed variability, and largely consists of contributions from aridity (measured by P/PE), total annual precipitation, fraction of precipitation in winter, mean slope, percent deciduous/seasonal vegetation cover, and rock depth, showing that these variables can roughly predict RC seasonality. The major contributors to the second PC are the latitude, winter PE, and annual variability in GF.

We also investigated the relationship between recession constants and spring onset dates in the Northeastern U.S., a region with a high density of MOPEX watersheds and high variability in the onset of spring (defined using first lilac bloom dates of the year (Schwartz et al., 2006)). In early spring years, mean June-August RC decreased by 13% compared to

normal years ($p < 0.02$), with a decrease of approximately 15% in June. March-May RC was not correlated with spring onset date, showing that spring onset mainly influenced RC during the period of the year with highest leaf cover, warmest temperatures, and longer time since leaf-out. A late spring onset did not significantly alter summer RC from years with normal spring onset dates ($p = 0.52$). This is an example of how earlier spring onset caused by climate change could affect streamflow properties, through changes in both temperature and vegetation activity.

The model results given in Table 2.2 indicate how significant the different seasonal contributions were to annual RC patterns for watersheds displaying three different types of seasonality: D_{long}, RC values staying within a 10% range, and G_{long}. Most watersheds displayed the D_{long} type seasonality, where mean dormant season RC is greater than the mean growing season RC. For these watersheds, removing seasonality for PET and vegetation parameters in model 6 led to a poor fit to observed RC (mean NSE< 0). Model 6 resulted in a switch in seasonality for D_{long} watersheds, as indicated by the negative sign of the mean seasonality measure. Seasonality was not reversed, on average, holding constant any one of PET, interception, or transpiration on their own. The dormant$\approx$growing group showed an even greater difference between models, though this is likely due to the fact that RC seasonality is small to begin with and thus any changes were proportionally large. For all three seasonality types, the differences between observed and modeled seasonality were largest for the simplest model (model 6). The model error in timing of the longest monthly RC was largest for the watersheds in which recession constants were similar or longer in the dormant season, using the simplest model version (model 6).

For D_{long} watersheds, holding transpiration constant reduced mean NSE from 0.46 ± 0.02 to 0.34 ± 0.02 and decreased the percent of observed seasonality captured from $69\pm6\%$ to $51\pm5\%$. In comparison, holding interception constant reduced average NSE by only 0.08 (0.46 to 0.38) and did not affect modeled seasonality (Table 2.2). In general, increased interception and transpiration both contribute to changes in flow generation with phenology, though transpiration has a larger contribution on average. PET provides the greatest contribution to seasonal variations in RC for the majority of watersheds, though the largest seasonal changes occur when PET, interception, and transpiration all act together to decrease RC in the summer.

2.4 Conclusion

Our observations of seasonal changes in the recession constant for most watersheds demonstrates the appropriateness of recession constant as a metric for capturing seasonal changes in flow generation mechanisms. For the Central and Northeastern regions, RCs are generally shorter during the growing season, as was found by Czikowsky and Fitzjarrald (2004). The opposite is true in the Northwestern region.

This study demonstrated the use of a novel alternative to paired catchment studies. Instead of comparing treated and untreated watersheds, we compared watersheds to themselves

	1. Full Model	2. Const. Int.	3. Const. Int. and T	4. Const. T	5.Const. PET	6.All Const.
Dormant RC>Growing RC (D_{long}, n=123)						
NSE	0.46(0.02)	0.38(0.03)	0.29(0.03)	0.34(0.02)	0.02(0.04)	-0.15(0.04)
Seasonality	0.69(0.06)	0.69(0.06)	0.52(0.06)	0.51(0.05)	0.08(0.05)	-0.15(0.06)
Timing Err.	1.61(0.16)	1.66(0.16)	1.53(0.14)	1.63(0.15)	2.24(0.16)	2.65(0.16)
Dormant RC≈Growing RC (n=121)						
NSE	0.31(0.02)	0.21(0.03)	0.15(0.03)	0.20(0.03)	-0.10(0.04)	-0.24(0.04)
Seasonality	0.45(0.18)	0.43(0.17)	0.33(0.14)	0.33(0.14)	-0.33(0.37)	-0.32(0.36)
Timing Err.	1.55(0.16)	1.79(0.16)	1.91(0.16)	1.76(0.16)	2.40(0.17)	2.81(0.16)
Dormant RC<Growing RC (G_{long}, n=72)						
NSE	0.30(0.04)	0.26(0.04)	0.17(0.06)	0.17(0.06)	0.12(0.04)	0.09(0.05)
Seasonality	0.58(0.37)	0.61(0.37)	0.57(0.32)	0.56(0.33)	0.42(0.10)	0.22(0.12)
Timing Err.	1.49(0.17)	1.51(0.17)	1.61(0.18)	1.67(0.16)	1.61(0.18)	1.63(0.19)
Percent of all watersheds where model created least RC variability						
%	<1	8	12	18	61	NA

Table 2.2: Model Test Outcomes: Each column gives statistics of results from models 1-6 described in the methods section. The results are divided between watersheds where dormant season recession constants were at least 10% longer than in the growing season (Dormant>Growing), those with growing season recession constants being at least 10% longer (Dormant<Green) and those with less than 10% $SeasRC$ (Dormant≈Growing). Each row gives a different goodness-of-fit measure of the model output compared to the observed data. An NSE value of 1 denotes a perfect fit. The "seasonality" measure gives the ratio of modeled seasonality (difference in mean recession constants between seasons) to the observed seasonality, so a value of 1 is the best fit possible. The timing error, in the last row of each section, gives the average number of months by which the model missed the observed month of maximum recession constant. Numbers in parentheses are standard error. For 61% of watersheds, model 5 provided the least month to month variability in RC, suggesting that PET is usually the dominant driver in seasonal RC changes.

using growing and dormant periods as two different treatments. Combining data analysis and a simple hydrological model, we measured effects of vegetation change without the secondary effects on soil associated with vegetation removal. Another advantage of this method is that it captures persistent patterns over a long time period, rather than initial responses to change as is the case with paired catchment studies. Such a method could be employed for analysis of the effect of vegetation on other hydrological behavior in addition to the streamflow recession explored here.

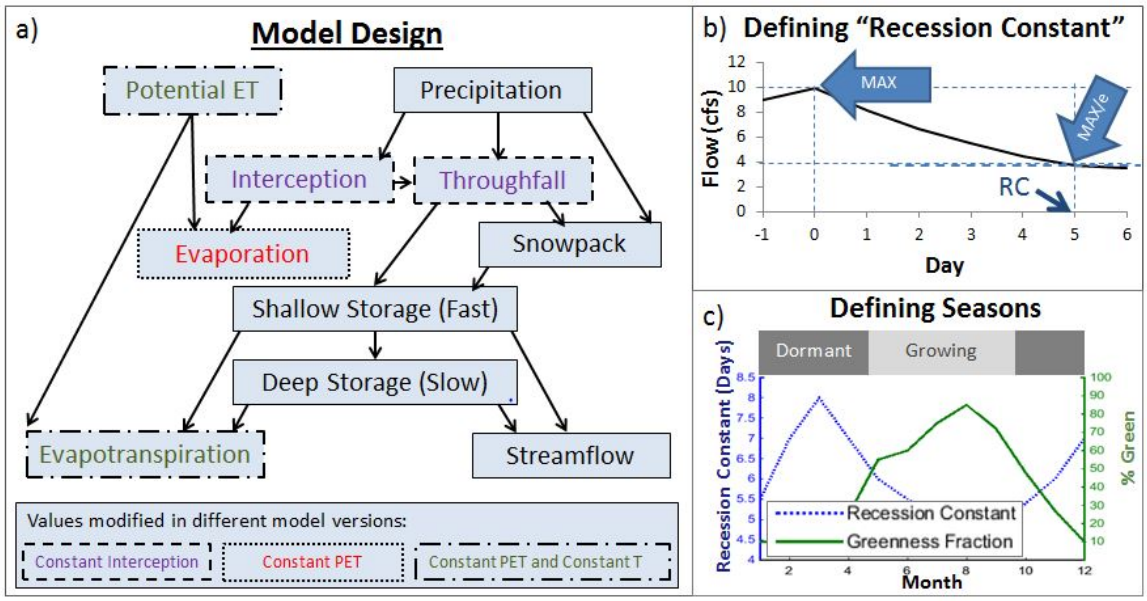

Figure 2.1: Diagrams explaining models and terminology. (a) Flow chart showing the partitioning of water in the two-bucket model. Boxes with non-solid edges represent portions of the model which are changed in our analysis to test sensitivity of streamflow to interception, transpiration, and PET. Precipitation is divided into snowpack or rainfall. Rainfall in turn can be intercepted by leaves or fall to the ground. (b) Explanation of our definition of "recession constant", the e-folding time of streamflow recession following rain-induced peak flow. This theoretical plot shows a recession constant of five days. (c) Definition of the growing season as the period when greenness fraction is at least 75% of the watershed's maximum. The lines shown are observed data from a watershed which demonstrates a clean inverse relationship between greenness fraction and recession constant.

a)

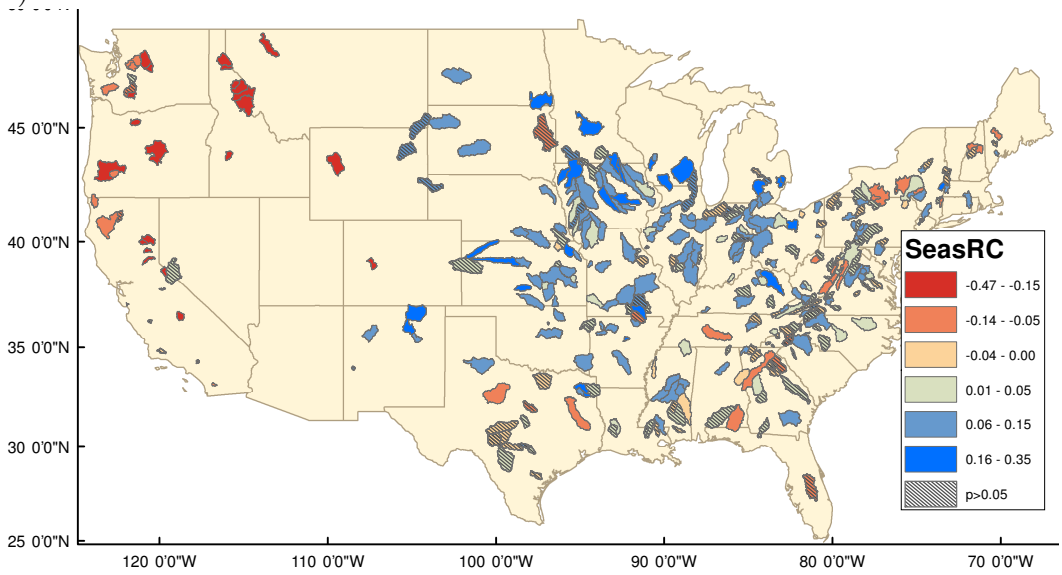

b)

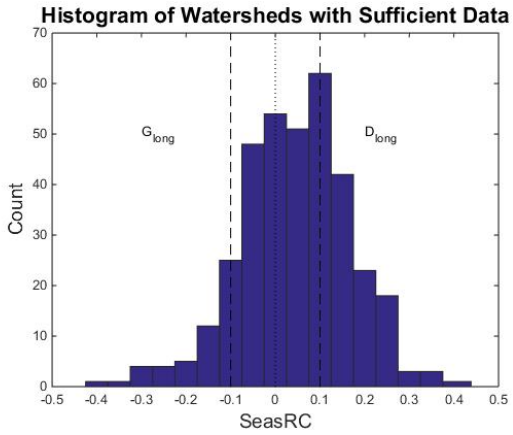

Figure 2.2: (a) Map of recession constant seasonality for all watersheds, for rain in the lowest quartile. Watersheds in red shades have G_{long} seasonality, while D_{long} watersheds are shown in blue. Watersheds with shading did not show a statistically significant difference in mean RC between growing and dormant seasons. (b) Distribution of SeasRC over all watersheds.

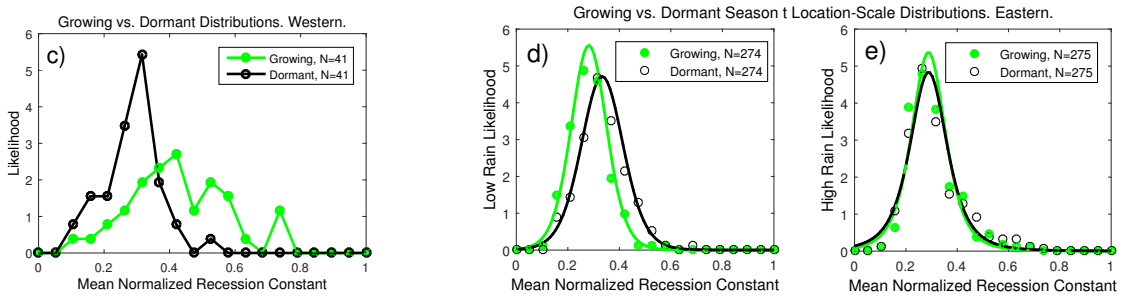

Figure 2.3: (c-e) Distributions of recession constants (normalized by that watershed's maximum) in each season for Western and Eastern watersheds. Sections d and e show empirical distributions of seasonally averaged RC for the eastern watersheds (longitude $> -100°$E, latitude $> 35°$N). The distributions are separated by the lower 50% (d) and upper 50% (e) of rainfall volume and fit with a parametric distribution. For larger amounts of rain, the seasonal effect is drowned out in eastern watersheds (e). For the western watersheds (longitude $< -110°$E, latitude $> 37°$N), rainfall amounts did not make a large difference so all recessions are shown together (c). The western distribution did not match a parametric distribution well, and thus only the raw distribution is presented here. The p value printed on each graph gives the probability that the means of the two distributions are equal (using a K-S test). In eastern watersheds (d and e) the recession constants are generally shorter during the growing season, while the opposite is true of western watersheds (c).

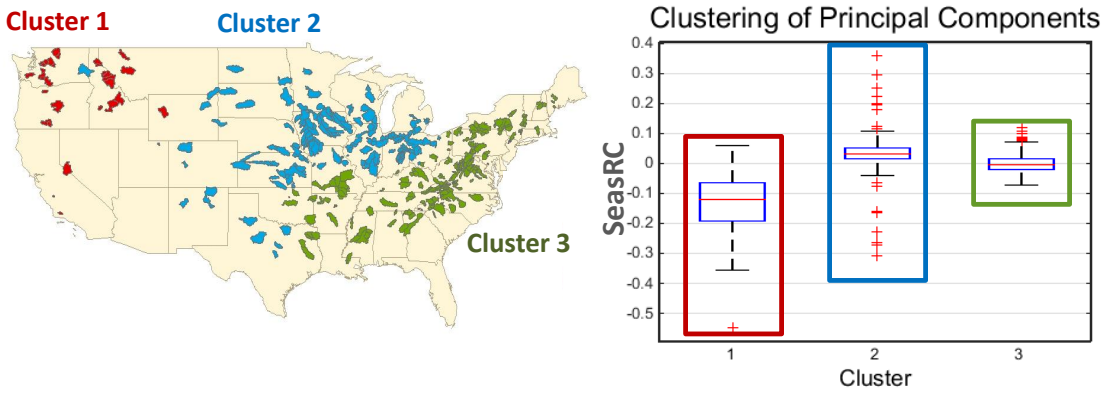

Figure 2.4: Result of clustering of the first five principal components of the watershed properties. Each cluster has a unique distribution of recession constants, showing the relationship of recession constant to the physical basin characteristics used to define the component space.

Chapter 3

Landscape Change Over Forty Years of Fire in the Illilouette Creek Basin

In the MOPEX project, I generalized hydrologic response to vegetation change over broad scales. In studying the Illilouette Creek Basin, in contrast, I wanted to gain a specific understanding of how vegetation cover impacted the water balance of this catchment at sub-watershed scales. Studying changes at these scales requires a detailed understanding of what vegetation changes have occurred across this landscape due to fire. This chapter describes fine-scale land cover changes in the ICB over time both in terms of land cover types and spatial structure.

3.1 Introduction

Landscape structure, as defined by the types and spatial organization of vegetation communities, is shaped by the interactions between disturbance events and succession following disturbance (Miller and Urban, 2000a). Succession trajectories vary depending on disturbance history, local site characteristics, and temporally varying conditions as young life-stages establish in disturbed sites (Johnson and Miyanishi, 2010). Disturbance processes are also affected by the landscape structure, which can influence disturbance frequency, spatial extent, and severity (Turner, 1989). These two-way interactions allow landscape composition to be thought of as non-equilibrium complex system, in which constant inputs of energy (in the form of disturbance) prevent the landscapes from achieving "steady state" conditions (Mori, 2011; Sousa, 1984). Removing these energy inputs, by suppressing disturbance events, would be expected to move landscapes towards a successional "steady state", which, for spatially uniform soil and climate conditions, could produce uniform vegetation cover (D'Odorico et al., 2006).

Homogenization of landscapes has been observed in response to the prevalence of fire suppression as a fire-management strategy in the Western USA during most of the 20^{th} Century. In the Sierra Nevada, the homogeneity of both the landscape and individual for-

est stands has increased compared to pre-1900 baseline conditions (Hessburg et al., 2005a; Perry et al., 2011; Scholl and Taylor, 2010; Stephens et al., 2015), and fire-suppressed forest stands have more than doubled in density since the early 1900s (Collins et al., 2011). In contrast, there are few opportunities to directly observe the response of landscape structure to increases in disturbance frequency due to fire. Simulations suggest that forest density and spatial autocorrelation of forest patches should decrease as fire disturbance rates increase (Miller and Urban, 2000b), with concomitant increases in the abundance of species that prefer open habitat such as shade-intolerant flowering plants (Pausas, 2006), and in fire- or disturbance-adapted shrub species (Pausas and Lloret, 2007).

Opportunities to empirically evaluate such predictions have generally been limited to considering the immediate effects of isolated disturbance events such as individual stand-replacing fires, yet the conclusions to be drawn are not always clear. Large, stand-replacing fires can increase or decrease species richness, and can reduce beta diversity (the ratio of regional to local species diversity, measuring differentiation between habitats), particularly if the fire results in colonization by a small number of disturbance-tolerant species (Burkle et al., 2015). Mixed severity fires, on the other hand, may increase beta diversity (Burkle et al., 2015; Perry et al., 2011). Such increases are theoretically consistent with increases in landscape heterogeneity in more frequently disturbed systems, since heterogeneity in natural landscapes is generally positively correlated with biodiversity (Seiferling et al., 2014).

However, drawing conclusions about landscape-scale effects of a changing disturbance regime from modeling or individual disturbance events alone is problematic - for example, fire return intervals can affect post-fire recruitment, even amongst fires with the same severity (Donato et al., 2009). Empirically evaluating the effects of increasing fire frequency on previously fire-suppressed landscapes is increasingly important as forest and land management agencies strive to find techniques to manage forested landscapes for resilience against likely increases in fire severity and drought stress projected to occur as a consequence of climate change (Westerling and Bryant, 2008; Westerling et al., 2006). The dense, homogeneous forests generated by decades of fire suppression are likely to exacerbate fire risks due to elevated fuel loads (Collins and Skinner, 2014; Taylor et al., 2014) and drought risks due to increased water demand from dense forest stands and uniformly forested landscapes (Goulden and Bales, 2014; Grant et al., 2013). Indeed, high intensity wildfire and large-scale insect outbreaks are altering the Sierra Nevada landscapes faster than they did before fire suppression and logging (Hessburg et al., 2015), and drought-related tree mortality has been increasing throughout the Western US (Hicke et al., 2016; Moore, 2015).

In the Sierra Nevada, vegetation communities are likely adapted to a frequent, lightning-induced fire regime (Hessburg et al., 2015). Consequently, "managed wildfire", a land management strategy in which naturally ignited fires are allowed to burn without intervention (subject to an approved fire management plan) is attracting increased interest. In 2016, three Californian National Forests (Inyo, Sequoia and Sierra National Forests) designated more than 50% of their total area to use managed wildfire (www.fs.usda.gov/detail/r5). Managed wildfire is anticipated to benefit landscapes by restoring a "natural" structure (Hessburg et al., 2015). Natural landscape structure is hypothesized to benefit local ecology

(e.g. species abundance and dispersal responding to changes in patch size and shape (Turner, 1989)), and hydrology (e.g. canopy interception (Andreadis et al., 2009), evaporative demand (Brown et al., 2005), and timing of snowmelt (Lundquist et al., 2013),). Despite the increasing interest in managed wildfire and its effects on landscape structure, empirical evaluations of how landscape structure changes in response to such a management regime are rare, largely due to the paucity of landscapes managed under a natural fire regime.

Here we address this gap by providing a detailed description of how forty years of managed wildfire has altered a previously fire-suppressed landscape in the Illilouette Creek Basin (ICB) of Yosemite National Park in the Sierra Nevada, California. ICB has operated under a managed wildfire policy since 1972, one of only two such long-running managed wildfire regimes in forested areas of California. We evaluate changes in the ICB using historical aerial imagery spanning the end of the fire-suppressed period through 2012. We present the results in terms of overall land cover compositional change, along with a range of metrics describing landscape patterns and vegetation patch structure (Turner, 1989). Results not only provide insight into possible trajectories of landscape structural change upon initiation of a natural wildfire regime, but also form a basis for evaluating the effects of fire-induced landscape compositional changes on basin-scale ecosystem functions, such as water cycling and carbon storage.

3.2 Methods

Study Area

The Illilouette Creek Basin (ICB) is a 150 km^2 watershed spanning elevations of 1800 m to ≈3000m in the Central Sierra Nevada region, located within Yosemite National Park, California, USA (119.50°W, 37.66°N). The climate is mediterranean with approximately 100 cm average annual precipitation, dominated by winter snow. Temperatures from nearby weather stations at similar elevations vary from average January daily minimum temperatures of -5°C to average July daily maximum temperatures of 25°C (2000-2015; http://www.wrcc.dri.edu/; stations: White Wolf, Crane Flat).

The basin is covered by coniferous forests (dominated by *Pinus jeffreyi, Abies magnifica, Abies concolor,* and *Pinus contorta*), shrublands (dominated by *Ceanothus cordulatus*), meadow environments containing grasses and forbs (including both dryland and wetland obligate species), and extensive exposed bedrock (Collins et al., 2007). The ICB was not logged and experienced minimal impacts from livestock grazing (Collins and Stephens, 2007). Fire suppression began in ICB in the late 19^{th} Century (Collins and Stephens, 2007) and continued until 1972, when Yosemite National Park began its "Natural Fire Management" program (van Wagtendonk, 2007). The ICB's first 20^{th} Century fire over 5ha in size was the 1600ha Starr King fire in 1974. Since then, there have been 27 fires over 20ha in size, and over 100 smaller fires. Fifty-two percent of the total basin area and ≈75% of the vegetated area have burned since 1972 (Figure 1.3). Fire frequency and extent during the managed

wildfire period beginning in 1972 are comparable to pre-suppression historical estimates (a 6.8 year recurrence interval, versus 6.3 historically, based on fire scar measurements, Collins and Stephens, 2007).

Data Sources

This study makes use of aerial photos, historical maps, and ground reference data to delineate patches of vegetation with common composition. Aerial imagery is increasingly popular for historical vegetation change analysis, and new computer products are increasing the objectivity and reproducibility of classification of aerial photos (Morgan et al., 2010). Aerial imagery offers several advantages for historical vegetation mapping. Given its high resolution, it is often possible to identify individual trees and large shrubs within the image, allowing manual interpretation of images and object-oriented classification. This contrasts with relying on interpretation of spectral signatures for classification, as would be required if the reconstruction were to be based upon satellite records such as Landsat. Landsat imagery is available on more frequent time intervals and with greater spectral resolution, but the coarse spatial resolution (80m from 1972-1978, 40m for 1978-1982, and 30m afterwards, landsat.usgs.gov) reduces accuracy when identifying different vegetation types and mapping them to changes in the landscape. Particularly because no ground truth data are available for the earliest part of our analysis, use of a high spatial resolution product is important.

The earliest aerial imagery of the ICB comes from a set of black and white images taken by Cartwright Aerial Surveys in 1969 and 1970, provided by the Yosemite National Park Archive. This imagery has approximately 0.5 meter spatial resolution (because it is film rather than digital, there is no exact resolution) and represents the fire-suppressed condition of the watershed.

National Aerial Photography Program (NAPP) aerial imagery from 1987, 1988, and 1997 (available from U.S. Geological Survey) were used to map the changing state of ICB vegetation following the institution of the managed wildfire regime. Images from 1987 and 1988 were combined to maximize spatial coverage of the watershed. NAPP imagery is 1 meter resolution and was recorded using color infrared film. The highest quality images of this area are from 2005 and 2012 National Agriculture Imagery Program (NAIP) datasets (Farm Service Agency and USDA, 2015). The NAIP imagery has a spatial resolution of 1 meter, a radiometric resolution of 8 bits, and contains red, green, and blue bands as well as an infrared band.

All images other than those from NAIP required orthorectification prior to classification. We used the ERDAS Imagine Leica Photogrammetry Suite (www.hexagongeospatial.com/ products/ producer-suite/ erdas-imagine), NAIP imagery for reference, and a LiDAR elevation map (Kane et al., 2015) for orthorectification. Where two or more images overlapped, the best of those images was chosen manually, in ArcMap, based on the clarity of individual objects (influenced by plane angle, contrast, glare, etc.).

We used existing vegetation maps of Yosemite to assist with mapping as much as possible. However, such maps are only available for a limited number of years, and most have lower

spatial resolution than our analyses require. The 1997 Yosemite National Park vegetation map (available at irma.nps.gov) provided the finest spatial resolution, and was used to verify the approximate extent of the different vegetation types where appropriate (e.g. we could not use the 1997 park map to verify the 2012 map in areas that had burned after 1997).

Vegetation Mapping

Vegetation classification was performed in eCognition (produced by Trimble, www. ecognition. com), an object-based analysis tool which uses color band values, texture, and shape to classify image objects. Object-based analysis facilitates the use of texture in classification, and also avoids the challenges associated with pixel-based analysis, including unmixing of spectral information in areas with fine-scale heterogeneity in land cover (Blaschke et al., 2014), and changing availability of color and infra-red bands across the images.

All years were classified into at least six land cover classes: granite, water, conifer forest, shrub, sparse meadow, and dense meadow. A seventh cover class, aspen, was added for the 1997 NAPP and all NAIP images. Meadows are defined as areas dominated by grasses and forbs; dense meadows have little to no bare ground and appear green in color summer aerial photographs (bright red in color infrared images), while sparse meadows have larger amounts of bare ground and appear brown in color photographs or green/beige in color infrared. The dense meadow category encompasses wetlands, but the aerial image analysis does not reliably separate true wetlands from areas with dense summer grass. Areas of standing dead trees with no discernible understory were classified as sparse meadows.

The 1969 black and white imagery was degraded both spatially and radiometrically, prior to classification, to enhance the capabilities of the texture algorithms and speed processing time (Caridade et al., 2008). The original data was 8-bit, ≈ 0.5 meter resolution and was degraded to 4-bit, 2 meter resolution. Only non-overlapping portions of the images were processed in eCognition to eliminate redundancy and to speed processing. Bodies of water were entered via ArcMap after the initial eCognition classification using delineations from NAIP imagery in order to retain smooth outlines that were not always captured in the degraded black and white imagery. Some images captured more fine-scale heterogeneity than others. To compensate for this effect, we merged any polygon with an area less than 700m^2 with the largest adjacent polygon. The value of 700m^2 was chosen to minimize the number of polygons removed while visually maximizing the similarity in types of structures captured in different maps.

To classify the images, we first identified exposed granite using color imagery, which helped to distinguish it from grassland, bare ground and sand. Ground reference locations of bare ground, solid rock, and sand helped in identifying the slight differences in color between these similar looking areas. Under the rationale that fire occurrence would not affect the distribution of the "rock" land cover type, the mapped locations of granite outcrops from later images were used directly in classifying the 1969 photographs. Granite was uploaded into eCognition as a thematic layer, using the "assign class using thematic layer" algorithm.

The 1997 aerial images were of lower quality than other years due to poor resolution and multiple areas with heavy glare that made it difficult to identify vegetation. To compensate for this, and to incorporate as much independent information into the classification as possible, we included the Yosemite National Park Service (NPS) vegetation map (irma.nps.gov) as a thematic layer in eCognition. Including the 1997 NPS map, which was created using aerial imagery originally, helped us to delineate some of the boundaries between vegetation types as well as identify vegetation types in areas with high levels of glare. Although it would have been simpler to use the 1997 NPS map instead of creating our own map for 1997, initial tests showed that we could not directly compare the NPS map to our other vegetation maps because of differences in the level of spatial detail and shape complexity captured.

For imagery not obtained from NAIP, unclassified sliver polygons remained in the exported classification in areas where individual images did not overlap perfectly. These slivers were classified manually in ArcMap. There were some small areas (<10%) of the watershed that were not covered by the available imagery. These missing areas do not include any of the areas where stand-replacing fire occurred in ICB. We therefore gap-filled these sites from the closest (in time) vegetation map that covered the missing areas.

Accuracy Assessment

The 2012 map was validated using 230 ground reference points mapped in 2013-2015. We mapped these points with a handheld Garmin GPS unit, with the goal of capturing transitions in vegetation cover type as well as mapping multiple examples of large stands within each cover class. Due to the inaccessibility of portions of the ICB, mapping was generally limited to within 1.5km of hiking trails. Sixty-six points were removed because they were within 50m of another ground reference point for the same vegetation type, in order to avoid skewing the results. We manually classified an additional 300 randomly selected validation points from the aerial imagery, in order to cover a broader area and increase the total number of validation sites.

We were unable to use the Yosemite NPS Vegetation map from 1997 for additional validation due to the mismatch in resolution between the the NPS map and our product. Not only do the maps we produced provide finer spatial resolution than the Yosemite NPS vegetation map, they are also more discriminatory in assigning an area as "forest". In contiguous patches with less than $\approx 15\%$ vegetation cover, we classified the patch as bare ground or granite, even if the park map labeled it as forest.

Other than the NPS map, no independent information is available to validate the maps for earlier years. Earlier classifications were validated by selecting random points in ArcMAP, visually identifying those points as belonging to one of the five vegetation classes, and then using these random points for validation. These points were selected using the Create Random Points tool in ArcMap, keeping a minimum of 50m between any two points. The goal was to have 500 total points, distributed proportionally among vegetation types, in each year. If needed, extra points were added in order for each mapped vegetation class

to include at least 10 verification points. Any large vegetation areas identified as being misclassified were manually corrected until overall accuracy reached 90%.

We used confusion matrices to calculate accuracy within each vegetation class for each year. Confusion matrices give the number of validation points mapped as a certain class (rows) which are identified as each vegetation class using visual inspection of the photos or actual ground reference points (columns). *Reliability*, also known as "user's accuracy", is the proportion of points mapped as belonging to a certain class which are classified correctly. *Overall Accuracy* is the proportion of points where the vegetation is mapped correctly, or the sum of values along the diagonal of the confusion matrix divided by the number of data points.

In addition to accuracy for individual years, we used transition confusion matrices to calculate our accuracy in capturing different transition types. The transition confusion matrix is the same as an individual confusion matrix, except that instead of dividing the map into individual vegetation classes it uses categories such as "conifer to conifer" or "conifer to shrub" (which would represent areas which remain conifer or that transition from conifer to shrub, respectively) (Congalton and Green, 2008). We created these transition confusion matrices for all sequential map pairs (e.g. 1969 to 1988 and 1997 to 2005) as well as for the larger time lags of 1969 to 2012, 1969 to 1997, and 1997 to 2012.

Identifying Landscape Change

Total cover was calculated for each vegetation type in each image. Because of the steep topography in this area, we adjusted area for the slope of the landscape in order to avoid underestimating land cover in steep areas (Dorner et al., 2002). We used our measures of classification accuracy for each vegetation type in each image in order to determine the statistical significance of our estimated changes in total area for each vegetation type (following Congalton and Green, 2008). For each map, we calculated the areas of each vegetation class that were converted into another class in a later map. For example, what proportion of the shrublands in 1969 remained as shrubland in each mapped year, and what proportion converted to each of the other vegetation classes?

Changes in patch sizes and distributions between the fire-suppressed and the contemporary condition were assessed using the FRAGSTAT software package (McGarigal et al., 2012). The landscape metrics we selected can be divided into two categories: landscape diversity metrics, which describe how heterogeneous a landscape is, and within-class properties, which describe the behavior of a specific vegetation class.

Landscape Diversity Metrics:

Diversity indices have been shown to capture fire-related landscape changes well (Romme, 1982). They describe heterogeneity by measuring how patches of vegetation are distributed spatially across the landscape.

Shannon's Evenness Index (SHEI) is the Shannon's Diversity Index (calculated using information theory) divided by the maximum diversity given the number of cover types present (McGarigal et al., 2012). An evenness index of 1 would mean that all vegetation types were equally represented in the landscape; higher evenness means more landscape diversity.

Simpson's Evenness Index (SIEI) is similar, but is calculated using the probability that any two cells selected at random would be different patch types (McGarigal et al., 2012). Again, a value of 1 would mean that all patch types cover an equal area, and a value near 0 would mean that one type dominated nearly all of the landscape.

Aggregation Index (AI) is a measure of how much each vegetation type is clumped into a few large groups (high aggregation) or spread into many small groups (low aggregation).

Patch Properties Within Each Class:

Patch properties describe local-scale heterogeneity and the size and shape of individual vegetation patches. For this study, we selected metrics which have been shown to be consistent across many different landscapes (Cushman et al., 2008):

Largest patch percent area (LPI) gives the percent of the total vegetated area taken up by the largest contiguous vegetation patch within each vegetation class. This metric gives an idea of the maximum area dominated by a single type of overstory.

Fractal dimension (FRAC) measures how complex and plane-filling the shapes are by using the relationship between the area and perimeter of a patch. As the dimension approaches 2, perimeter is maximized for a given area of coverage, while for simple geometries such as squares or circles the dimension is 1 (McGarigal et al., 2012).

For example: a vegetation class with a low fractal dimension whose largest patch covered a large area indicates a spatially homogeneous region. On the other hand, a high fractal dimension suggests an increase in the total length of boundaries between patches of different types, thus increasing local heterogeneity.

Varying Resolution

Spatial resolution can significantly affect the computed values of landscape-scale metrics (Kelly et al., 2011; Wu, 2004). We tested the sensitivity of our metrics to resolution by converting our vectorized vegetation maps into raster maps at resolutions of 5, 30, 90, and 500 meters (FRAGSTATS requires converting vectorized maps into gridded datasets). We re-calculated all metrics with these varying-resolution maps and compared the results to each other.

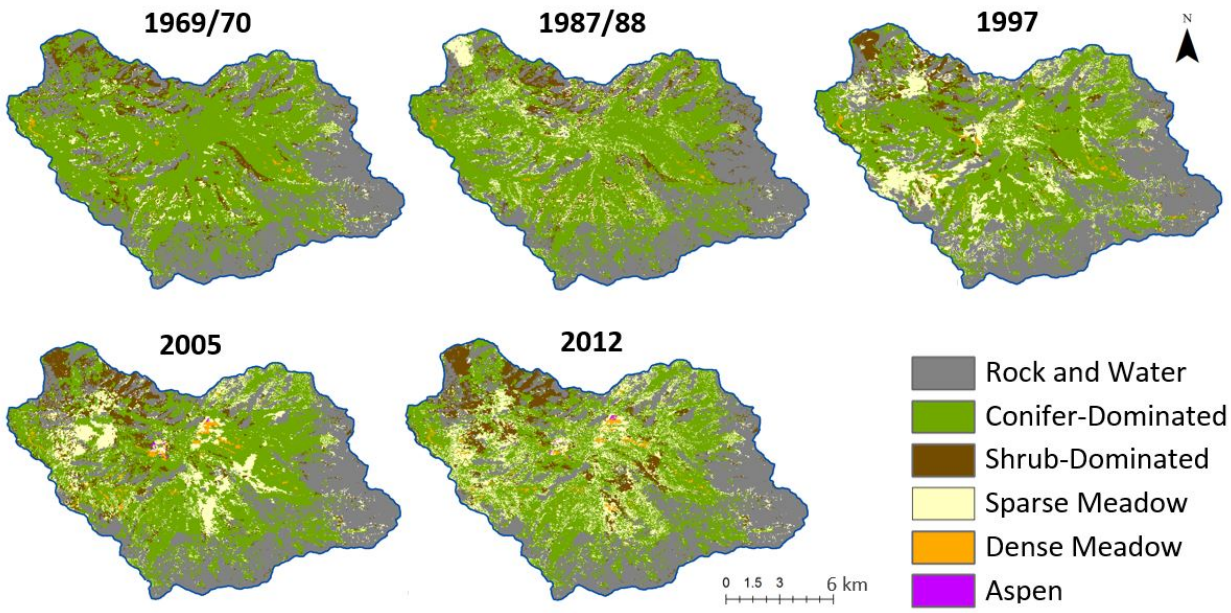

Figure 3.1: Maps created from aerial imagery in five different decades showing non-vegetated areas (rock and open water), conifer forest, shrublands, sparse meadows, dense meadows, and aspen stands.

3.3 Results

Vegetation Mapping

The final vegetation maps created from each set of aerial images reveal clear changes over time (Figure 3.1). Many forested areas are replaced by other vegetation types, and some shrub patches expand into high severity burn areas. Figure 3.2 shows the total landscape area covered by each vegetation type in each year (adjusted for land surface slopes). There were significant changes in total area for every land cover class from 1969 to 2012. However, the significance of some image-to-image changes within that time period are unclear when the change is less than our level of classification accuracy (Figure A.1).

Across the whole 1969-2012 period, conifer cover decreased by 21km^2 (24%), shrublands increased by 4km^2 (35%), sparse meadow area increased by 17km^2 (199%) and dense meadows increased by 1km^2 (161%). Sparse meadow area increased significantly from 1969-1997 after which its total area remained steady. Shrublands initially decreased in area, but then increased. This pattern likely arose from a delay in colonization of burned areas by shrubs. Dense meadow area generally increased, but dropped slightly between 2005 and 2012, possibly due to drought conditions in 2012 (http://droughtmonitor.unl.edu/). In 2012, it had been 8 years since the most recent stand replacing fire in ICB, and vegetation had grown in to some of the large, sparsely vegetated patches present in 1997 and 2005. The 1997

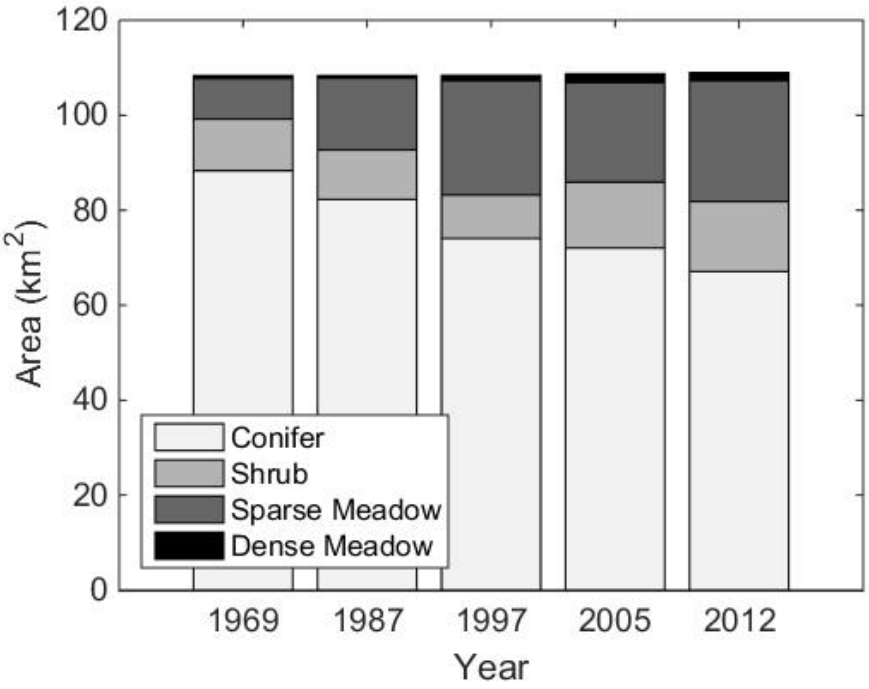

Figure 3.2: Total area of each vegetation class for each year's map. Conifer cover steadily decreases. Shrub area decreases initially but then increases as burned forests and shrublands are colonized by shrubs. Sparse meadow initially increases dramatically but roughly levels out by 1997, while dense meadow area increases slowly and steadily.

and 2005 maps were created from imagery taken relatively soon after large stand-replacing fires (nearly 2000ha burned from 1994-1996, and a 2000 ha fire burned in 2004). These fires created large areas of sparsely vegetated grassland. Although woody recruitment into these burned sites may have begun in 1997 and 2005, any seedlings or saplings would be too small to detect in aerial photography.

Most of the area covered by the 1969 conifer forest (61-73%) was also conifer in 2012 (Table A.3), either because it did not experience stand-replacing fire or conifers had regrown post-fire. Approximately 10% of the conifer area transitioned to shrubland by 2012, 16-26% to sparse meadow, and 2% to dense meadow. Areas dominated by shrubs in 1969 either remained as shrubs in 2012 (40-44%), transitioned to conifer (24-52%), or were replaced by sparse meadows (19%) and a negligible portion shifted to dense meadow. Most 1969 sparse meadows remained sparsely vegetated (54%), but a large portion transitioned to forest (39%). There was very little dense meadow present in the basin in 1969, and conifers encroached upon up to 40% of this area by 2012, while the rest remained as meadow. For the 1987/8-2012 period, results are similar but only 43% of 1987/8 sparse meadow remains sparse meadow in 2012, and 20% transitioned to shrubs.

We compared our maps to the publicly-available LANDFIRE product, a 30m resolution map of existing vegetation cover (EVT) for 2012 (LANDFIRE, 2012b), an estimate of "peak" vegetation cover (for fire suppressed conditions), and a mapped estimate of pre-European settlement vegetation cover (pre-fire suppression) referred to as the biophysical settings or BPS map (LANDFIRE, 2012a). We found reasonable agreement between the 2012 EVT layer and our 2012 map (54% forest cover versus our estimate of 41% forest cover, and 4.5% shrubland cover versus our estimate of 8.7%). Some of the differences in cover between the EVT layer and our 2012 map partly arise from discrepancies in classification of the ICB as barren/sparsely vegetated or as open water - 20% of ICB was classified this way in EVT, versus 33-36% in our maps. EVT does not distinguish between dense and sparse meadows, preventing a direct comparison of these values. The LANDFIRE peak vegetation layer was similar to our 1969 vegetation map. The BPS layer, however, did not closely resemble the current landscape. For example, the BPS layer suggests 79% of the watershed would support forests, but only 1% would be shrubland. This is more consistent with the 1969 fire suppressed conditions in ICB than conditions under the current fire regime.

Accuracy Assessment

Greater than 85% total accuracy in the classification was achieved in each year's vegetation map, ranging from 87% for 2012 to 94% for 1969. Accuracy varied between vegetation classes (Table 3.1). Confusion matrices, detailing sources of error in the classifications for different years, are provided in Appendix A (Tables A.1 and A.2). Confusion matrices for changes over time, using the methods of Congalton and Green (2008), are also presented in Appendix A (Table A.3). Collapsing all changed versus unchanged points, 94% of the area mapped as remaining unchanged is truly unchanged, and 76% of the area mapped as having changed vegetation class from 1969-2012 actually experienced a change. Within the areas of change, transitions from one vegetation class to another were captured with variable accuracy, ranging from only 14% for the uncommon sparse-shrub transition, to 93% accuracy for the conifer to dense meadow transition.

Year	Conifer	Shrub	Sparse	Dense	Overall
1969	0.97	0.88	0.80	0.90	0.94
1988	0.96	0.87	0.77	0.80	0.92
1997	0.91	0.91	0.88	0.80	0.90
2005	0.95	0.89	0.94	1.00	0.92
2012	0.89	0.94	0.78	0.90	0.87

Table 3.1: The accuracy (proportion of the vegetation map that is classified correctly) of our vegetation maps varies between years and vegetation classes.

Common classification errors included bare ground being classified as conifers, due to shadows being mis-classified as trees by the eCognition algorithm. The eCognition algorithms

also sometimes had difficulty differentiating between shrubs and trees. Other sources of error include low camera angles in parts of some images, which impairs detection of edges, particularly at forest boundaries, and can result in trees obscuring small meadow or rock features. It should also be noted that the rigor of the accuracy assessments was not constant across the maps: For the 2012 map, actual ground reference points were included in the accuracy assessment in addition to manually classified points from the aerial photograph. This is likely why the 2012 map accuracy is slightly lower than that of the other maps.

Varying Resolutions

We calculated patch-level and landscape-level indices at resolutions from 5m to 500m. None of the indices changed significantly with scale, except for a few individual values at the 500m level. At all scales, the trend of each metric over time remains the same. This scale-independence gives us high confidence that these indices accurately represent changes in the vegetation structure, rather than being an artifact of the mapping process. Because of these results, we did not deem it necessary to present results from various spatial resolutions. Therefore, all further results in this paper are calculated from maps at 5m resolution. The supplementary material gives examples of some of these calculations (Table A.4).

Identifying Landscape Change

FRAGSTAT operates on planar area, which can be problematic in highly sloping regions. Correcting total vegetation areas to account for surface slope increased total area in the 2012 image by 4% for conifers and sparse meadows, 7% for shrubs (which generally grow in steeper areas), and 1% for dense meadows (generally found on relatively flat ground). While this correction was incorporated into our calculations of total coverage, the differences were not large enough to require modifying FRAGSTAT calculations.

Using landscape metrics offers a quantitative measure of the increased spatial complexity in the ICB. Figure 3.3 shows consistent and parallel increases in both Shannon's and Simpson's evenness indices, and a decrease in the aggregation index (meaning the landscape became more fragmented). We measured a steady increase in both Shannon's Evenness Index (from 0.44 to 0.70) and Simpson's Evenness Index (from 0.42 to 0.73) for the 1969-2012 period. The aggregation index decreases from 95 to 87 over this period, although not monotonically, showing a trend toward more distributed vegetation patches over time.

Patch size generally decreased over time, regardless of vegetation type. The 25th percentile of patch sizes (across all vegetation types) was $75m^2$ in 1969 and $50m^2$ in 2012. The median patch sizes were $875m^2$ in 1969 and $250m^2$ in 2012 (3.5 times smaller).

LPI decreased over time for conifers, but increased for all other vegetation classes (Figure 3.4a). The large 1997 and 2005 sparse meadow LPI values are due to a large burned area that hadn't grown back yet (Figure 3.4c). By 2012, much of this sparse meadow had regrown with shrub or conifers. Area-weighted fractal dimension showed an increasing trend for all vegetation classes, suggesting that the vegetation patches are adopting an increasingly

(a)

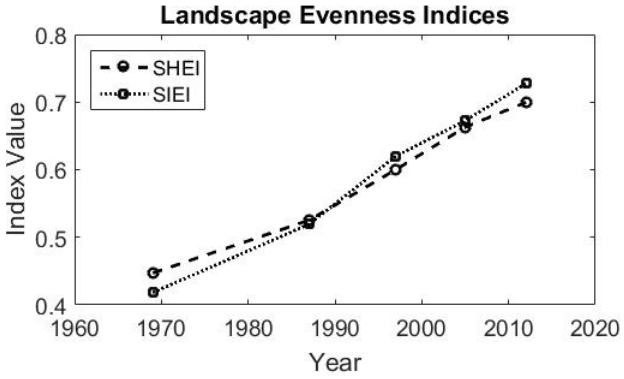

(b)

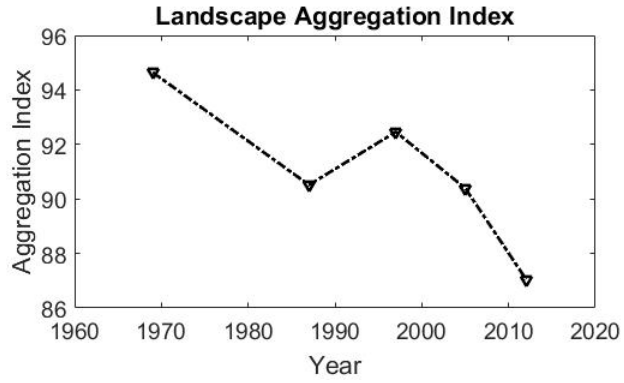

Figure 3.3: (a) The landscape-scale indices Shannon Evenness Index (SHEI) and Simpson's Evenness Index (SIEI) both increase over time, indicating an increase in landscape heterogeneity. (b) The landscape aggregation index has a downward trend over time which also is a measure of increasing heterogeneity.

complex suite of geometries (Figure 3.4b). The fractal dimension increased even during the fire-free period of 2005-2012, suggesting that regeneration processes as well as fire contribute to increasing vegetation patch shape complexity. Data from 1997 are omitted from Figure 3.4b. When initially calculated, the 1997 image had an anomalously low fractal dimension. This image was partially classified using the Yosemite Vegetation Map to compensate for low aerial imagery quality, and we interpret the low fractal dimension as arising from the relatively coarse resolution of the 1997 NPS map.

3.4 Discussion

These results suggest that the re-introduction of fire to the ICB through the managed wildfire regime has increased landscape heterogeneity and complexity, primarily by fragmenting and

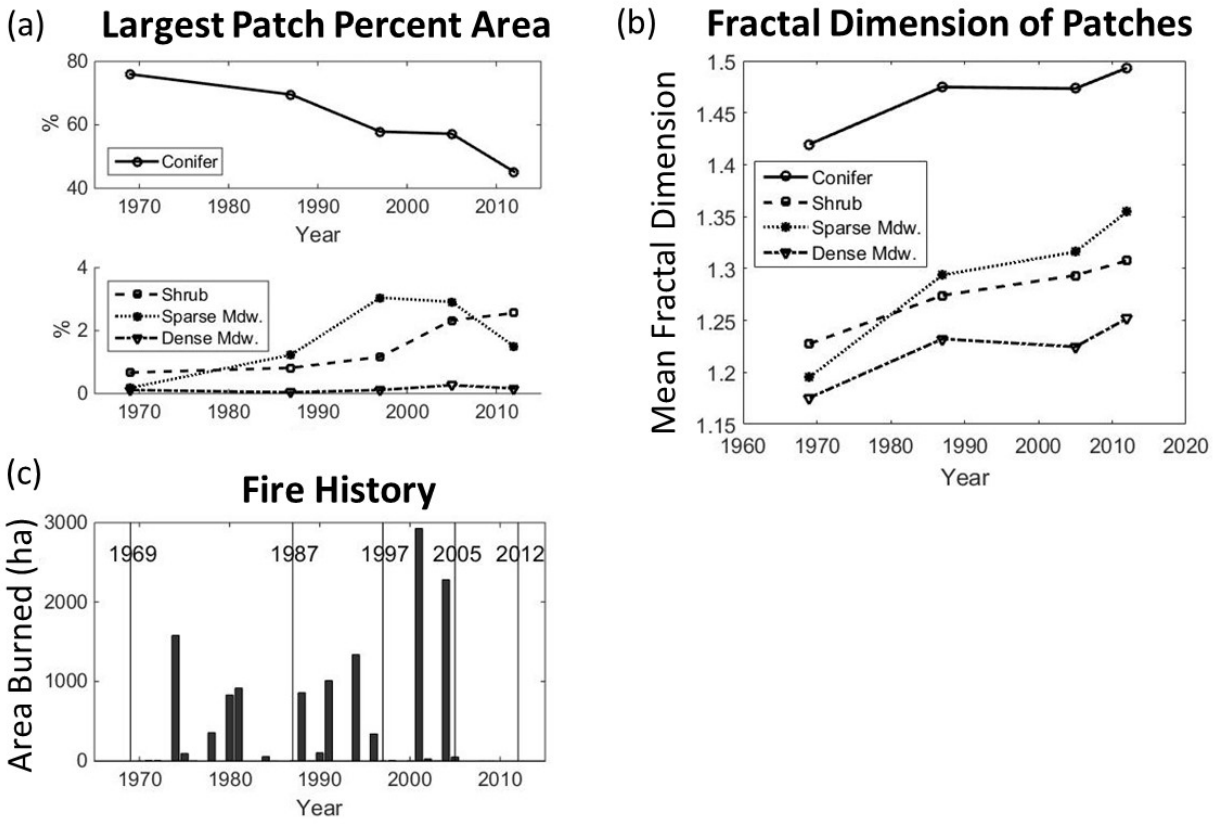

Figure 3.4: (a) The percent of the vegetated landscape covered by the largest patch of each vegetation type. Conifer is shown separately from the other vegetation types because of the difference in scales of the patch sizes. (b) Area weighted fractal dimension of the patches within each vegetation category. (c) Total area (ha) burned each year (bars) in the context of years mapped (vertical lines).

reducing the area covered by conifer forest. All measures of heterogeneity, both landscape metrics and patch metrics, showed that heterogeneity increased from 1969 to 2012. Although landscape metrics can be challenging to directly relate to ecological outcomes, and only reflect selected kinds of landscape change (Li and Wu, 2004), the trends in landscape metrics that we have identified in the ICB appear to be both informative and robust: Multiple metrics point towards the same trend of increased heterogeneity and complexity, the metrics were independent of the resolution of the datasets used for their computation, and the metrics we used have been independently shown to be ecologically relevant across many landscapes. Furthermore, our results are consistent with recent field studies which have identified high levels of landscape heterogeneity in the ICB (Collins et al., 2016).

A range of ecological consequences may be expected to follow from the increased landscape complexity in the ICB. From literature, and from awareness of the requirements of

many plant species in the ICB (e.g. species dependent on open areas or on recruitment under shrub canopies), we would anticipate increases in biodiversity from the reestablishment of fire regimes (Bird et al., 2008; Seiferling et al., 2014). There is some evidence of such increases occurring in ICB. Pollinator diversity in ICB is positively correlated with diversity in understory vegetation and fire history (Ponisio et al., 2016). Understory vegetation richness and total understory cover in the ICB are slightly elevated in open areas compared to dense forests, on average (Wilkin, 2016). We also anticipate that increased fragmentation and reduced patch sizes in the landscape would decrease connectivity of available fuels (Miller and Urban, 2000a), reducing the risk of extreme fire in the ICB. Indeed, Collins et al. (2009) found many areas of self-limiting fires within the ICB. The reduction in connectivity of conifer area, however, may be partially offset by increases in shrub patch sizes, since dense shrublands propagate fire relatively easily.

Finally, there is scope for the landscape-level changes to have hydrologic relevance. Our maps show a decrease in forested area of more than 20%, which has been shown to be a large enough effect to cause measurable streamflow changes in many other watersheds (Brown et al., 2005; Wine and Cadol, 2016). Dense forests are likely to have the greatest water use of the vegetation types in the ICB (Goulden and Bales, 2014), meaning that reduction in forest cover likely translates to reduced overall loss of water through transpiration. In addition, replacement of dense forests with sparser forest cover, shrubs, and open areas may increase snow retention and reduce water loss from canopy evaporation and sublimation (Grant et al., 2013; Lundquist et al., 2013). Potentially, managed wildfire could therefore provide a forest management approach consistent with contemporary interest in supporting streamflow yields from Sierra Nevada watersheds and reducing drought stress in forests (Boisramé et al., 2016; Grant et al., 2013).

The use of aerial photography for mapping vegetation change was effective, but was also time consuming and required finding and purchasing imagery from multiple sources. Since landscape analysis results were similar at 30m and 5m scales, it might be reasonable to rely on the 30m resolution of recent Landsat imagery to describe changes in landscape patterns from fire, as long as the imagery can be classified accurately.

Our accuracy assessment suggested that individual maps had high accuracy, but classification errors arose when mapping specific transitions over time from one land cover class to another. Despite classification errors, the most common transitions were clearly from mixed conifer to either shrub or sparse meadow. These observed transitions are consistent with the known biology of the dominant species in the ICB. For instance, the dominant shrub species (*Ceanothus cordulatus*) establishes quickly in disturbed areas thanks to its ability to propagate both via seed and re-sprouting (www.fs.fed.us/database/feis/plants/shrub/ceacor/all.html#81), and sparse meadow conditions are likely to prevail during the period required for tree establishement after fire if conditions are not favorable to fast grass or forb recruitment. Wildfires are known to affect the establishment and maintenance of mountain meadows, although most work focuses on forest encroachment on meadows rather than creation of new meadows in previously forested areas (Helms and Ratliff, 1987; Ratliff, 1985). We observed some wetland encroachment during our study period, which is likely associated

with the fire-intolerant *Pinus contorta* which grows in a variety of moisture conditions and commonly encroaches on meadows (Helms and Ratliff, 1987). Removing conifer trees with fire or other means can also restore aspen stands (Jones et al., 2005). Although we could not positively identify tree type in the black and white photos, our field observations show that at least one of the large aspen stands mapped in 2012 grew following high severity fire in a conifer-dominated forest.

There may be complex interactions between the land cover classes that our large-scale analysis cannot capture. For example, *Pinus jeffreyi*, *Abies magnifica*, and *Abies concolor* have been shown to have higher post-fire seedling survival rates in *Ceanothus*-dominated patches compared to bare patches (Zald et al., 2008). Fires are also likely causing changes in species composition that could not be captured by our maps. For example, the fir (*Abies*) species and *Pinus jeffreyi* in the ICB are more fire tolerant and generally grow in relatively dry soil (Fites-Kaufman et al., 2007; Fowells, 1965), while *Pinus contorta* is fire-intolerant but readily grows in open areas following fire (Helms and Ratliff, 1987; Stuart and Sawyer, 2001). These species would be expected to fill different niches in a landscape with frequent fire.

All computed landscape-level metrics showed clear trends, rather than appearing to saturate or approach anything resembling a dynamic equilibrium, suggesting that the restored fire regime has not yet returned the ICB landscape to a state of "natural variability" in which the landscape structure remains within a range set by natural habitat and disturbance conditions rather than human intervention (Swanson et al., 1994). Model predictions suggest that restoration of similar landscapes having experienced a century of fire suppression could take over 200 years (Miller and Urban, 2000b), without factoring in the complications implied by non-stationary climate. The landscape of the ICB today conforms to the description of historical Western US forests given by Hessburg et al. (2015): a patchwork of small ($<$ 100ha) to large (1,000-10,000ha) patches of vegetation including forest, shrubland, grassland, bare ground, and dead trees, suggesting that the current landscape is beginning to approximate the conditions that prevailed before fire suppression. There are few guidelines available to assist with the restoration of landscape-scale heterogeneity to fire suppressed forests (Collins et al., 2016). The analyses presented here provide an important resource: a detailed description of the heterogeneity caused by a natural fire regime in the Sierra Nevada, and thus an approximation for landscape-level targets for alternative management regimes, or guidance as to what could be expected if managed wildfire were introduced into other Sierran forests.

3.5 Conclusion

The alleviation of fire suppression in the ICB reintroduced an agent of change to a landscape which had been artificially protected for nearly 100 years. Landscape metrics do not appear to have stabilized or peaked yet, suggesting that the landscape is still recovering from the history of fire suppression. While we would expect the landscape to ultimately come into a dynamical equilibrium set by the fire regime and local climate, in which individual points

on the landscape may change but the landscape composition and patch characteristics are approximately stationary (or vary within a natural envelope), the ICB does not yet appear to have reached such a state. While it is unclear what the end point of the managed wildfire regime is likely to be in terms of landscape composition, especially in light of climate non-stationarity, it is clear that frequent, mixed severity wildfires in the ICB reintroduced heterogeneity to the landscape and increased the amount of non-forest land cover.

Clearly, there are many potential benefits to adopting wildland fire use. There are nearly 10,000km^2 of wilderness area in the Sierra Nevada within the same climate zone as ICB, where wildland fire use could likely be implemented safely and successfully (Boisramé et al., 2016). Despite the long timescales that might be required to restore forests to a relatively stable natural state, forty years of change were clearly sufficient to impose changes that could increase biodiversity, reduce plant water consumption, decrease the risks of extreme fire and enhance the resilience of forests.

Co-author acknowledgement: Some of the text in this chapter was provided by Sally Thompson, Maggi Kelly, and Julia Cavalli as part of a manuscript being prepared for publication.

Chapter 4

Relating Soil Moisture to Vegetation Cover and Fire History

This chapter covers my use of field measurements to relate soil moisture to vegetation cover within the ICB at different times of year. These field measurements informed a statistical model which inferred changes in soil moisture caused by the ICB's restored fire regime using vegetation maps of the watershed's fire-suppressed state and current state (described in Chapter 3).

4.1 Introduction

Subsurface water stores are necessary for sustaining vegetation growth and dry season streamflow. The factors that control this water store are hypothesized to respond to long term changes in vegetation structure associated with altered fire regimes. These responses can vary in spatial and temporal scale, and can potentially result in either increased or decreased net storage, depending on which processes dominate. For example, the replacement of dense forests with non-forest vegetation (particularly grasslands, wetlands or forbs) via stand-replacing fires is likely to result in reduced watershed-scale transpiration and interception, thereby increasing soil water storage (Brown et al., 2005; He et al., 2013; Zhang et al., 2001, e.g.), but stand-replacing fires can also result in higher soil evaporation rates due to increased solar radiation incident on the ground, or lower infiltration rates due to reduced litter cover and/or soil water repellency following fire, all of which would reduce soil water storage (Helvey, 1980; Lane et al., 2010; Neary et al., 2005).

Fire effects on soil moisture may also vary depending on the time and season. Regrowth following a fire can lead to a high water demand by dense, fast-growing vegetation and therefore decrease soil moisture storage to levels below those from pre-fire conditions (Lane et al., 2010; Neary et al., 2005; Tague and Dugger, 2010). This increase in water demand due to regrowth is not observed everywhere, even in experiments involving the same tree species (e.g. Lane et al. (2010) and Webb and Jarrett (2013)). Snowpack is an important

water source that can be greatly affected by fire-related changes. The increased temperature of blackened trees and reduced shading in burned areas have the potential to cause higher melting and sublimation rates of snowpack (Neary et al., 2005; Tague and Dugger, 2010), thus reducing water available for soil storage. Conversely, thinning a forest by creating gaps (as happens in moderate severity fires) can lead to greater snow accumulation and a longer snowmelt period compared to dense forests (Ellis et al., 2013), coupled with reduced transpiration demand, thus increasing soil water availability. Different plant water use profiles, rooting depths and canopy structures in turn alter micrometeorological conditions below ground and beneath the canopy and change the local water balance (Brown et al., 2005; Ma et al., 2010; Rambo and North, 2009; Zhang et al., 2001). More details on the interactions between fire, vegetation cover, and hydrology are given in Chapter 1.

Much of the existing work on fire's effects on the water balance focus on large individual fires (Brown et al., 2005; Helvey, 1980, e.g.). For a frequently burned watershed such as Illilouette Creek Basin (ICB), net long term changes in water storage might be different than those seen after isolated, large disturbances. Simple models of fire in mediterranean ecosystems show that feedbacks could lead to higher average soil moisture under a frequent fire regime compared to fire suppressed conditions (Ursino and Rulli, 2011). Such increases could even be part of a feedback loop that helps reduce the severity of future fires by increasing fuel moisture (Miller and Urban, 2000a).

There are few opportunities to test the hypothesis that a frequent fire regime will increase soil water storage relative to a low fire-frequency situation. Watersheds with frequent fire regimes are rare, and we do not know of any with long term monitoring of groundwater or soil moisture. Even if such long term monitoring did exist, quantifying subsurface water storage (especially at the watershed scale) always involves high levels of uncertainty. This leaves few options, then, for field-testing the hypothesis that a frequent fire regime increases subsurface water storage.

The Illilouette Creek Basin (ICB) provides a valuable field site in which to study fire-regime effects on water storage. Its wilderness status means that soil and surface hydrology are relatively undisturbed by humans. There are tradeoffs, however: portions of this basin are not easily accessible for measurement, and wilderness regulations limit the amount of soil disturbance that is allowed for research purposes (U.S. Congress, 1964).

One option would be to use soil wetness indices from remote sensing to track moisture changes over time under a changing fire regime (Musick and Pelletier, 1988). However, soil moisture condition cannot be captured via remote sensing in areas with dense vegetation cover (Crist and Cicone, 1984). Instead of relying on remote sensing, we chose to take manual measurements of surface soil moisture, allowing us to capture soil moisture under any vegetation canopy.

Shallow soils can be readily accessed and measured without extensive soil disturbance; even though surface soil moisture cannot be directly extrapolated to full subsurface storage, it has been found to be closely related to water table depth (Sörensen et al., 2006). Vegetation maps have successfully been used to estimate spatial distributions of soil moisture in the past (Milledge et al., 2013). The type of vegetation growing at a location frequently indicates

the presence of hydrological conditions that favors that vegetation type (e.g. Araya et al., 2011; Milledge et al., 2013; Mountford and Chapman, 1993). For example, *Pinus contorta* establishes in intermediately wet areas of meadows (Helms and Ratliff, 1987), and *Ceanothus cordulatus* is able to grow in harsh, dry sites (Fites-Kaufman et al., 2007). Within the ICB, Kane et al. (2015) found relationships between water balance and forest structure, further suggesting that vegetation observations can be related to water availability. We should, therefore, be able to use maps of vegetation changes over time to infer changes in soil moisture over time, as long as we have a clear relationship between vegetation and moisture.

We can strengthen our understanding of soil moisture variation by including topographic variables as well as vegetation. Topographic variables have also frequently been used to estimate soil moisture, especially the topographic wetness index, which combines information on the slope and upslope contributing area of a given location (Sörensen et al., 2006). Topographic wetness index, however, can be less effective at predicting soil moisture during dry periods, and cannot be relied on as a fully predictive measure of moisture (Western et al., 1999).

The study presented here aims to determine the long term soil water storage changes that have resulted from restoring the fire regime of the ICB. In order to do this, I upscaled field measurements to the entire watershed using variables related to vegetation type, fire history, and topography.

All of the field observations in this thesis are from drought years, meaning that we do not have clear views of the soil moisture regimes under a typical year (precipitation during the winter of 2015/2016 was near-normal, however), and have no observations from a wet year. Understanding soil moisture during drought years, however, is disproportionately important since drought years are when landscapes are likely to be water limited and therefore even small increases in water retention can have a big impact.

These field observations were also all taken at least nine years after the most recent fire. This means that the measurements do not represent short-term post-fire effects of fires on soil moisture such as water repellency of soil or depletion due to rapid vegetation regrowth in the first few years following fires.

This study asks the following questions:

- Is surface soil moisture a useful indicator of ecologically-relevant water storage?
- Is vegetation a useful indicator of surface soil moisture values, and is this relationship stable from year to year?
- How has changing the fire regime in the ICB altered soil moisture at the watershed scale and at smaller, vegetation stand scales?

4.2 Methods

Field Measurements

Surface soil moisture was extensively mapped in ICB in the summers of 2014-2016. Over 6000 measurements were made in 90 sites. These sites were selected to cover representative conditions including: burn severity, time since fire, soil type, slope, aspect, elevation, and vegetation cover, and to capture as many combinations of different conditions as possible (Figure 4.1, Table C.1).

Each site was measured between one and six separate times over the three year study, capturing both early and late summer moisture when possible. This time period falls within a drought in California which has seen not only low precipitation but also historically high temperatures (Dettinger and Anderson, 2015; Griffin and Anchukaitis, 2014).

Measurements were made with a 12cm time-domain reflectomer (TDR) Hydrosense II probe (Campbell Scientific, 2015). All measurements were recorded in terms of volumetric water content (VWC). The VWC is the proportion of the total volume of the soil matrix that consists of water, ranging from 0 for completely dry soils to ≈ 0.6 for saturated, highly porous soils (pure water would have a VWC of 1).

For most plots we took 30 soil moisture measurements within a 30m by 30m grid. If initial observations showed the site to be highly homogeneous in both vegetation cover and moisture, this number was reduced to 25 measurements. Occasionally extra measurements were added between grid points to capture the variability of highly heterogeneous areas. When an obvious gradient in soil moisture was present, such as in many wetland sites which were bordered by dryer uplands, a transect of at least 30m in length was used instead of a grid (still with $\geq$30 measurements), in order to ensure that the gradient was captured. At each plot, we noted dominant vegetation cover (to species level when possible), slope, aspect, and the presence of burned snags or fire scarred trees. We also recorded either the corners of the plot grid or the ends of the transect using a Garmin GPS. Latitude and longitude were assigned to each measurement point based on its location within the grid or transect.

Thirty-seven measurement plots were selected from previously identified plots used by the UC Berkeley Stephens Lab (Collins et al., 2016). Forty-nine new plots were selected to capture combinations of slope, aspect, burn severity, and vegetation cover that did not exist in the pre-existing plots. These new plots were either selected randomly using arcGIS (while staying within reasonable access of trails) or selected opportunistically once in the field. In total, 90 different plots were measured at least once. Fifty five plots were measured at least twice, 27 plots were measured at least four times, and seven plots were measured six times. Decisions about the selection of plots to be measured were based on prioritizing those sites which would provide the most information and cover the most variable set of conditions, given time constraints. For example, some of the plots that were extremely dry when measured in June were not re-sampled in later summer trips, under the assumption that the soil would still be very dry.

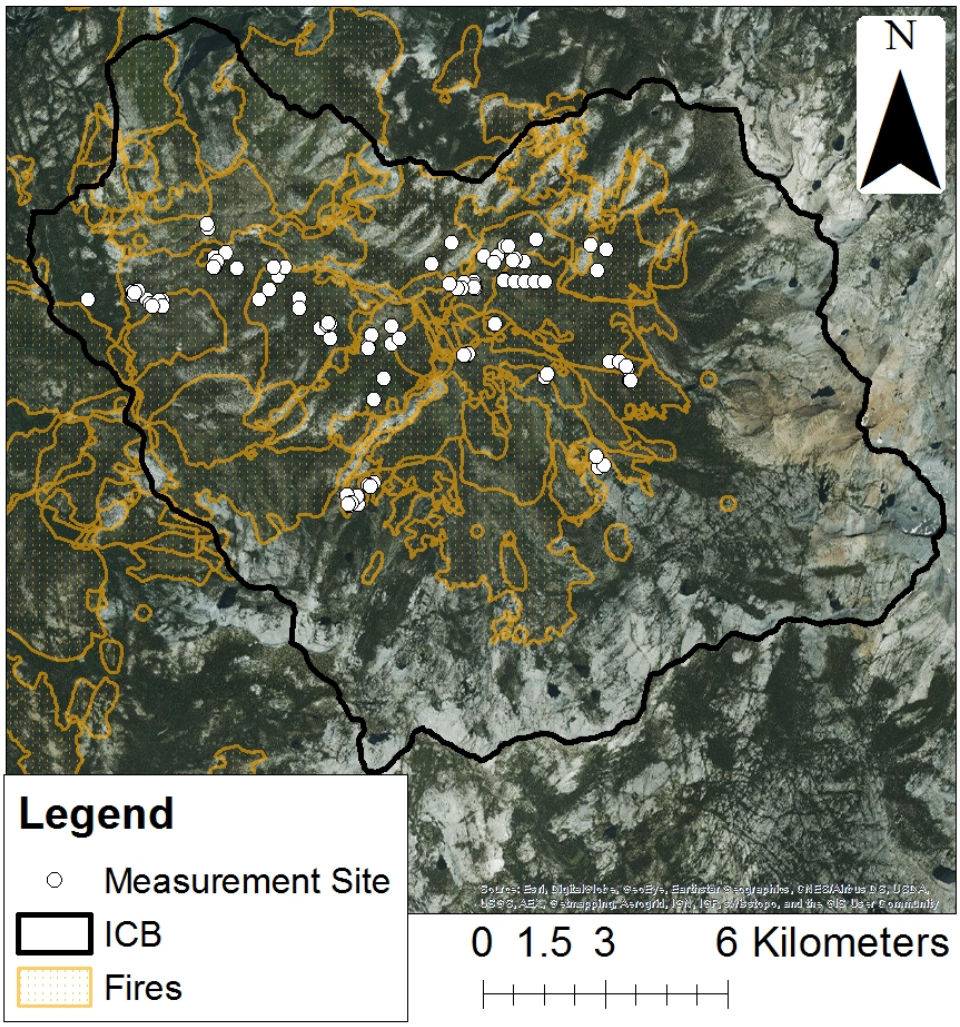

Figure 4.1: Locations of soil moisture measurement sites and perimeters of all fires since 1970. Imagery source: Esri.

Relating surface and root-zone soil moisture

We verified that summer soil moisture was correlated with root zone soil moisture with two independent methods. In the first method, we took pre-dawn and mid-day leaf water potential measurements and correlated the water potentials with surface soil moisture. In the second method we compared continuously-monitored soil moisture at depths of up to one meter to shallow soil moisture in three sites.

Pre-dawn measurements of leaf water potential are widely used as a proxy for root-zone averaged soil moisture, under the assumption that plants have reached hydraulic equilibrium with soil water potential overnight when transpiration was halted (Bréda et al., 1995; Dawson et al., 2007). More negative predawn leaf water potentials are associated with drier soils. Midday leaf water potentials represent a combination of transpiration and soil moisture conditions. We measured leaf water potential using a model 1505D pressure chamber from PMS instrument company (http://www.pmsinstrument.com/). This measurement involves cutting a healthy stem from a plant, placing the leaf end inside a sealed vacuum chamber, and then slowly adding pressure from a compressed Nitrogen gas cylinder until water begins to seep out of the cut end of the stem. The pressure required to force water out of the stem is assumed to be equal in magnitude and opposite in sign to the water potential inside the stem.

We measured different species in different locations throughout the watershed and compared these measurements to measured surface soil moisture. Each time we performed these measurements, we chose one site within a riparian zone, so we could use the riparian plants' leaf water potential as a reference value for non water-stressed plants. The species measured were whitethorn ceanothus (*Ceanothus cordulatus*), willow (multiple unidentified *Salix* species), lodgepole pine (*Pinus contorta*), Jeffrey pine (*Pinus jeffreyi*), and aspen (*Populus tremuloides*). At each location and each measurement time we collected samples from at least three different individuals of each species present. Not all measurement locations had members of all species present, and in some spring measurements we could not measure deciduous species (willow and aspen) because they had not yet grown leaves. We collected these samples from the same height and the same side (e.g. north or south) on each plant within each site. The conifer species often had sap leak out of the stem before the first water drops, which made identifying the initial water drops' appearance difficult.

In three locations located within 200m of each other, soil moisture probes were buried horizontally at approximately 12cm, 60cm, and 1m beneath the soil surface (12cm Campbell Scientific Soil Water Content Reflectometers, TDRs, www.campbellsci.com/cs655). We dug a hole to the maximum depth, inserted the probes horizontally into undisturbed soil at the desired depth, and then refilled the hole with the same soil, compacting the soil as the hole was refilled. Exact depths at each location varied depending on ability to dig deep enough and in one case reaching the water table before 1m, and these exact depths were recorded. These TDR probes recorded soil moisture every 10 minutes beginning July 2015. We routinely measured surface soil moisture near the buried TDRs with a handheld TDR to verify that the 12cm buried probe was recording values similar to the values recorded by

the handheld TDR, to compare the responses of the in-situ TDR and the mobile TDR used for the majority of field measurements. We expected some differences between the two due to different measurement domains - an average over the top 12cm for the handheld TDR, and a horizontal average across soil at 12cm depth for the in situ TDR. See Appendix D for more details on these continuous measurements.

Statistical Analyses

Variability of Soil Moisture in Space and Time

In order to gain an initial understanding of how sensitive VWC was to different spatial variables, VWC was related to each measured location's topography, fire history, and vegetation cover using correlations and a simple linear regressions. Measurements from different years and seasons were also compared in order to determine the variability in VWC at each plot both within years and between different years.

Spatial Data Sources

Field measurements were related to spatial variables using maps of topography, fire history, and vegetation cover created in Arc GIS (www.arcgis.com). The values of individual variables for each measurement point were extracted from these maps using the points' geographic coordinates.

All topographic variables (slope, aspect, etc.) were derived from a LiDAR elevation map of the ICB, coarsened to a resolution of $10m^2$ (Kane et al., 2015). The aspect index is transformed from aspect via the formula $0.5(1 - cos(Aspect - 30))$ where the aspect is the number of degrees from north of the downhill direction at the measurement location. This index moves the aspects that have similar solar radiation to be closer to each other, and avoids the issues of aspects near the minimum and maximum values of 0 and near 360 actually being similar. Topographic Wetness Index (TWI) is calculated using the equation $TWI = ln\frac{a}{tan(s)}$, where a is the upslope contributing area and s is local slope. This equation gives all positive values, with larger numbers more amenable to high moisture and values near zero likely to be dry. Topographic Position Index is calculated using the equation TPI =int$((elev-$focalmean$(elev, annulus, 150, 300)) + .5)$, following Weiss (2001), where $elev$ is the point's elevation in meters and the "focalmean" function as used here takes the mean elevation over a ring surrounding the point with inner diameter of 150m and outer diameter of 300m. The "int" function refers to rounding to the nearest integer. A negative TPI indicates a valley while positive values indicate ridges and a value near zero indicates an area that is neither convex nor concave.

Vegetation types followed the categories available from the classification of historical and contemporary aerial photos in Chapter 3: sparse, dense meadow, shrub, aspen, and conifer. Because *Pinus contorta* was the only conifer species observed growing in areas with relatively high soil moisture during our field visits, the conifer classification was further divided

into "*Pinus contorta*" and "other conifer". Areas mapped as conifer based on aerial photo classification (Chapter 3), and that were identified as *P. contorta* in the Yosemite National Park 1997 vegetation map (available at irma.nps.gov) were classified as *Pinus contorta* in the final maps used for spatial analysis.

Time since fire was calculated using a digital fire atlas consisting of all fire perimeters for which a record exists dating back to 1930 within Yosemite National Park (available from irma.nps.gov/Portal). If there were no fires during this period, years since fire was set to 100. The fire atlases are a best approximation of actual burn perimeters, but do not provide information on the spatial heterogeneity of burning within fire areas (Morgan et al., 2001). We used satellite-based estimates of fire severity developed by Collins et al. (2009) to characterize this heterogeneity within fire areas for all fires over 100 ha since 1972. For fires that occurred in 1984 or later (n = 11) a relative version of the differenced Normalized Burn Ratio (RdNBR) was used, derived from Landsat Thematic Mapper images (Miller and Thode, 2007). Fire severity data for fires prior to 1984 (n = 8) were derived from Landsat MSS images, which only had 4 bands (as compared to 7 bands on the Landsat Thematic Mapper sensor) and had larger pixels (66 m, as compared to 30 m for the later sensor). As a result, fire severity data from fires that occurred between 1972 and 1983 were developed using a relative version of the difference between pre- and post-fire Normalized Difference Vegetation Index (RdNDVI) (Collins et al., 2009; Thode, 2005). Fire severity class (unchanged, low, moderate, high) for each soil moisture measurement site was extracted from the nearest 30-m (or 66-m) resolution raster cell. Thresholds for RdNBR fire severity classes were taken from Miller and Thode (2007). Thresholds for RdNDVI were developed from the RdNBR thresholds because there was insufficient historical field data to calibrate MSS images. Where pre-1984 fire locations had reburned after 1984, we used post-1984 fire severity since it is more accurate and likely to be more relevant to soil moisture conditions measured in 2014-2016.

Modeling Soil Moisture

Soil moisture was related to site condition using a random forest model (Liaw and Wiener, 2015). This model does not include any hydrologic processes explicitly (such as evaporation or rainfall). Instead, it is a regression method which estimates the most likely VWC value for a given set of topographic and fire history variables based on fitted relationships between VWC measurements and the topography and fire history in those measurement locations, the dominant vegetation cover, and date of measurement.

Random forest models predict a continuous variable by creating a large number of regression trees, using a random subset of all possible predictor variables to create each tree, and then averaging the predicted values of all of the trees. Each regression tree works by dividing the data into smaller and smaller groups, or nodes, until a stopping criterion is reached. At each step, the data in one node is divided into two more nodes based on the division in the predictors that maximizes the separation in values between the two nodes. The value of a new point in the variable space is computed by following the path from the first node to the

appropriate terminal node. The random forest method avoids issues of over-fitting that can result from using only one regression tree, and allows for fitting non-linear responses between variables and predictors (Grmping, 2009; Kane et al., 2015).

All data were randomly divided into a training dataset (75% of all data) and a test dataset (25%). Model performance was evaluated using root mean squared error (RMSE) and correlation coefficient.

This random forest model predicts soil moisture (as a continuous value) using current vegetation type, vegetation type in 1969, upslope area, slope, aspect index, elevation, topographic position index (Weiss, 2001), topographic wetness index, distance from nearest stream, year of measurement (2014, 2015, or 2016), day of year the measurement was taken (e.g. 152 for June 1), years since last fire, times burned since 1970, and maximum fire severity as predictor variables. We used the RandomForest package in the R program to fit the model, and set the minimum node size to 5 and the number of trees to 500, the number that minimized the RMSE of the model (Liaw and Wiener, 2015).

The measurement year variable was used to indirectly account for different weather conditions in each year. For example, 2015 had three times more summer precipitation than the other two years (120mm in May-September, Yosemite Southern Entrance Station, www.ncdc.noaa.gov), while 2016 had the most winter precipitation (890mm in the winter of 2015/2016 compared to <400mm the previous two winters). Rather than accounting for weather explicitly, we included "year" as a random effect in the model, meaning that it is assumed that VWC can respond to predictors differently in each year for reasons independent of the other explanatory variables in the model (Clark, 2007). The model accounts for there being unknown differences between years when finding the best fit to the data. In this specific case, when running the random forest model for prediction, changing the "year" variable should make the modeled soil moisture reflect the weather and other unknown effects particular to that year.

Model Simulations

Once the random forest model was trained to field measurements of VWC, I used the model to upscale soil moisture measurements to the whole basin. Using maps of topographic variables, fire history, and vegetation described earlier, I estimated soil moisture at thousands of points on a fine grid over the whole watershed. For each model run, I had to assign a date to the simulation since day of year and year are included in the predictor variables. Beyond extrapolating measured values to the whole watershed, this random forest model was also used to explore hypothetical scenarios. For example, I simulated what basin-scale soil moisture would have been like in 2015 if fire suppression was still in effect by setting the simulation date to August 2015 but using the 1969 vegetation map for the current vegetation type, setting time since fire to 100 years (because the random forest model behaves nonlinearly, the exact number of years used for unburned sites is not important as long as it is significantly larger than the time since our earliest mapped fire in 1974), and setting both times burned and maximum severity to zero.

4.3 Results

Field Measurements

Relationship between VWC and vegetation type

In ICB, we found that vegetation type was closely associated with the summer surface soil moisture content, as shown in Figure 4.2. Dense meadows had the highest median VWC throughout the summer (0.33 in May to 0.14 in August). At the beginning of the summer, conifers had the next-highest median VWC (0.15), but were comparable with other dry vegetation by the end of summer, at 0.04 VWC. Shrublands and sparse meadows had comparable soil moisture values at the beginning of summer (0.11 and 0.12, respectively), but the meadows exhibited a more rapid dry down, dropping to 0.03 median VWC by June while shrubs only dropped to 0.05.

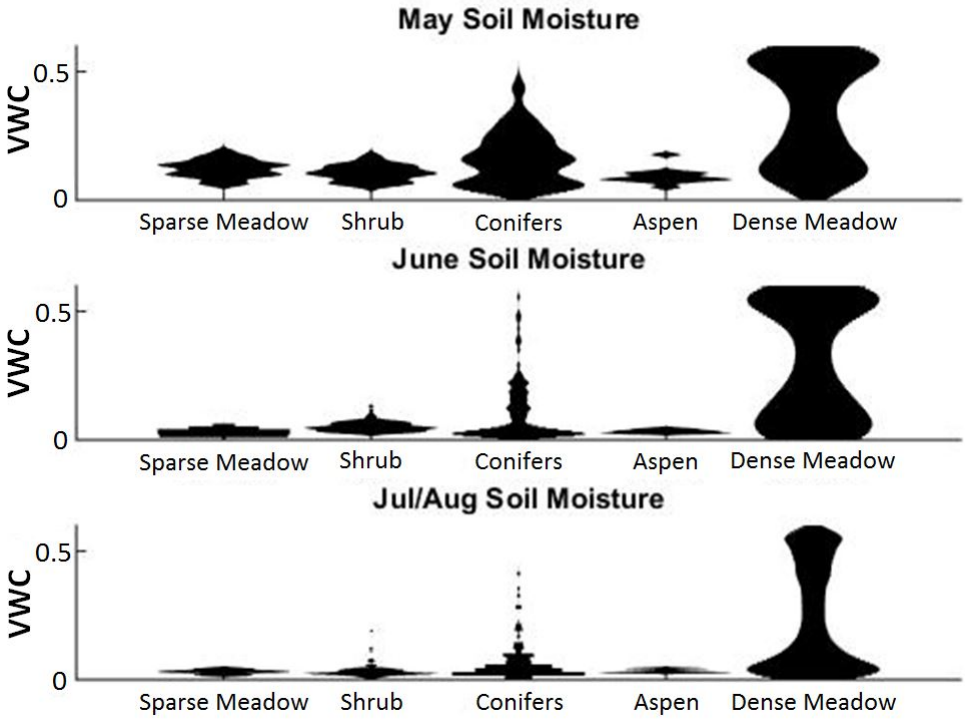

Figure 4.2: Plots of the distribution of soil moisture under each vegetation class for the same measurement locations in May, June, and July/August for 2014 and 2015. The results are divided between locations dominated by sparsely vegetated meadows, shrubs, conifers, aspen, and dense meadows. Soil moisture is given as the volumetric water content (VWC). The width of the shape for each category is proportional to the number of observations at that VWC value.

The areas which consistently had the highest VWC were persistent wet meadows - areas

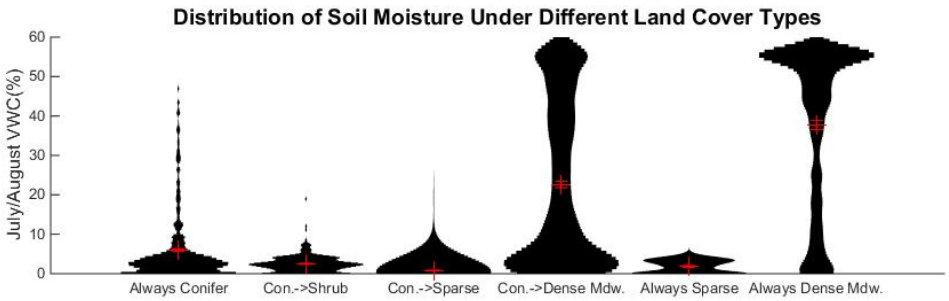

Figure 4.3: Violin plots of the distribution of soil moisture measurements from June and July of all three summers. The results are divided into the following categories: always conifer (conifer cover in both 1969 and 2012), burned conifer forests replaced by shrub, sparse meadow, or dense meadow, and sites that were sparse meadow in both 1969 and 2012 or dense meadow in both years. Soil moisture is given as the volumetric water content (VWC). The width of the shape for each category is proportional to the number of observations at that VWC value. Red crosses show the mean and standard error within each vegetation category.

that were mapped as wet meadow from the 1969 aerial photographs and continued to be identified as such in all subsequent mappings using more recent aerial photos (Figure 4.3). Sites which had been conifer forest in 1969 and subsequently burned and transitioned to dense meadow by 2012 were the next wettest category. Other conifer sites, or sites that were conifer forest in 1969 but transitioned to other vegetation classes by 2012, were uniformly drier. Even in late summer, clear differences between dense meadows (either persistent or recently formed) and all other locations are clear (Figure 4.3). Different vegetation classes had different mean VWC values, but there was also a large amount of variability within each vegetation class. In order to capture this within-class variability, in Figures 4.2 and 4.3 the data are presented as violin plots which show the distributions of the data in each category, especially pointing out the long tail of distribution for conifer plots and the bimodal nature of the dense meadow measurements (most measurements are either very wet or very dry, with few points in the middle).

Wet Meadow Persistence

Some wet meadows stayed saturated throughout the summer, while others dried dramatically. Within persistent meadows (those that were meadows from 1969 through 2012), we did not find a clear predictor for which meadows stayed saturated and which dried. The individual meadows' late summer moisture appeared independent of predictors such as upslope area or fire history.

Of the twelve wet meadows with repeat measurements, two were significantly wetter in late summer of 2016 compared to 2015, and two were significantly drier. The remaining did

not show a difference in late summer soil moisture between the two years.

Relationship between surface measurements and root zone soil moisture

These observed patterns in soil moisture appear to be indicative of the state of deeper sources of plant-available water. Predawn water potentials show that surface soil moisture is correlated with root zone soil moisture, although there is a fair amount of variability in this trend (Figure 4.4A).

Our measurements of the top 12cm of soil using manual TDRs closely matched the values measured by the 12cm deep horizontal TDRs.

When digging to install the continuously-monitoring TDRs, we found the soil to be at least 90cm deep in all three sites. The soil texture varied slightly both between sites and with depth, but was generally loamy sand (Appendix D). Within each weather station, correlation between daily VWC at 12cm and at 90-100cm ranged from 0.69 for the closed canopy site to 0.77 for the shrub site. Correlation between shallow and deep daily VWC for all measurements from all stations was 0.87. Excluding winter months (October-April) raised this correlation to 0.96. Daily VWC at the shallowest and deepest TDRs is shown in figure 4.4B.

Model Accuracy and Upscaling

The random forest model predicted the observed soil moisture values with an RMSE of 0.08 and coefficient of determination (r^2) of 0.91. This fit is very high compared to simple regression models used to predict soil moisture in other studies (Western et al., 1999, e.g.). The model accounted for 81% of the observed variation, and generally has low errors (Figure 4.5A). Vegetation was the most important predictor of water content (Figure 4.5B). The model shows realistic patterns of moisture across the landscape, even in areas outside of the portion of the watershed where we were able to take measurements (Figure 4.6).

Relationship Between VWC and Landscape Parameters

Although VWC was not strongly correlated with any individual parameter, there were clear responses to most predictor variables after controlling for the effects of other variables. Figures 4.7 and 4.8 show the partial dependence of the random forest model on different topography and fire history variables. The partial dependence is calculated by taking the average of all VWC values across all possible values for each of the variables except for one variable which is held constant. The model captures the fact that soil moisture is more likely to be high at low slopes and low topographic position index, indicative of valley bottoms (Figure 4.7B and F). There is a large jump in mean VWC around a topographic wetness index of 5 (Figure 4.7E). Locations that are unburned or burned at low severity are more likely to have high VWC (Figure 4.8).

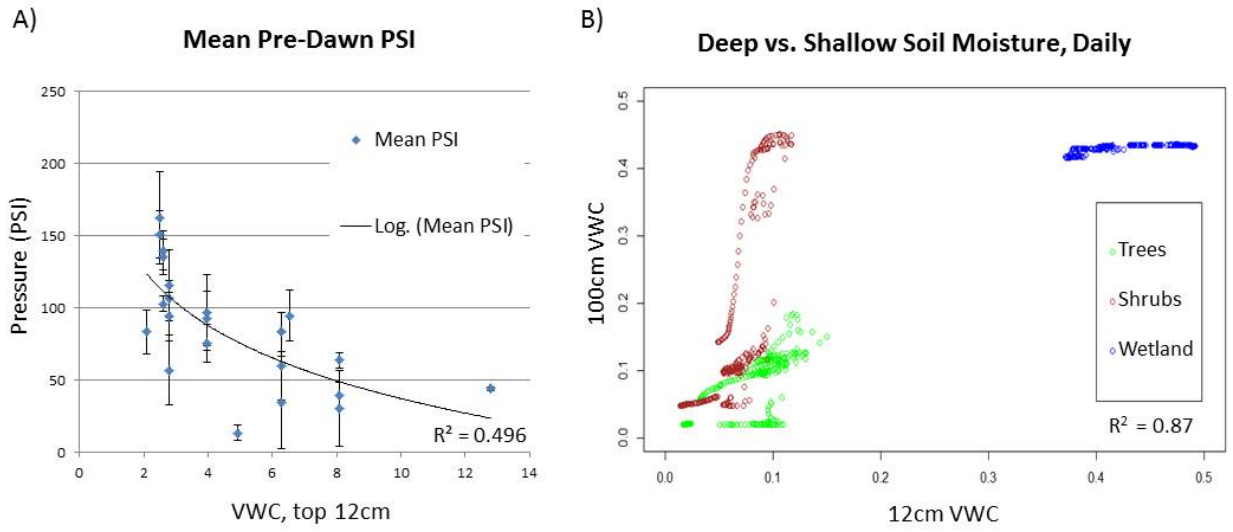

Figure 4.4: (A) A negative trend between surface soil VWC and the absolute value of pre-dawn leaf water potential suggests that when surface soil moisture is low the root zone also has low moisture (and therefore a more negative water potential). (B) On most days, shallow and deep daily measurements of VWC are closely related (all measurements are shown here, but removing winter soil moisture provides an even more robust correlation).

When using a simple linear regression, the sign of the coefficient on each variable matches the sign of the slope of these partial dependencies, except for aspect and time since fire. In the linear regression, TPI, slope, and vegetation types in both 1969 and 2012 were the most significant predictors of measured VWC ($p<0.00001$). The linear regression, however, only had an r^2 of 0.43, much lower than the random forest fit (although within the range of r^2 values achieved via regression models of soil moisture in Western et al. (1999)).

Year to Year Variation and Seasonal Trends

Although the general relationships between sites remained constant over all years, there was some variation in individual sites from year to year (Figure 4.9). Some wetland meadows, such as Mono Meadows, were always saturated through June but became unsaturated by the end of summer. Some spring-fed areas had roughly constant soil moisture throughout the summer, but most sites had lower soil moisture in July than in June. For most sites, 2014 had the lowest soil moisture.

The year to year variability had low importance in the random forest model (Figure 4.5B), but there was an effect nonetheless, with mean VWC being 0.01 higher in 2016 compared to 2014 on average, independent of all other variables (Figure 4.10A).

A

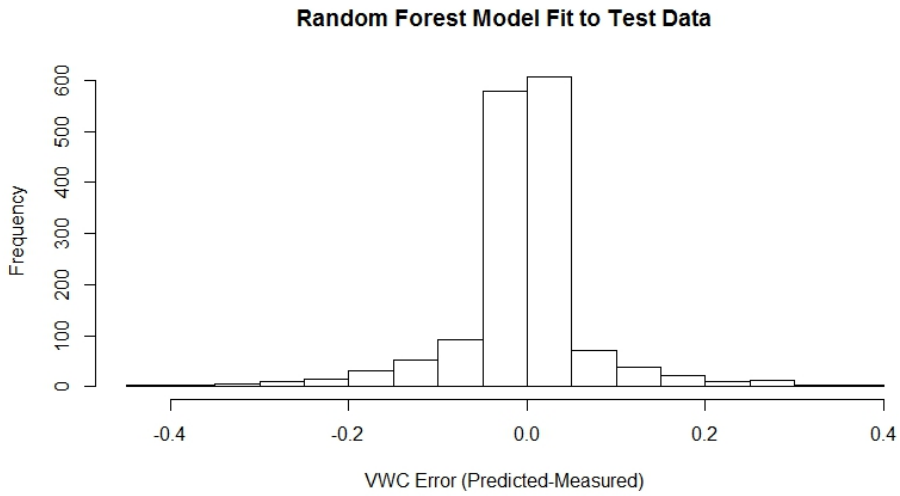

B

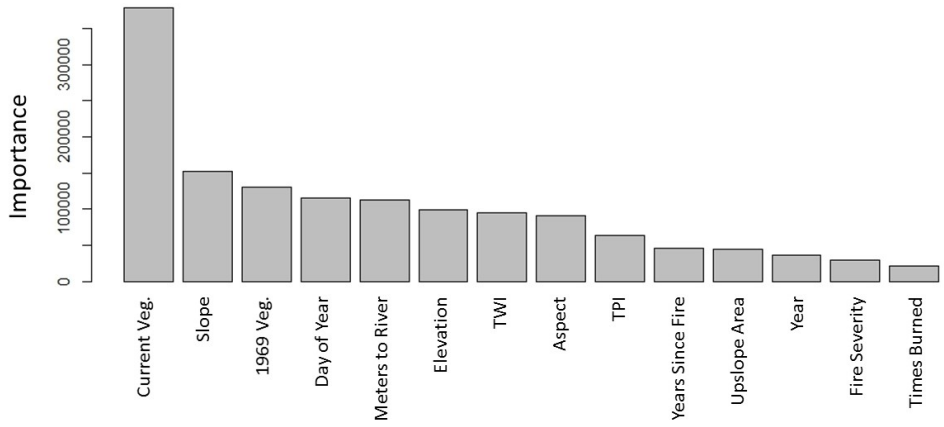

Figure 4.5: A: Histogram of individual errors in modeling the test dataset showing that most predicted VWC values are within 0.05 of the true value. B: The relative importance of each input variable to the random forest model (importance is related to the reduction in error when that variable is included). The variable with the highest importance is the current dominant vegetation. The next most important variables is slope, and the values of local slope, vegetation cover in 1969, day of year, distance to the nearest river, elevation, topographic wetness index (TWI) and aspect, all have similar importance. Topographic position index (TPI), years since fire, upslope area, year of measurement, maximum fire severity, and number of times burned all have relatively small contributions to the model.

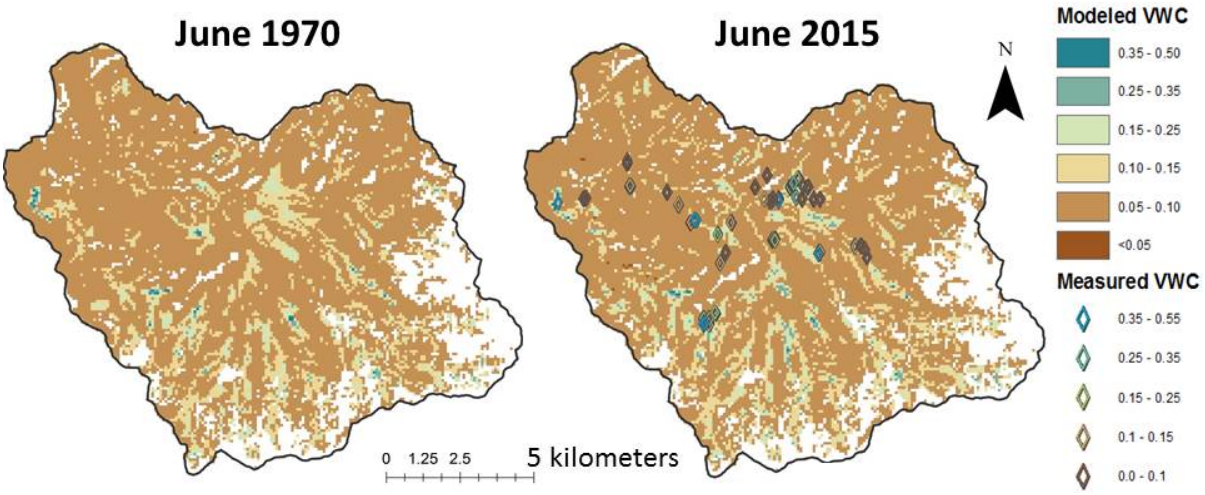

Figure 4.6: Maps showing modeled soil moisture for June using vegetation and fire history from 1970 and 2015. Areas shown in white are either exposed bedrock or outside of the ICB boundary. The modeled values here are aggregated to 90 meter resolution. The 2015 map also shows measured soil moisture values from May and June of 2015.

For 24 sites we were able to measure in three different periods in the summer (usually May, June, and late July or early August), we calculated percent change in VWC (relative to the mean) versus day of the year. The sites grouped well by vegetation type, ranging from forested hillslopes and sparse meadows drying at a rate of 2%/day to riparian areas drying at just under 1%/day and permanent wetlands not drying at all. Shrub sites dried at just over 1%/day on average. Forested riparian areas dried twice as slowly as forested hillslopes in terms of % decrease per day, but both dried at similar rates in terms of VWC (-.001/day). Sparse meadows dried proportionally faster than seasonally wet meadows, but the rate of drying in terms of VWC/day was nearly identical for all meadows (-.001/day), except permanent wetlands. In terms of water storage, shallow soil water loss ranged from 0.7mm/day to 0.1 mm/day (averaged over two months). The random forest model showed a decrease of 0.6%/day across all possible sites, but suggests that there are sharp decreases at the end of May (around the time snow has finished melting) and again in late June (when temperatures start to peak) rather than a uniform drying throughout the summer (Figure 4.10B). This downward trend throughout the summer is much greater in magnitude than the year-to-year variability (there is a VWC difference of 0.02 between 2014 and 2016, Figure 4.10A, compared to 0.10 for May to August, Figure 4.10B).

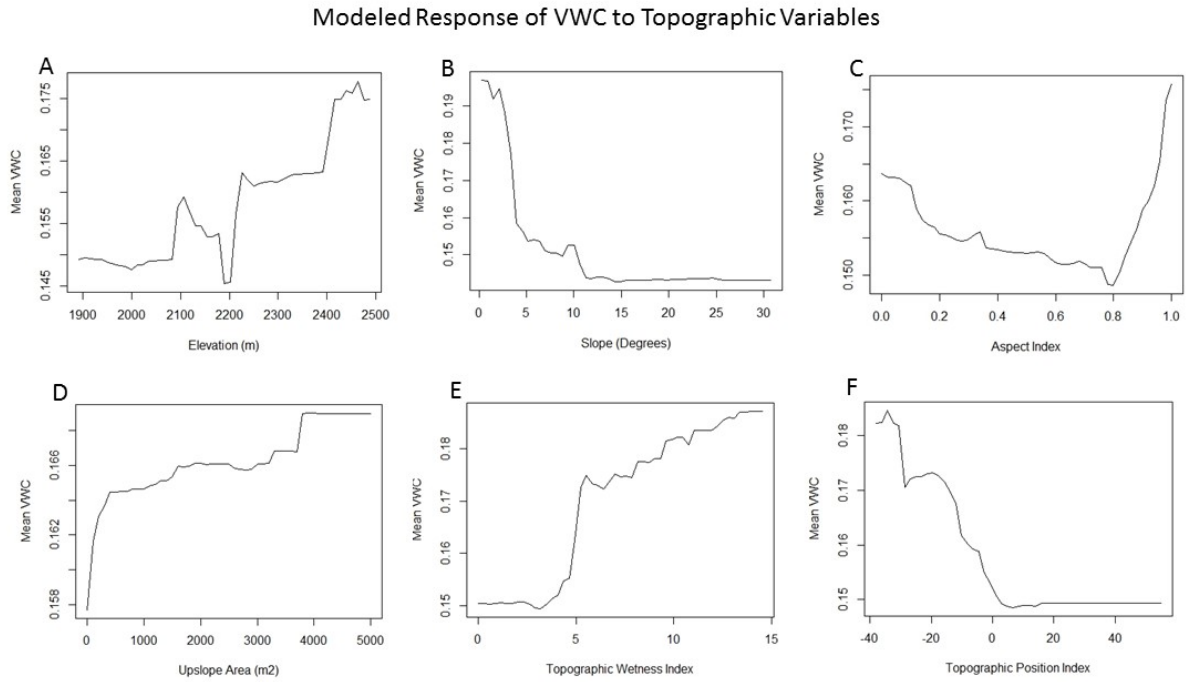

Figure 4.7: Partial dependence of VWC on slope, aspect index, elevation, topographic wetness index (TWI) and topographic position index (TPI), according to the random forest model. Note that not all y axes have the same range.

Modeled Effects of Landscape Change on Soil Moisture

We used the model to explore potential basin-scale effects of the mapped vegetation changes on soil moisture in ICB. At the whole basin scale, the model predicted very minimal differences in spatially average surface soil moisture between burned and unburned conditions, despite the large changes in vegetation cover: mean June VWC was 0.0018 (3%) higher under contemporary vegetation compared to 1969, and in August the difference was 0.0022 (5%), assuming 2014 weather conditions. Dramatic changes, however, were predicted in the wetness of individual sites. Figure 4.11 shows the change in August VWC between the 1969 vegetation conditions and the 2012 vegetation map plus fire history as of 2014 (a positive value indicates that soil moisture is higher under 2014 conditions). The site-specific effects of slope, aspect, topographic position, contributing area, and elevation were explicitly controlled for, and the model assumes no difference in weather between the two model scenarios. Burned forest sites that regenerated with dense meadow (and potentially wetland) vegetation increased in predicted June VWC by as much as 0.31 (for comparison, some of the most highly saturated sites had a VWC of approximately 0.55). These large local increases in soil moisture were offset by widespread, minor decreases in soil moisture; the greatest decreases (down to -0.17) were modeled in locations where conifers encroached on meadows.

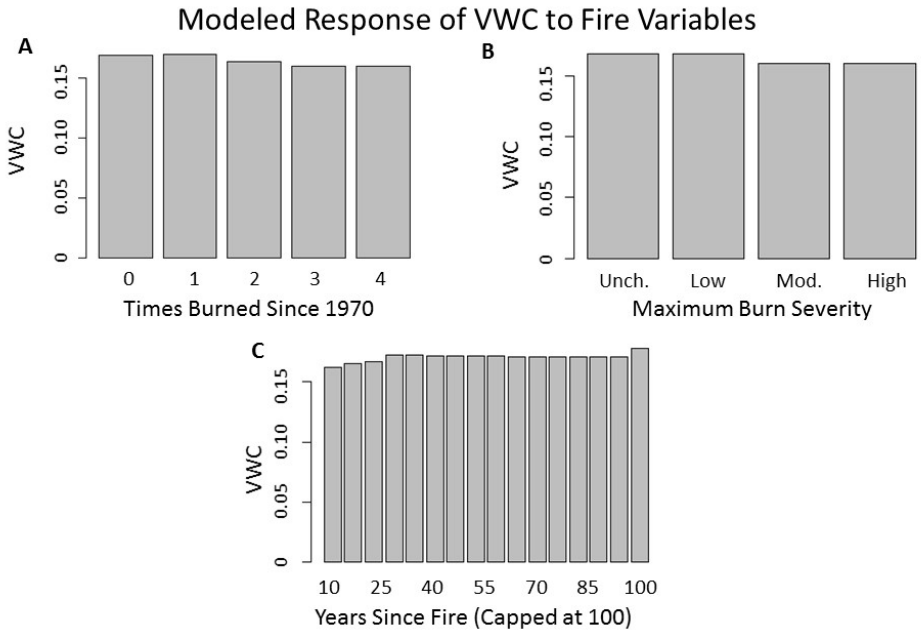

Figure 4.8: Partial dependence of VWC on (A) number of times burned since 1970, (B) maximum fire severity (unburned, low, moderate, or high), and (C) years since fire (the cap is set to 100 years since we do not have consistent maps for dating older fires).

The maximum increase in modeled August VWC was 0.28, slightly less than the June value of 0.31, but in some locations the increase from 1969 to 2014 was greater in August than in June.

4.4 Discussion

Surface soil moisture and deeper, root zone moisture are clearly correlated though they do not present a one to one relationship. The scatter of data from the leaf water potential measurements suggest that not all individual plants growing in areas with the same surface soil moisture experience exactly the same root zone moisture. It is also possible that some of this scatter is due to nighttime transpiration during periods of high evaporative water demand (Dawson et al., 2007; Sellin, 1999). The general trend, however, is for sites with wetter surface soil to have plants with less negative leaf water potential values (and thus wetter root zone soil). This trend shows that our surface soil moisture measurements are related to the actual soil moisture experienced by even deep-rooted plants.

The mean surface soil moisture was statistically different under multiple vegetation categories. We were able to use vegetation maps, as well as topographic information and fire history, to predict soil moisture throughout the basin. Vegetation cover was the strongest predictor of soil moisture, followed by local slope. Pre-fire vegetation was the third most

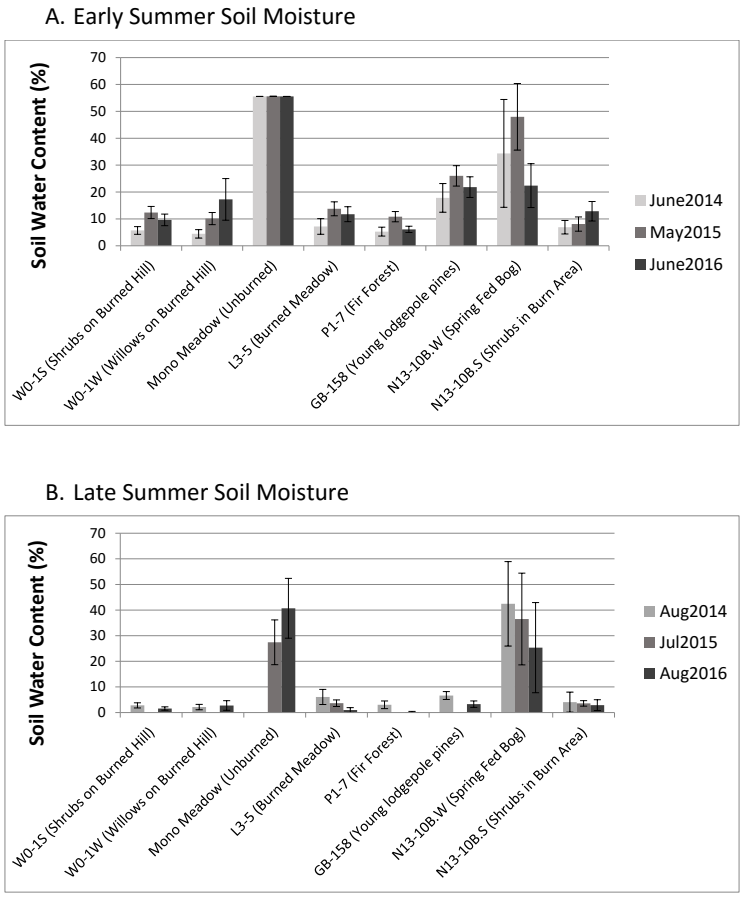

Figure 4.9: This plot shows a subset of sites spanning a range of fire histories and land cover for May-June (A) and July-August (B). Some sites are missing one year of July-August data (a missing bar does not indicate a value of 0). Error bars denote standard deviations.

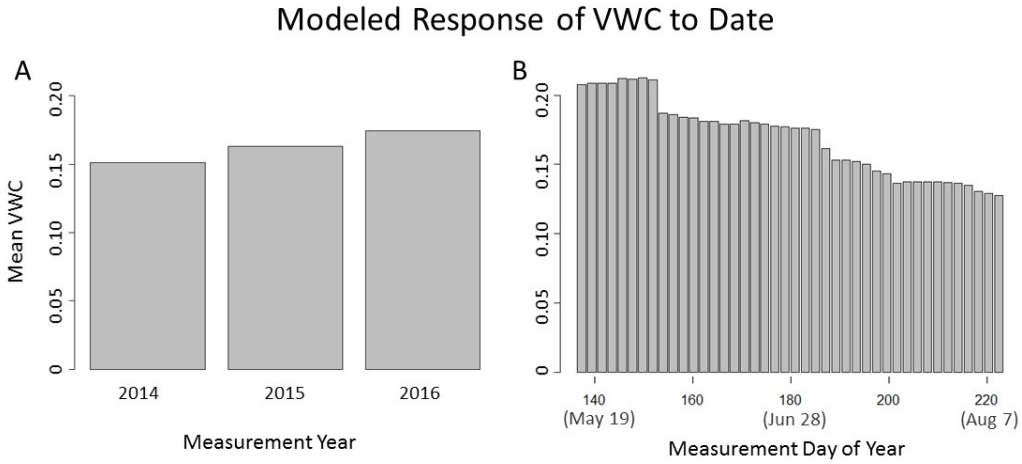

Figure 4.10: Partial dependence of VWC on (A) the measurement year and (B) the number of days after the previous December 31 that the measurement was taken, according to the random forest model.

important predictor of soil moisture. The relatively high importance of pre-fire vegetation is likely mostly driven by the fact that locations which were already meadows in 1969 had much higher mean soil moisture than other vegetation categories (Figure 4.3).

The relationships between fire and soil moisture are complicated by the interplay of cause and effect in these systems. Low soil moisture in frequently burned areas (Figure 4.8) could be due to frequent fires drying out the soil, or it could reflect the fact that dry soils are generally associated with drier fuels which are more likely to burn with higher consumption and to ignite in the first place. Similarly, the fact that unburned areas have the highest mean soil moisture is likely due to the fact that many of these unburned areas are wet meadows that do not easily burn. Fire does appear to affect soil moisture through stand replacement: in locations where a forest burned and is now replaced by a dense meadow, VWC is nearly three times as high as in areas that remain forested, on average, and dense meadows are the only locations where we measured saturated soils (Figure 4.3).

Some wet meadows appear to be fed by springs, which may confound our statistical model which attempts to predict moisture based on surface topography without subsurface flow path data. The fact that some wetlands had higher water content in summer 2016 compared to 2015 could indicate that those specific wetlands were highly dependent on snowpack, since water year 2016 had much more snow than water year 2015. The two wetlands that were drier in 2016 could be responding to reduced summer rainfall in 2016, indicating that different wetlands may have very different geologic controls dominating their hydrology. The fact that most of our wetland sites stayed relatively wet throughout all three

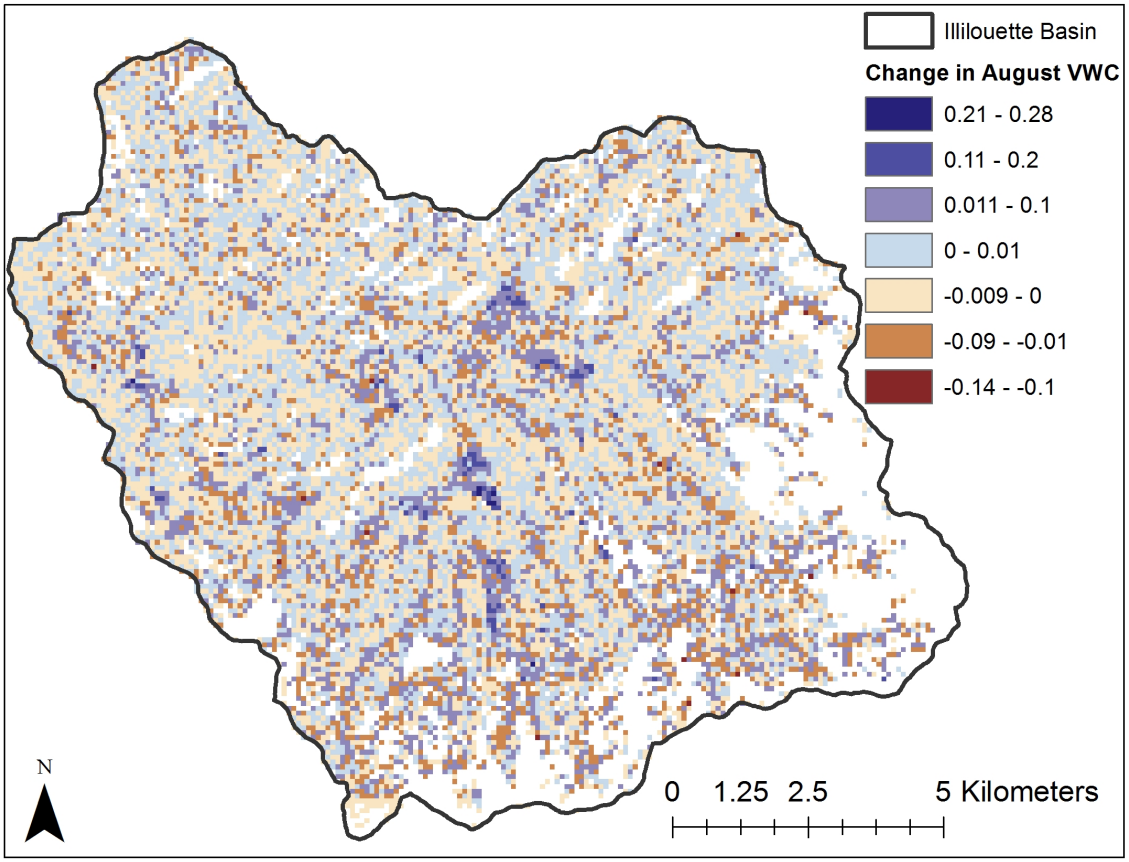

Figure 4.11: Using a random forest model trained to field measurements, we estimated the difference in soil moisture under current conditions compared to what soil moisture would have been if there had been no fires in ICB since 1900. The measurement date variable was set to early August 2014. Dark blue areas denote increases in soil moisture, while orange denotes a decrease and tan or pale blue indicates almost no change.

drought summers suggest a high drought resistance in this watershed.

Differences in midday water potential show differences in water use by different species (Appendix B). Most notably, willows appear more water stressed than *Pinus* jeffreyi, suggesting that willows indicate areas which normally have higher soil moisture (in non drought years). An example of willows likely establishing in wetter areas is site W0-1W, a willow-dominated site which had higher mean VWC than the adjacent shrub-dominated site, W0-1S, in 2016 but not in earlier, drier years (Figure 4.9). These pockets of willow will merit further attention in field studies conducted in future, non-drought years.

The most dramatic fire-related VWC increases shown by the random forest model were associated with locations that were forested in 1969, experienced high severity fire, and were colonized by dense meadow. Most of these areas had elevated soil moisture even when they

were forested (compared to other forested areas, according to the model), and became even wetter following the vegetation shift. Based on this modeling result and observations in the field, I have developed the following hypothesis: Areas that transition from forest to wet meadow (rather than to a more xeric vegetation type) following fire have local topography and geology which facilitates soil moisture storage in these areas. Such areas may even have been wetlands before, but in relatively dry years during fire suppressed periods trees were able to colonize (Helms and Ratliff, 1987) and the high water demand of these trees further reduced the soil moisture. Once these trees and their high transpiration demand were removed, enough water was available for the soil to come closer to saturation, making the ground less favorable to tree seedling growth and more favorable for grasses and forbs.

4.5 Conclusions and Next Steps

Our model suggests that late summer soil moisture in ICB is approximately 5% higher on average currently than it would be if fire suppression had continued. In early summer this increase was only 3%, suggesting that effects of changing vegetation cover is most important to changing water balance toward the end of the dry season. Within individual areas there were some very large increases in soil moisture due to fire, as well as some moderate decreases.

This project demonstrates that surface soil moisture measurements can be upscaled to the watershed scale using vegetation maps. We also showed that surface soil moisture was a good indicator of root zone moisture, especially during the summer.

Although our random forest model fit the data well and captured nonlinearities in the relationships between predictor variables and soil moisture, this type of model does not account for spatial autocorrelation of soil moisture, which can be important in capturing large scale moisture patterns (Western et al., 1998). Further work will explore modeling soil moisture with linear mixed effects models that explicitly account for spatial autocorrelation.

Chapter 5

Comparing Drought Resilience and Runoff to Control Watersheds

This chapter combines information from chapters 3 and 4, as well as additional datasets, to explore the general eco-hydrological changes that can be observed in the ICB following the implementation of a managed wildfire policy.

The contents of this chapter were originally published in *Ecosystems* in 2016, as an article titled "Managed Wildfire Effects on Forest Resilience and Water in the Sierra Nevada," DOI 10.1007/s10021-016-0048-1. The co-authors are Sally Thompson, Scott Stephens, and Brandon Collins.

5.1 Introduction

Projected warming and drying of the western United States climate is expected to simultaneously increase fire risks in the Sierra Nevada and to reduce the winter snowpack that feeds 60% of California's contemporary water supply (Barnett et al., 2004; Department of Water Resources, 2008; Dettinger and Anderson, 2015; Goulden and Bales, 2014; Westerling and Bryant, 2008). Fire risk and water supply in the Sierra Nevada (and much of the western United States) are linked together by the condition and function of the forests that cover approximately 70% of montane landscapes, provide fuel to fires, and regulate hydrological processes including interception, surface energy balance and transpiration (Soulard, 2015). These forests are also vulnerable to climatic extremes. For example, ongoing drought led to the death of up to 10.5 million conifers in the southern Sierra Nevada in 2015 alone (Moore, 2015), with complex consequences for future fire risk, wildlife habitat, and hydrology. Forest management has the potential to alter the relationships between forest condition, forest hydrology, and fire risk in the Sierra Nevada through manipulating tree densities, tree spatial patterns, and surface fuel loads. In particular, fire suppression, which has been practiced in the Sierra Nevada for the past century, has had negative impacts on forest resilience (the ability of a system to absorb impacts before a threshold is reached where the system changes

into a different state, Gunderson, 2000), raising the question of whether alternative management strategies could improve the montane forests' ability to cope with disturbances, including those posed by climate change (Holling and Meffe, 1996).

Fire suppression in the Sierra Nevada has increased the fractional forest cover of the landscape, forest canopy density and stand homogeneity (Scholl and Taylor, 2010; Stephens et al., 2015). These changes elevate total fuel loads and the risk of extreme fire (Collins and Skinner, 2014; Taylor et al., 2014). Forest transpiration demands and interception rates also increase with stand and canopy density. Goulden and Bales (2014) showed that evapotranspiration (ET) increases exponentially with increased Normalized Difference Vegetation Index (NDVI, a measure of forest greenness and density). For example, an increase in NDVI from 0.70 to 0.77 (a 10% change) is projected to increase ET from 764 mm/yr to 934 mm/yr (a 22% change) (Goulden and Bales, 2014). Fire suppression is also likely to result in the replacement of non-forest vegetation (particularly grasslands, shrubs, wetlands or forbs) by trees (Lauvaux et al., 2016; Norman and Taylor, 2005). Such vegetation changes are likely to reduce streamflow yields (e.g. Brown et al., 2005; Zhang et al., 2001). Indeed, contemporary Sierra Nevada mixed conifer forests transpire at rates of 760 mm/year (Bales et al., 2011), as much as four times higher than grasslands and meadows (Loheide and Gorelick, 2005).

Assessing the net effects of vegetation change on water demand at basin scales, or at the scale of the whole Sierra Nevada, is complicated due to the variety of mechanisms through which vegetation and water interact. For example, conifers are relatively inefficient at extracting water from dry soils, and may use less water than drought-adapted shrub communities when water is scarce (Royce and Barbour, 2001). However, coniferous forests may also obtain as much as a third of their water from fractured rock beneath the developed soil (Bales et al., 2011), meaning that conclusions drawn from observations made in shallow soils could under-estimate conifer water use (Royce and Barbour, 2001). The increased temperature of blackened trees and reduced shading in burned areas may also increase melting and sublimation rates of snowpack, as well as evaporation rates from bare soil, partly negating gains in water obtained from burned forests' reduced transpiration and interception (Neary et al., 2005).

Overall, fire suppression facilitated an expansion and increase in the density of coniferous forests in the Sierra Nevada, which has increased fire risk, landscape homogeneity and, probably, plant water use. In the context of a warming, drying and increasingly fire-prone climate, these consequences are likley to reduce the resilience of the montane landscape. New forest management strategies are called for to encourage increases in forest resilience, water supply and diversity. Forest management strategies have traditionally focused on canopy thinning (Stephens and Moghaddas, 2005), prescribed burning (Fernandes and Botelho, 2003), and other forms of fuel reduction (Agee and Skinner, 2005). These strategies hold the primary goal of reducing surface and ladder fuel loads, with reducing plant water demand being a secondary outcome (Grant et al., 2013). An alternative forest management strategy, 'managed wildfire', has received relatively less attention (Collins and Stephens, 2007). Managed wildfire uses fire as a forest treatment, but differs from conventional prescribed burning in that it relies on natural ignition events. Managers refrain from intervening with the progres-

sion of naturally occurring fires as long as there is an approved fire management plan, which specifies intervention (i.e. suppression) if other management goals (safety, or air quality for instance) are threatened.

The fire characteristics associated with managed wildfire are distinct from those associated with prescribed burning. Managed wildfire encompasses more diverse and heterogeneous fire patterns, differing from prescribed burns in terms of intensity, extent, spatial pattern, severity, and burning duration (Collins et al., 2011). Managed wildfires typically create high severity burn areas that can cause stand-replacement which, unlike lower intensity prescribed burning, can change landscape-scale vegetation composition and structure (Collins and Stephens, 2010) and increase the heterogeneity of vegetation cover (Hessburg et al., 2005b, 2015). Prescribed burns, thinning and other fuel treatment options have traditionally not achieved similar increases in landscape diversity. Thanks to this heterogeneity, forests with restored fire regimes may represent a more resilient state for montane ecosystems than the contemporary fire supressed condition - at least in the sense that more resilient forests are less likely to be catastrophically altered by severe disturbance (Holling and Meffe, 1996; Kane et al., 2014; Millar et al., 2007).

Despite these intriguing qualities, managed wildfire has been only minimally used for forest management: for instance only two locations in the Sierra Nevada have an extensive history of managed wildfire (Collins and Stephens, 2007). Obvious constraints and challenges associated with managed wildfire include identifying safe and appropriate locations for its use, transitioning to a natural fire regime from fire suppressed conditions, and minimizing risks to people and property. In spite of these constraints, future use of managed wildfire is likely to increase. In 2015, three national forests in the southern Sierra Nevada (Sierra, Sequoia, and Inyo National Forests) have proposed over 50% of their land base for use of managed wildfire to restore more natural vegetation structure and patterns. There is relatively little information on how, and over what timescales, the introduction of such managed wildfire treatments could alter long-term landscape composition and ecosystem functioning, including water use.

We expect that managed wildfire will add heterogeneity to vegetation cover (Hessburg et al., 2005b, 2015). The associated reduction in fuels and competition among trees should increase forest resilience to fire and drought (Stephens et al., 2009; van Mantgem et al., 2016). Due to reduced interception and transpiration, we also predict increased streamflow and summer soil moisture (Brown et al., 2005). Yosemite's Illilouette Creek Basin (ICB) provides a unique opportunity to evaluate these hypotheses, being, to our knowledge, the only long-term managed wildfire area in the western United States coupled with a long-term stream gage. Previous research in this watershed has focused on fire patterns (e.g. Collins and Stephens, 2010), forest structure (e.g. Kane et al., 2014), and diversity in plant and pollinator species (Ponisio et al., 2016). By combining findings from earlier studies with new datasets and analyses, this paper provides the first investigation of watershed-scale change in vegetation cover and its effects on water resources and drought resilience within this basin. Specifically, we summarize "lessons learned" from the 40 year application of managed wildfire in ICB, focusing on three major topics: (i) vegetation changes induced by

the managed wildfire regime, (ii) the effect of vegetation change on water resources in ICB, and (iii) the effects of vegetation change on fire characteristics and forest resilience.

5.2 Methods

Vegetation change

Vegetation change from the fire suppressed condition (1969) to the present managed wildfire condition (2012) was assessed using an object-oriented image analysis (eCognition) of aerial photography. The imagery sources are contemporary aerial photographs (National Agricultural Imaging Program 2012, four-band, 1 m resolution, Farm Service Agency and USDA, 2015) and black-and-white aerial photographs from 1969, capturing the basin condition near the end of the fire suppressed period (Yosemite National Park Archive, 8-bit 0.5 m resolution, produced by Cartwright Aerial Surveys). The black and white photography was orthorectified in the ERDAS Imagine Leica Photogrammetry Suite, and then spatially and radiometrically degraded (from 8-bit, 0.5 meter resolution to 4-bit, 2 meter resolution) to improve the performance and processing speed of the classification algorithms (Caridade et al., 2008). Where two or more images overlapped, the best of those images was selected manually for classification based on the clarity of individual objects.

The orthorectified photos were classified as granite, water, mixed conifer forest, shrub, sparse meadows, aspen, and dense meadows. Meadows are defined as areas dominated by grasses and forbs; dense meadows have little to no bare ground and appear green in summer aerial photographs, while sparse meadows have larger amounts of bare ground and appear brown. The dense meadow category encompasses wetlands, but the aerial image analysis was not able to reliably separate true wetlands from areas with dense summer green grass. Granite was identified using the 2012 imagery first, where it is more easily distinguishable from grassland than in the black and white imagery. Mapped granite outcrops from 2012 were then applied to the 1969 map, under the rationale that fire would not affect the distribution of rocky land cover. The 2012 classification was validated using 274 ground-truth points mapped in 2013-2015. The 1969 vegetation class maps were validated by randomly selecting point locations and comparing a visual classification of the points to the automated classification. Greater than 90% accuracy in the classification was achieved. Changes in landscape composition between the fire-suppressed and the contemporary condition were assessed in terms of landscape composition, patch size and Shannon's evenness index, using FRAGSTAT (McGarigal et al., 2012). Total cover was calculated for each vegetation type in each year, accounting for slope of the landscape. Classification uncertainty was propagated into the change estimates (following Congalton and Green, 2008).

For more details on the vegetation mapping and FRAGSTAT analyses, see Chapter 3.

Forest mortality during drought

The US Forest Service maps new tree mortality (defined by yellow to reddish brown trees) in the Sierra Nevada every summer using aerial surveys (Moore, 2015). These mapping surveys have high levels of accuracy: Only 4% of tree mortality or injury was missed, and damage type was identified correctly 83% of the time (Coleman et al., 2015).

We used these data to compare drought-associated tree mortality (not caused by fire) between ICB and nearby forests in 2014 and 2015. 2014 was the year when the Forest Service first observed a large increase in tree mortality related to the current drought (Moore, 2015). Although most mortality was attributed to insects or diseases such as mountain pine beetle (*Dendroctonus ponderosae*) and cytospora canker(*Cytospora kunzei*), the susceptibility of the trees to mortality from these stressors was likely increased by drought (Allen et al., 2010). Although a full analysis of the effects of fire history on drought-related forest mortality would require explicitly accounting for dispersal rates of beetles and other damaging agents, detailed localized weather, and groundwater availability, such an analysis is beyond the scope of this paper. Instead, we compare mortality within ICB to multiple control watersheds: (i) the control watersheds described below under "Runoff ratio analysis", and (ii) comparable watersheds adjacent to ICB having had less than 15% of their area burn since 1994. All control areas lie within the same elevation and climatic zones as ICB, and thus should experience similar drought stress, and they have all experienced fire over less than 15% of their area in the past 20 years. The watersheds used here are defined using the 12-unit watershed delineations available from USGS (http://nhd.usgs.gov/wbd.html), and are all approximately the same size (48-193km^2, compared to 158km^2 for the ICB). For each of these control areas, we calculated the drought-related mortality per km^2 of forest by dividing the number of dead trees by the total forested area (defined using the LANDFIRE existing vegetation type layer, LANDFIRE, 2012b).

Soil moisture measurements

The changes in vegetation structure induced by the managed wildfire regime were expected to lead to changes in the local water balance. A location's vegetation cover frequently indicates local hydrological conditions favoring that vegetation type (e.g. Araya et al., 2011; Milledge et al., 2013; Mountford and Chapman, 1993), and different plant water use profiles, rooting depths and canopy structures also alter micrometeorological conditions beneath the canopy and change the local water balance (Brown et al., 2005; Ma et al., 2010; Rambo and North, 2009; Zhang et al., 2001). Therefore, vegetation and soil water storage are expected to covary.

Details of the soil moisture measurements are given in Chapter 4. The analyses presented in this chapter only use soil moisture data from 2014 and 2015.

Each site was measured between one and five separate times over the two year study, capturing both early and late summer moisture when possible. Measurements were made with a 12cm time-domain reflectomer (TDR) Hydrosense II probe (Campbell Scientific,

2015). All measurements were recorded in terms of volumetric water content (VWC). The VWC is the proportion of the total volume of the soil matrix that consists of water, ranging from 0 for completely dry soils to ≈ 0.6 for saturated, highly porous soils (pure water would have a VWC of 1). Soil moisture was related to site condition using a random forest model (Liaw and Wiener, 2015), which was subsequently used to upscale the soil moisture results to the whole basin, using geospatial data and the vegetation maps. For modeling purposes, vegetation cover was assigned based on the broad vegetation classes inferred from the aerial imagery: sparse meadow, dense meadow, mature conifer, conifer recruitment, and shrub.

The random forest model predicts soil moisture (as a continuous value) using the following predictor variables: vegetation type, upslope area, slope, aspect, topographic position index (Weiss, 2001), topographic wetness index, distance from nearest stream, years since last fire, and maximum fire severity. In order to model change in soil moisture as a consequence of fire, we ran the model under 1969 (fire suppressed) and 2012 conditions. The first model run used the 1969 vegetation map, time since fire set to 100 (reflecting the duration of fire suppression), and both times burned and fire severity set to 0. The second model version used the 2012 vegetation map and actual fire data as of 2012. We then subtracted the modeled VWC values for 1969 from the modeled 2012 values to calculate the change. Note that this model does not include meteorological data, and thus the model results represent the change we would expect under identical climatic conditions with only the fire history and vegetation cover being different.

Random forest models predict a continuous variable by creating a large number of regression trees, using a random subset of all possible predictor variables to create each tree, and then taking the average predicted value of all of the trees. Each regression tree divides the data into smaller and smaller groups, or nodes, until a stopping criterion is reached. At each step, the data in one node is divided into two more nodes based on the division in the predictors that creates the largest separation in values between the two groups. The value of a new point in the variable space is computed by following the path from the first node to the appropriate terminal node. This method avoids issues of over-fitting that can result from using only one regression tree, and allows for fitting non-linear responses between variables and predictors (Grmping, 2009; Kane et al., 2015). We used the RandomForest package in the R program to fit the model, and set the minimum node size to 5 and the number of trees to 100 (100 trees minimized the RMSE of the model) (Liaw and Wiener, 2015). All data were randomly divided into a training dataset (75% of all data) and a test dataset (25%).

Details of the data sources for the predictor variables used in the model are given in chapter 4, though the random forests model used in this chapter is slightly different from that used in Chapter 4.

Runoff ratio analysis

Runoff from the ICB is first gaged at the Happy Isles Gage on the Upper Merced Watershed, where the ICB comprises approximately 30% of the gaged area. To determine if any changes in flow characteristics could be discerned at Happy Isles and potentially be attributed to

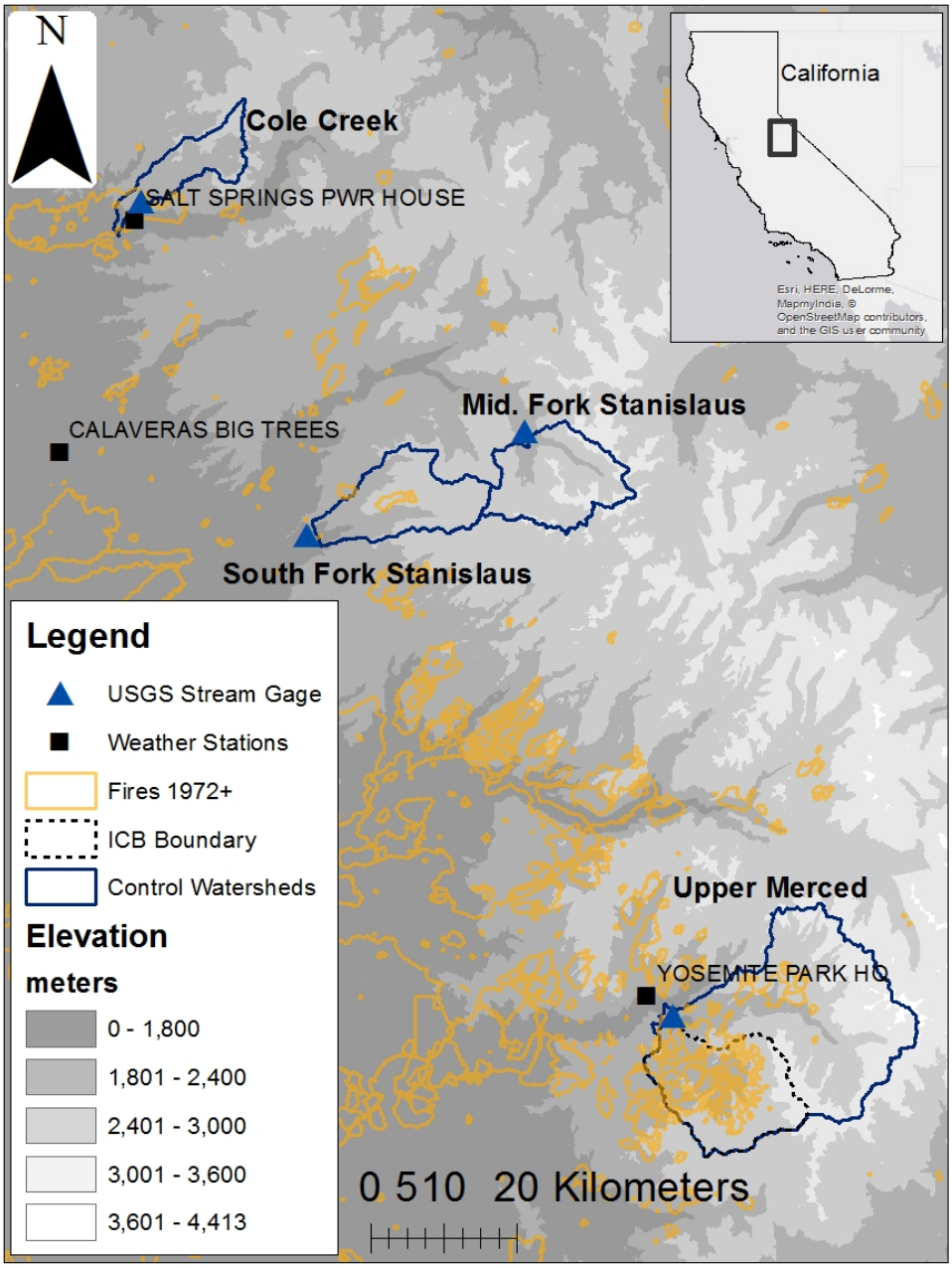

Figure 5.1: Map of control watersheds, stream gage locations, and the locations of the closest weather stations with records of over 10 years within each time period (pre and post 1974) shown in the context of elevation and fires occuring after 1972.

Watershed Name	Area (km^2)	Elevation (m)	Flow (m^3/s)	PPT (m)	Veg (%)	Burned (%)	Earliest Data
Upper Merced	453	1200-3700	2.9	1.2	76	23.0	1915
MF Stanislaus	119	1900-3400	1.8	1.5	55	0.2	1938
SF Stanislaus	112	1600-2900	1.7	1.6	88	3.3	1913
Cole Creek	53	1000-2600	0.4	1.5	91	14.7*	1927

Table 5.1: All watersheds are of comparable size, elevation range, median streamflow, annual precipitation (PPT), and percent vegetated area (from LANDFIRE). The "Burned (%)" column gives the percent of the area of each watershed known to have burned since 1930. The control watersheds have all had very little area burned in recorded history, and have only experienced one or two fires compared to 74 in the Upper Merced Watershed. Streamflow data is available for at least 35 years before the ICB's change in fire management (as shown in the "Earliest Data" column). Annual precipitation for this table is calculated from PRISM. *The 14.7% burned area in Cole Creek is due to a fire in 2004; prior to this only 1% of the watershed had been burned.

changes in ICB, we divided the flow timeseries into pre- and post-1973 time periods, and normalized annual (water year, October-September) flow by annual precipitation to obtain the annual runoff ratio. Trends and changes in the distribution of annual runoff ratio were computed for both time periods at Happy Isles, and for three nearby USGS stream gages measuring flow from control watersheds with comparable area, vegetation, topography and elevation, but where fire suppression has continued. The gages are: Upper Merced River at Happy Isles (USGS #11264500), Middle Fork Stanislaus River at Kennedy Meadows (#11292000), South Fork Stanislaus River at Strawberry (#11296500), and Cole Creek near Salt Springs Dam (#11315000). Approximately 25% of flow at Happy Isles is from Illilouette Creek (James Roche personal communication). Details for all watersheds are given in Table 5.1, showing that the control watersheds have comparable elevation ranges, climate, and vegetation cover to the Upper Merced watershed. Locations of the control watersheds, stream gages, and weather stations are shown in Figure 5.1. We also compared the ecological similarity of the watersheds using the LANDFIRE Biophysical Settings layer, which models potential vegetation under historic fire regimes prior to European settlement, taking into account climate, substrate, and topography (Rollins, 2009). The most common potential vegetation category for all watersheds is Mediterranean California Red Fir Forest, suggesting that the watersheds are comparable from a biophysical perspective (LANDFIRE, 2012a). Precipitation is sparsely gaged in the Sierra Nevada, so we conducted the analysis with 3 precipitation datasets: the point-scale measurements made at the weather station closest to each basin, and gridded climate products PRISM (Oregon State University, 2004) and ClimSurf (Alvarez et al., 2014).

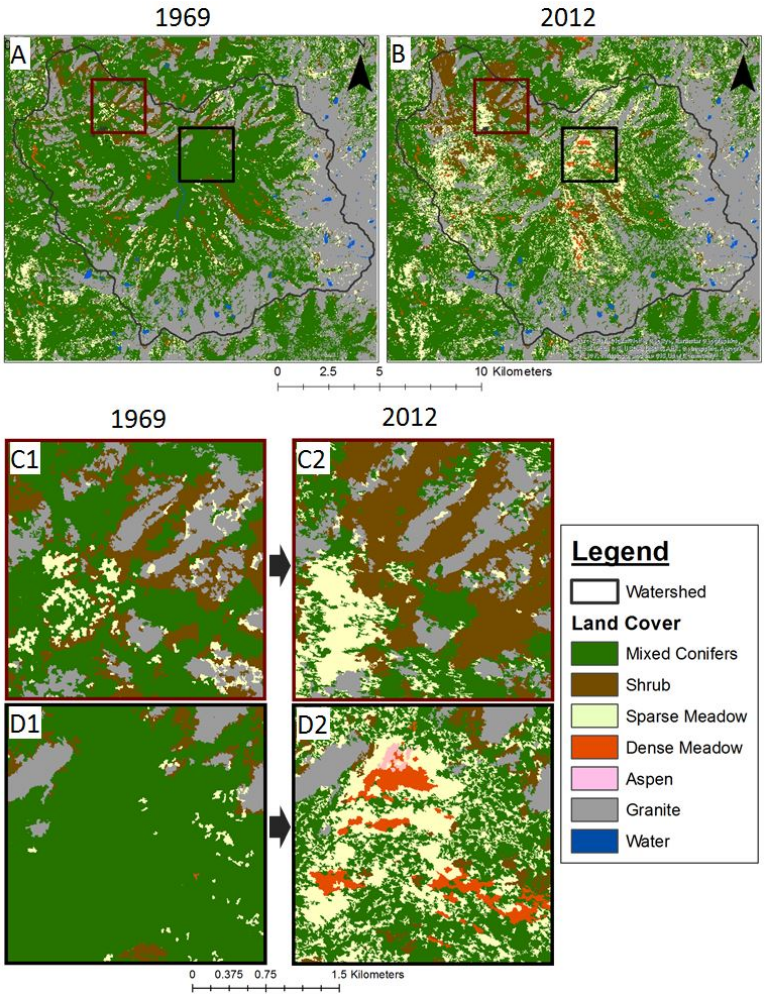

Figure 5.2: Maps of land cover in the Illilouette Creek Basin in 1969 (after 100 years of fire suppression) and 2012 (40 years after fire regime change). Insets show an area where both sparse grasslands and shrublands have expanded post-fire (C1,C2), and another that has generally changed from conifer cover to more open vegetation (D1,D2).

5.3 Results

Vegetation change following introduction of managed wildfire

Following the introduction of managed wildfire, the vegetation cover in ICB became more heterogeneous and less dominated by coniferous forest (Figure 5.2). Figure 5.2 Panels C and D show examples of common transitions that occurred during the managed wildfire regime: coniferous forest to shrubland (C1-C2) and coniferous forest to a mix of dense meadows and sparse grassland (D1-D2). Quantitatively, forest cover declined by 22% (from 109 km^2 to 84 km^2), while the area of meadow vegetation increased by 200% (0.8 km^2-2.4 km^2) and

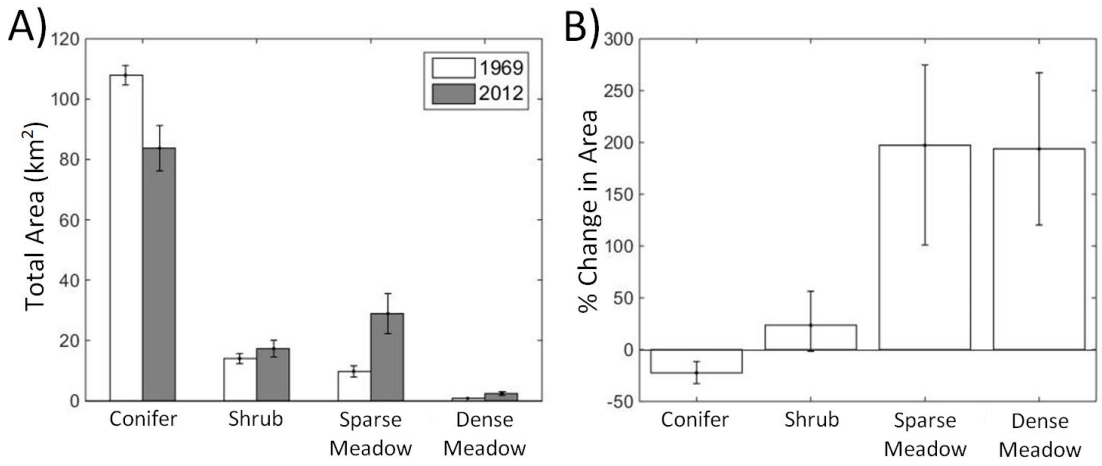

Figure 5.3: Change in vegetation cover in terms of total area covered in each year (A) and as a percent change in area covered (B). Error bars represent the level of uncertainty in the vegetation mapping. For example, if conifers were mapped with 90% accuracy, then the error bars for conifer would show ±10% of the area calculated. Aspen is not included due to difficulty identifying aspen in the black and white 1969 images making quantification of change in area highly uncertain.

shrublands by 24% (14 km^2-17 km^2) (Figure 5.3).

The organization of the landscape also changed following the introduction of the managed wildfire regime. Today the ICB contains a greater number of distinct vegetation patches, with a wider range of size characteristics, than in 1969. Forest patches declined in area (e.g. the largest forest patch decreased by 38%, from 51 to 32% of the basin area) and other vegetation type patches expanded (e.g. the largest shrub patch increased from 0.4 to 1.7% of the basin area, and the largest meadow patch increased from 0.1 to 0.9% of the basin area). The basin-scale Shannon's evenness index, which summarizes the structural diversity in the landscape on a scale from 0 to 1, increased from 0.65 to 0.80 from 1969 to 2012, consistent with an increase in structural diversity.

Effects on soil moisture and hydrology

In ICB, vegetation type was closely associated with the summer surface soil moisture content (Figure 4.2). Dense meadows had the highest median VWC throughout the summer (0.33 in May to 0.14 in August). At the beginning of the summer, conifer patches had the next-highest median VWC (0.15), but were comparable to other dry vegetation by the end of summer, at 0.04 VWC. Shrublands and sparse meadows had comparable soil moisture values at the beginning of summer (0.11 and 0.12, respectively) and end of summer (with 0.03 and 0.05 respectively).

We used a random forest model to isolate the effect of vegetation on local summer soil

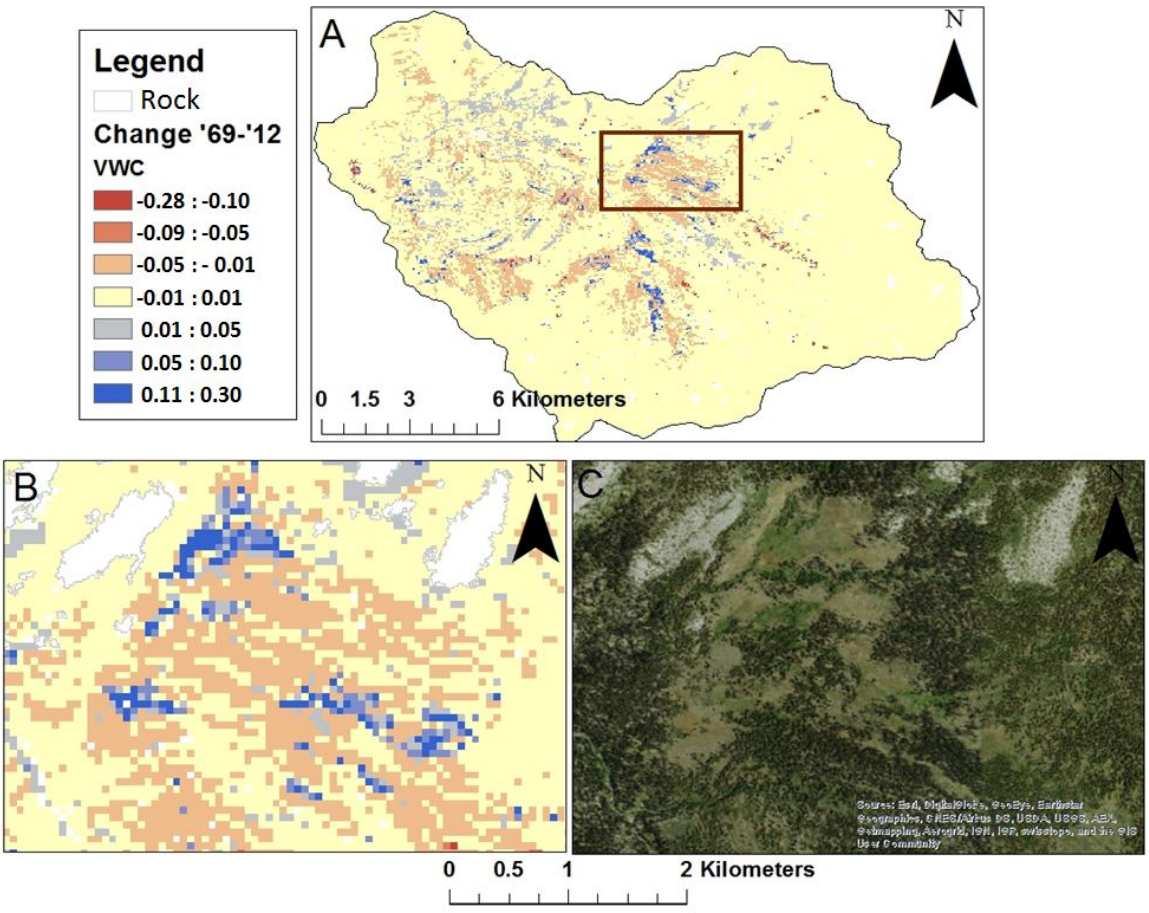

Figure 5.4: (A) Map of ICB showing change in summer mean volumetric water content for the top 12cm of soil from 1969 to 2012, calculated using a random forest model. This probabilistic model does not include any information on weather, only vegetation, topography, and fire history. Areas in blue represent an increase in water storage. Areas in red experienced a decrease in water storage, while areas in yellow experienced little to no change. (B) Close-up of VWC change in an area with a variety of changes in soil moisture. (C) 2014 aerial imagery (Esri inc.) of the region shown in (B) with extent given in (A).

moisture. The model results predicted the observed soil moisture values with an RMSE of 0.07 and coefficient of determination (r^2) of 0.76, with vegetation significantly predicting differences between sites. We found that the random forest model performed best when it was broken up into two separate sub-models: one for early summer and one for late summer. We trained the early summer sub-model on data taken in late May and early June, and the late summer sub-model using data from late July and early August.

We used the model to explore potential basin-scale effects of the mapped vegetation changes on soil moisture in ICB. At the whole basin scale the model predicted minimal

	Weather Stations (1940-2000)		PRISM (1940-2012)		ClimSurf (1950-2000)	
Watershed	Change	p-Value	Change	p-Value	Change	p-Value
Upper Merced	13%	0.43	2%	0.36	0.0%	0.65
MF Stanislaus	-6%	0.26	-1%	0.60	-6%	0.05
SF Stanislaus	-8%	0.41	-4%	0.66	-9%	0.06
Cole Creek	-7%	0.00	-11%	0.05	-12%	0.02

Table 5.2: Percent change in median pre-1973 and post-1973 annual runoff ratio (total streamflow divided by total precipitation) using three sources of precipitation data: remote weather stations and gridded precipitation estimates from PRISM and ClimSurf. Depending on the data source, start dates for the pre-1973 era are either 1940 or 1950, and end dates for the post-1973 era are either 2000 or 2012. Using only data from 1950-2000 for all datasets does not alter the sign of the change in runoff ratio for any of the watersheds, and only slightly changes the magnitude and p-value. All watersheds show a decrease in runoff ratio after 1973 except for the Upper Merced Watershed (which includes ICB).

changes in spatially averaged soil moisture, despite the large changes in vegetation; these changes were slightly positive for June (ΔVWC=0.003, an 8% change) and negative for July (ΔVWC=-0.004, a 4% change). Dramatic changes, however, were predicted in the wetness of individual sites. Figure 5.4 shows the change in mean summer VWC (calculated by averaging early and late summer values) between the 1969 vegetation conditions and the 2012 vegetation plus fire history. The site-specific effects of slope, aspect, upslope area, and elevation were explicitly controlled for. Burned forest sites that regenerated with dense meadow (and potentially wetland) vegetation increased in predicted summer VWC by as much as 0.3 (for comparison, some of the most highly saturated sites had a VWC of approximately 0.5). These large local increases in soil moisture were offset by widespread, minor decreases in soil moisture; the greatest decreases were modeled in locations where conifers encroached on meadows.

The pre- and post-1973 runoff ratio changes computed using three different precipitation datasets for the ICB and three control (unburned) watersheds are shown in Table 5.2. The sign of any detected change in runoff ratio differs between the Upper Merced and the control basins, with Upper Merced tending towards relatively stable or positive trends in runoff ratio, and the other basins either decreasing or stable. The significance of observed trends is not consistent between basins and datasets.

Effects on tree mortality during drought

Aerial surveys by the USFS during the severe drought years of 2014-2015 show minimal levels of tree mortality within ICB, despite extensive tree death due to beetles and other drought-associated causes of mortality in adjacent, mainly unburned areas. These surveys

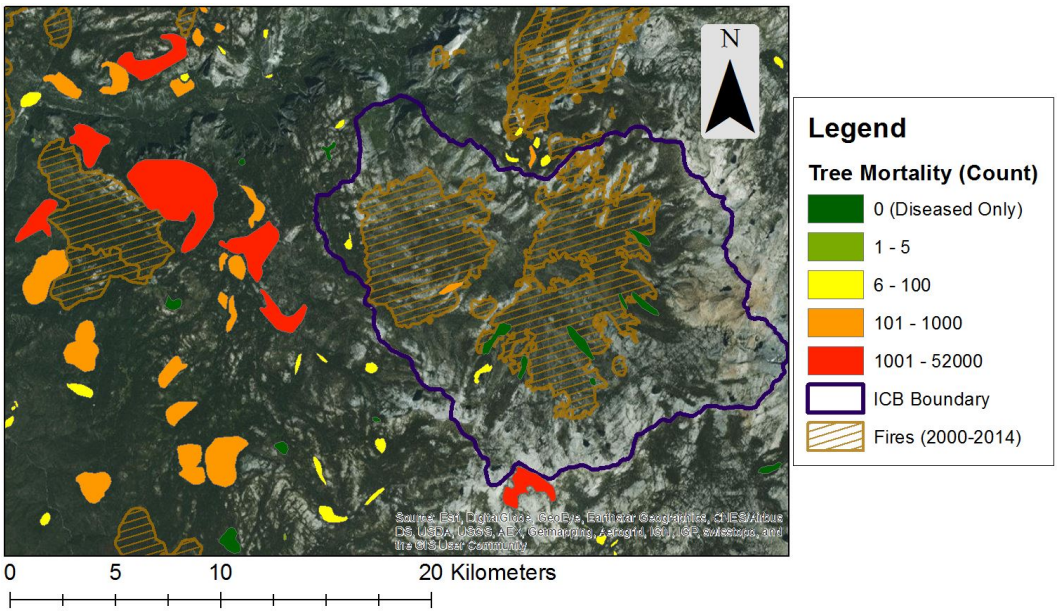

Figure 5.5: Map of drought-related tree mortality and disease areas in 2014, along with all fires since year 2000. The number of recently dead trees is much higher outside the ICB than within it. There is very little overlap between burned sites and large mortality patches, despite burned areas still containing many large trees (as shown in this aerial image from 2014, provided by Esri inc.).

match our qualitative field observations of tree health in the area. In 2014, approximately 47 trees per km^2 of forest died within fire-suppressed watersheds adjacent to ICB that were climatically similar, compared to only 4 dead trees per km^2 of forest within ICB. Table 5.3 gives a summary of tree mortality in similar areas, showing that ICB has the lowest mortality in this set of watersheds. Suggestively, areas of drought-related tree mortality are mostly located in unburned regions. Figure 5.5 shows an example of an area adjacent to ICB with 2014 beetle-killed tree areas occuring at the edges of previously burned areas but not overlapping with them. The only mapped tree mortality within the burned portion of the ICB occurred in areas that had experienced only low severity fires, and the largest patch was only 20 ha in extent, compared to patches of mortality up to 680 ha located within 10 km of the ICB. (For more details, see supplementary figure C.1.)

5.4 Discussion

Managed wildfire in ICB has dramatically altered the composition and structure of the landscape. At the end of the fire suppressed period, the vegetated parts of the basin formed essentially a single, homogeneous forested patch (Figures 5.2A,5.3A). Fire has fragmented the vegetation cover in ICB, resulting in an increase in the distribution of vegetation patch

Region	Conifer Area (km2)	Dead Trees 2014	Dead/km2 2014	Dead Trees 2015	Dead/km2 2015	Ratio 2014	Ratio 2015
ICB	80.6	325	4.0	1040	12.9	1.0	1.0
Table 5.1 Watersheds:							
MF Stanislaus	39.3	351	8.9	540	13.8	2.2	1.1
SF Stanislaus	71.7	11024	153.8	23352	325.8	38.1	25.2
Cole Creek	36.0	544	15.1	6294	174.6	3.7	13.5
Adjacent Watersheds in Same Elevation Range:							
Bridalveil	49.5	6094	123.0	33505	676.9	30.5	52.4
Chilnualna	34.7	306	8.8	10579	304.8	2.2	23.6
USF Merced	87.6	1787	20.4	5348	61.0	5.1	4.7
Total	171.8	8187	47.6	49432	287.7	11.8	22.3

Table 5.3: Summary of drought-related tree mortality during the summers of 2014 and 2015 in the ICB compared to similar watersheds with fire suppressed landscapes. These watersheds include both the control watersheds used in the runoff ratio analysis as well as fire-suppressed watersheds adjacent to ICB and falling within the same elevation range. The "Ratio" columns give the proportion of tree mortality density in a given region to the density in the ICB, showing that all regions have a higher density of drought-related tree mortality than the ICB.

sizes, and an increase in the proportion of the basin covered by meadow and shrub vegetation types. Changes in understory vegetation and in forest structure were not captured by our analysis of the historical imagery, though they have been observed in other studies within the ICB (Kane et al., 2015; Ponisio et al., 2016). The bulk landscape classification therefore presents a conservative estimate of the true degree of vegetation change in the ICB.

The change in vegetation composition and organization in the ICB also changed the patterns of fire occurrence and effects. Contemporary fires in the ICB occur with relatively high frequency, but are predominantly of low to moderate severity, interspersed with relatively small patches of stand-replacing fire (Collins and Stephens, 2010). This pattern is consistent with our understanding of how historical fires burned in these landscapes (Collins et al., 2009; Collins and Stephens, 2007; van Wagtendonk et al., 2012). Similar fire patterns are not observed in comparable forests where fire suppression continues (Miller et al., 2012a). Fires in suppressed forests create uncharacteristically large stand-replacing patches, and burn with a greater proportion of stand-replacing effects (Miller and Safford, 2012; Miller et al., 2009), consistent with the theoretical prediction that removing natural variability from a landscape reduces its ability to recover when disturbance (e.g. catastrophic fire, drought, or insect outbreak) eventually occurs (Holling and Meffe, 1996; Holling, 2001).

Two main factors drive the divergent fire patterns in the ICB relative to the fire suppressed Sierra Nevada. First, in forests with continued fire suppression, the only fires that burn a significant area are those that "escape" initial suppression efforts. "Escape" fires tend to burn under extreme weather conditions, compounding the already fuel-loaded condition of many Sierra Nevada forests, leading to uncharacteristically extensive and severe wildfires

(Finney et al., 2011; North et al., 2015). In contrast, the fires in ICB burn under a broad range of fire weather conditions (Collins et al., 2007; Miller et al., 2012a). Second, the frequency and extent of fires in the ICB is such that fuel consumption by previous fires limits the spread and intensity of subsequent wildfires (Collins et al., 2009; Parks et al., 2014; van Wagtendonk et al., 2012). This 'self limiting' characteristic of the fires is directly linked to the increased heterogeneity and more even patch-size distribution of vegetation in ICB (c.f. Figure 5.2) - a more heterogeneous landscape results in more obstacles to fire spread, while reductions in forest cover reduce the landscape-scale fuel loads.

Intriguingly, the ICB may also exhibit resilience to *other* forms of disturbance. Although the 2011-2015 drought conditions in California are estimated to have killed over 10 million trees in the southern Sierra Nevada (Moore, 2015), forest mortality in ICB during this period appears to be minimal. The only control watershed with comparably low drought mortality was the The Middle Fork Stanislaus, which was likely less susceptible to drought because it is in the higher end of the elevation range. Other watersheds had up to 52 times higher rates of drought mortality than the ICB. This low incidence of drought mortality in burned areas is consistent with van Mantgem et al. (2016), who found that, during the drought year of 2014, burned stands under 2100m in elevation had a lower occurence of tree mortality than areas that had not experienced fire in over 100 years.

In addition, we observed multiple persistent wetlands throughout the record-breaking drought summers of 2014 and 2015. While it would be premature to attribute the low drought-related forest mortality rates or wetland persistence in ICB directly to the managed wildfire regime, such drought resilience is consistent with expected effects of reducing forest extent, forest density and understory vegetation, all of which would reduce competition for limited water supplies (Grant et al., 2013).

Observations to date suggest that vegetation cover is meaningfully associated with summer soil moisture in ICB. Introduction of the managed wildfire regime led to the expansion of densely vegetated meadow areas in which surface water availability is likely much higher than under the previously forested state. Indeed, we regularly found instances of wetland vegetation regenerating amidst burned conifer stems; and yet the coniferous forest sites we measured never exhibited the summer-long saturated soil conditions found in wet meadows. We hypothesize that fire suppression enabled woody plant invasion and dessication of meadow margins (due to increased plant water uptake), and that the reintroduction of fire has re-opened those meadow regions, providing new habitat for wetland plants and year-round water sources (Norman and Taylor, 2005).

The basin-scale consequences of the observed changes in vegetation remain unclear, despite data that tentatively suggest the ICB is maintaining or increasing water yields while similar, but unburned basins are reducing water yields. Further investigations of the effects of vegetation change on water balance are clearly essential. Relevant issues include understanding how snowpack and soil moisture dynamics respond to the different vegetation types, and how patch-scale changes in vegetation and water availability scale up to produce changes in runoff response.

Although the measured differences in runoff ratio change between the Upper Merced

River and the control watersheds are small, they represent a lower bound on the influence of wildfires on this area's streamflow: Any slight flow regime change at Happy Isles related to wildfire is expected to stem from a larger change (proportionally) within ICB, since ICB is the sub-watershed with the greatest proportion of burned land feeding into the Happy Isles Gage. Tentatively, the managed wildfire regime may have either stabilized or increased the runoff yield from ICB, but further analysis is needed to test this hypothesis. Ongoing work focuses on basin-scale hydrologic modeling that propagates the changes in vegetation structure in ICB into estimated hydrologic response, and allows us to explore how these changes might propagate into overall watershed function.

Our paired watershed analysis is promising, but contains a high level of uncertainty. Unfortunately, all three control watersheds are smaller than ICB and located further north. We looked into using several larger and more southern watersheds, but they all either had large gaps in the flow record or were strongly affected by reservoirs (such as the Tuolumne River below Hetch Hetchy). We believe that runoff ratios should be comparable between these watersheds, however, since weather variations over time are similar among all watersheds being compared. The watersheds also have similar elevation ranges and are all on the western side of the central Sierra Nevada, and thus should experience similar proportions of snow versus rain as well as similar evaporative demand. These watersheds also all have streamflow records spanning at least 35 years before and after the change in ICB fire regime, allowing us to calculate reliable statistics.

Both the streamflow analysis and our analysis of drought-related tree mortality are limited by the difficulties in completely controlling for variations in biological and physical characteristics of the basins. Until more basins are exposed to managed wildfire treatments, these differences are likely to be impossible to completely control for statistically, and empirical comparisons between basins will remain subject to uncertainties induced by such variability.

Overall, our analyses of data from ICB show a variety of lines of evidence pointing to eco-hydrological benefits of managed wildfire in this watershed. The most obvious effect is the vegetation changing to be less dominated by forests. The modelled re-organization of soil moisture during summer indicates that these vegetation changes may restructure and influence hydrological processes at the scale of the ICB. It is possible that this restructuring also leads to changes in streamflow yield, although capturing the true magnitude and importance of any such changes requires further study. These changing hydrological processes may also be responsible for the relatively low drought-related mortality seen in ICB and adjacent burned forests during the drought years of 2014 and 2015. It is possible that our observations of soil moisture, streamflow, and forest health could be influenced by other factors besides fire, such as climate and landscape, despite our efforts to account for such factors in our analyses. The fact that these variables are all behaving in ways that are consistent with our hypotheses, however, is suggestive of the influence of the current fire regime.

Scalability

Replicating the resilience of ICB in other basins across the Sierra Nevada is a top land management priority (USDA-FS, 2011). Managed wildfire appears to be a promising tool for this purpose. While managed fire is clearly not a suitable tool for all areas, there is potential to expand managed wildfire to meet restoration objectives. The current revisions of the Land and Resource Management Plans for National Forests (NF) in the southern Sierra Nevada propose creating two new "zones" for binning NF lands that emphasize using managed wildfire for resource benefit. Previous plans only allowed for this type of managed wildfire in a few discrete areas; under the proposed revisions, 69-84% of the land in each NF in the southern Sierra Nevada is included in these two zones. This indicates considerable potential for increased use of managed wildfire. An important objective of these programs is to allow fires to burn under a range of fuel moisture and weather conditions, as opposed to the fairly extreme conditions associated with "escaped" wildfires that often occur on Forest Service lands due to an emphasis on suppression (Miller et al., 2012a; North et al., 2015). It is worth noting that a majority of the area of the new zones is in watersheds at around 2000 m elevation. This elevation band coincides with a peak in evapotranspiration in the Sierra Nevada, indicating that changes in vegetation water use could be significant for the hydrology of these basins (Goulden et al., 2012).

The Sierra Nevada are highly heterogeneous in terms of topography and geology, and thus observations from the ICB should not be directly extrapolated to the entire region. However, 19100 km^2 of the Sierra Nevada lie in a comparable climate and elevation range to the ICB according to PRISM climate data (Oregon State University, 2004) and USGS elevation maps (USGS, 2015). Over half of this area is designated wilderness, representing an area in which the risk of wildfires threatening homes or other structures is reduced (University of Montana, 2015). Based on this analysis, there is potential to scale up the ICB experiment by nearly 100-fold over some 9800 km^2, or 18% of the total area in the Sierra Nevada.

5.5 Conclusion

The Illilouette Creek Basin provides an example of a successful return to a natural fire regime after decades of fire suppression. This transition was achieved without significant negative effects, and has resulted in reduced fire risk, greater resilience to both fire and drought, greater landscape diversity in vegetation and hydrologic terms, and potentially an increase or stabilization of water yields. The resulting landscape is likely closer to the pre-European settlement ecosystems to which Sierra Nevada species are presumably best adapted.

The most preliminary aspect of the results presented here are the hydrological analyses. Despite documenting spatially explicit and vegetation-dependent differences in water availability, the mechanisms driving these differences are yet to be quantified in the ICB, while the consequences of changing vegetation composition for runoff yields remain preliminary. Recently installed soil moisture and weather observation stations (Appendix D), along with

mechanistic hydrological modeling (Chapter 6) are helping further our understanding of the changes in ecosystem function induced by managed wildfire, and the implications for the management of Californian forests, water resources and landscapes.

Chapter 6

Using the RHESSys Ecohydrological Model to Quantify Hydrologic Changes due to Wildfire

In the previous chapters, assessments of change have been based upon vegetation, vegetation as a proxy for water availability, or changes in water balance measured over scales larger than the ICB. In this chapter, a mechanistic model is used to quantify physical changes in response to the known vegetation change, and assess streamflow generation changes within the ICB separate from UMW.

6.1 Introduction

The hydrologic effects of large, high severity fires have been fairly well studied (Brown et al., 2005; Helvey, 1980; Mayor et al., 2007; Pierson et al., 2001). Little is known, however, about the effects of frequent, mixed severity fires on watershed hydrology, relative to the fire-suppressed conditions that prevail in many forested watersheds. The Illilouette Creek Basin (ICB) in Yosemite National Park is one of the only areas where these effects can be studied. Fire suppression began in this region in the late 19th century (Collins and Stephens, 2007) and continued until 1972, when Yosemite National Park began its "Natural Fire Management" program and allowed naturally ignited fires to burn within the ICB (van Wagtendonk, 2007). The duration of the managed wildfire program and the large total proportion of the basin area that has burned since 1972 (52% of the total area and ≈75% of the vegetated area) make it an ideal place to study the landscape effects of managed wildfire. Although ICB was impacted by approximately 100 years of fire suppression (only 8 ha are known to have burned between 1880 and 1973), fire frequency and extent since the onset of the managed wildfire program in 1972 is similar to that in the non-fire suppressed historical period (a 6.8 year recurrence interval, versus 6.2 historically, based on fire scar measurements, Collins and Stephens, 2007). The ICB is located near long-term weather and

streamflow monitoring stations in Yosemite National Park. This unique fire history coupled with long term hydrologic records provides a valuable opportunity to study the long term hydrological effects of a restored, near-natural fire regime in the Sierra Nevada (Collins and Stephens, 2007). Understanding changes to the hydrologic cycle in the Sierra Nevada is especially important because much of California's water infrastructure is dependent on flows from these mountains (Department of Water Resources, 2008).

Contrasting effects of vegetation cover on the water balance, especially snow accumulation, make the prediction of hydrologic responses to fire regime shifts in the Sierra Nevada uncertain. Changing vegetation composition following fire can alter water demands, interception, and the surface energy balance driving snowmelt (Bart et al., 2016). Sublimation of intercepted snow reduces snowpack, and longwave radiation from trees can melt snowpack, but shading helps to protect snow on the ground from melting or sublimating (Lundquist et al., 2013). Even if total snow storage is unchanged, altering vegetation cover can shift the timing of spring snowmelt, and the snowmelt period can be lengthened in gap-thinned forests due to snow in gaps and forests melting at different times (Ellis et al., 2013). Hydrologic response to fire is variable over time as well as space: thinning from fire reduces transpiration demands initially, which generally increases soil moisture, but eventually regrowth following a fire can lead to a high water demand by dense, fast-growing, re-establishing vegetation that reduce soil moisture storage to levels below those from pre-fire conditions (Lane et al., 2010; Neary et al., 2005).

There are very few locations in Western U.S. mountains where pre-suppression fire regimes have been restored to fire suppressed landscapes. Where such situations do exist, hydrological monitoring is sparse relative to the spatial variability in mountainous areas. Therefore, statistical or empirical evaluations of the effect of the fire regime change on water balance are necessarily constrained, and mechanistic modeling provides perhaps the best pathway to understanding these effects.

Models also allow us to estimate spatially distributed values of variables such as soil moisture and snowpack which have high uncertainty using remotely sensed products (especially under dense canopy cover, e.g. Todd and Hoffer (1998)) or are only available at high resolution for a limited number of years (e.g. Airborne Snow Observatory data, http://aso.jpl.nasa.gov/).

In this study, we use the Regional Hydro-Ecologic Simulation System (RHESSys) model to study the effect of the ICB's current fire regime on the watershed's water balance. RHESSys offers the capacity to represent processes such as snow dynamics and subsurface water flow, which have been shown to be critical for representing variations in evapotranspiration (ET) in mountainous terrain (Lundquist and Loheide, 2011). RHESSys also represents dynamic changes in vegetation and litter cover, as well as how these changes alter the water and energy flows (Tague and Band, 2004); capturing such processes is necessary for representing long term fire regime effects on hydrology. For this study, we focus on long term effects of the fire *regime* in this watershed, rather than only studying the effects of single fires or the first few post-fire years in which surface runoff is generally affected (Vieira et al., 2015).

RHESSys was selected for this project in part because it has been successfully used to model hydrologic change in the Sierra Nevada in numerous previous studies, including changes related to fire. Saksa (2015) found that in headwater catchments an 8% reduction in vegetation due to prescibed burning could lead to a 14% increase in streamflow in some watersheds. Vegetation type conversions have also been shown to alter streamflow if associated changes in interception and transpiration are great enough (Bart et al., 2016). RHESSys models have also shown that conifer transpiration in the elevation range of the ICB is highly sensitive to precipitation (Christensen et al., 2008) as well as to snow accumulation and timing of snowmelt (Tague and Peng, 2013). Evapotranspiration has also been shown to be sensitive to lateral redistribution of soil water, making it important to capture spatial organization when predicting landscape-level responses to water balance changes (Tague and Peng, 2013).

This study uses RHESSys to quantify the extent to which repeated managed wildfires in the Illilouette Creek Basin have altered the watershed's hydrology at multiple spatial scales. We begin with the hypothesis that this model is capable of capturing the impact of repeated fires on UMW. If this is successfully verified, we hypothesize that the model will show that the current fire regime has led to the following changes compared to fire suppressed conditions at the watershed scale (both in UMW and ICB): increased peak snowpack, increased summer low flows, increased runoff ratio, increased soil moisture, higher peak flows, decreased evapotranspiration, and decreased climatic water deficit. At smaller scales (hillslopes or vegetation stands), responses to the fire regime are likely to be highly variable.

Previous modeling studies related to fire and hydrology have generally either focused on a single event and its effect over time (Seibert et al., 2010, e.g.) or used theoretical patterns of repeated fires (Miller and Urban, 2000b; Ursino and Rulli, 2011, e.g.). In this study, in contrast, actual fire history and its associated vegetation cover changes are explicitly included in a model of a watershed with a frequent, mixed severity fire regime. Observational data are used to parameterize the fire-induced changes to the landscape over multiple decades, and the model is used to estimate hydrologic impacts of these changes.

6.2 Methods

RHESSys Model Details

RHESSys is a spatially distributed eco-hydrological model that simulates water and energy cycles as well as carbon and nitrogen cycling, as described in Tague and Band (2004). Required parameters include: daily precipitation, daily maximum and minimum temperature, a DEM file for topography, vegetation maps, and soil maps. Model outputs include streamflow and subsurface water stores, as well as fluxes and stores of carbon and nitrogen. The movement of water through the model landscape is affected by interception of precipitation by vegetation and litter, infiltration, evaporation, root water uptake, and subsurface water fluxes. The model has a hierarchical structure, with homogeneous vegetation layers within

patches of homogeneous soil moisture. These patches, in turn, are contained within hillslopes that drain into different stream segments to produce streamflow (via saturation-excess overland flow or subsurface flow). The hillslopes are all within a basin which drains to a single outlet. In our implementation, weather inputs vary from patch to patch based on elevation lapse rates and the mean topographic aspect's effect on solar radiation. At a daily timescale, water is gained through precipitation or lost through ET, sublimation, or streamflow, and water is redistributed spatially via subsurface flow and overland flow.

The soil column is divided into a saturated and an unsaturated layer. Vertical fluxes into and between these layers are modeled using a mass balance equation driven by infiltration (calculated using Philip's infiltration equation), drainage, and evapotranspiration. In this implemenation of RHESSys, lateral redistribution of saturated water from uphill patches to adjacent downhill patches is calculated based on soil transmissivity, local slope, and the width of the border between patches. Potential evapotranspiration is calculated using the Penman-Monteith equation, and actual evaporation and transpiration are limited by available water as well as maximum exfiltration rates from soil and stomatal conductance for plant leaves. Precipitation is divided between rain and snow based on spatially-variable air temperature values. Snow melt is modeled using a quasi-energy budget approach that includes radiation, sensible and latent heat, and advection melt due to warming by incoming precipitation. Incoming solar radiation is altered by vegetation canopy and/or snowpack according to Beer's law. Vegetation growth is controlled by available water, energy, and nutrients. More details on the modeling of water flow through soils in RHESSys is given by Tague and Band (2004).

Study Area

The main focus of this study is the ICB, a 150 km^2 basin within the Upper Merced Watershed (UMW) in Yosemite National Park, California, USA (Figure 6.1). Unfortunately, ICB is not suitable for calibration and validation due the limited streamflow data available for Illilouette Creek. Discharge from the UMW, in contrast, has been recorded at the Happy Isles stream gage in Yosemite since 1915, and therefore we use the full UMW as the model domain for calibration purposes (nearly 1/3 of the area of the 470 km^2 UMW is located within the ICB). The UMW spans a 1230m to 3800m elevation range, compared to an 1800m to 3000m range for the ICB alone. This region experiences a mediterranean climate. Average January daily minimum temperatures ranged from -5°C to 1°C, while average July daily maximum temperatures ranged from 24°C to 25°C (2000-2015; http://www.wrcc.dri.edu/; stations: White Wolf, Crane Flat). Average annual precipitation (Oct-Sep) ranged from 47 to 60 cm (for years 2000-2015), and is dominated by winter snow. The basin is covered by coniferous forests (dominated by *Pinus jeffreyi, Abies magnifica, Abies concolor* and *Pinus contorta*), rocks, meadows and shrublands (dominated by *Ceanothus cordulatus*) (Collins et al., 2007). Mean flow in the Upper Merced River (UMR) at Happy Isles was $10m^3/s$ (for 1965-2015; nwis.waterdata.usgs.gov).

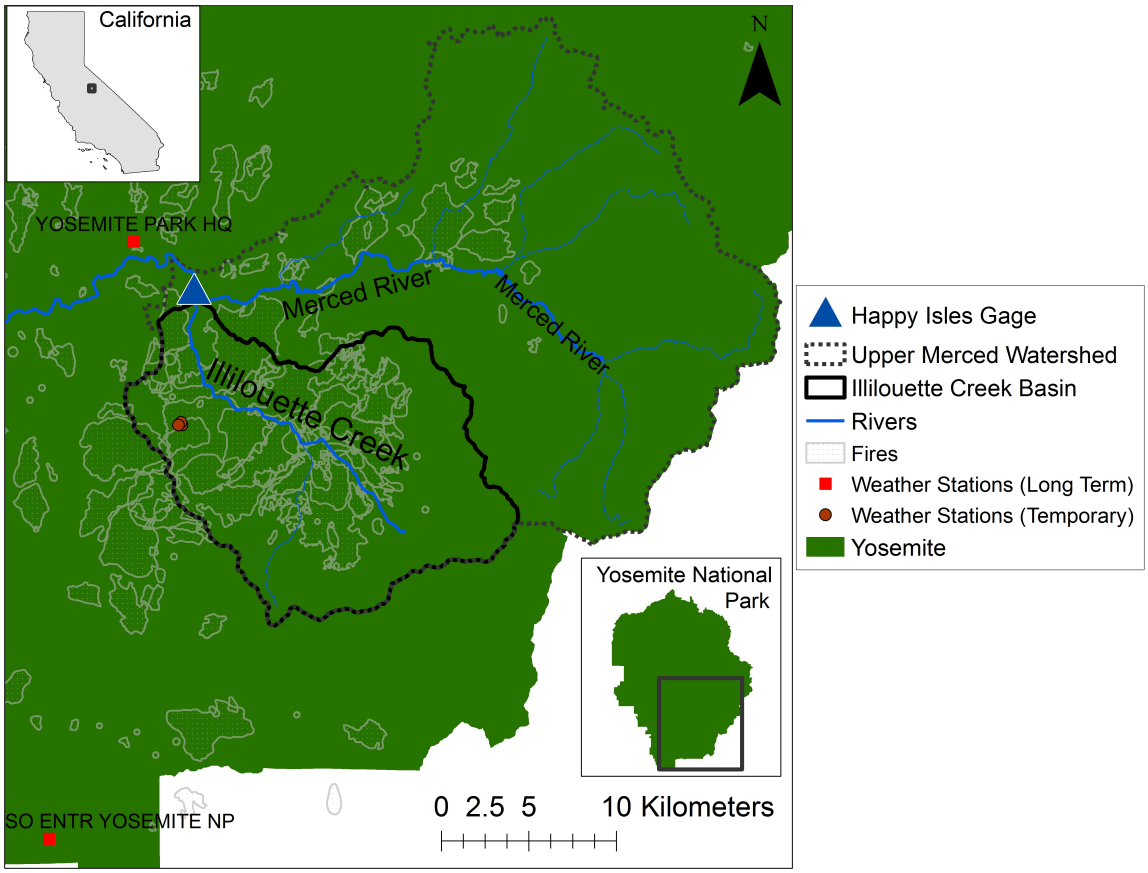

Figure 6.1: Location of the Upper Merced Watershed, Illilouette Creek Basin, the Happy Isles stream gage, and weather stations. The main stems of the Merced River and Illilouette Creek, along with their major tributaries, are also shown. All fires from 1974-2012 are shown with outlines and texture within the fire boundary.

The only long term streamflow data available includes water from areas outside of the ICB, and therefore a hydrologic model such as RHESSys is the only option for estimating streamflow changes for the ICB itself, rather than the full UMW. Although some UMW fires since 1972 have occurred outside of the ICB boundaries, the ICB has a greater percent burned than the UMW overall (Figure 6.1) and thus ICB should have a greater response to the natural fire management program than UMW.

Spatial Data Inputs

The RHESSys model is divided into patches defined by topography. First we used the r.watershed function in GRASS GIS to delineate hillslopes, and then these hillslopes were divided into elevation bands. These elevation bands were created at 100m increments for hillslopes with steep slopes, which are generally high rocky areas far from streams, and 25m

for low slopes, which are generally riparian or meadow areas where we are most interested in capturing finer scale hydrology.

Vegetation is divided into conifer forest, hardwood, shrub, wet meadow, dry grassland, and unvegetated. We used vegetation maps for 1969, 1988, 1997, 2005, and 2012 created from aerial photographs (Chapter 3).

We used Yosemite National Park's 1997 vegetation map to identify riparian areas, wetlands, and exposed bedrock. Soil type is divided into solid rock, talus, riparian, sandy loam, and sand. The sandy loam soil is set deeper in valley areas than on steep slopes, using topographic position index to define valleys versus slopes. Any area labeled as exposed bedrock in the 1997 Yosemite map is set to solid rock, while all other rock areas identified in our 2012 vegetation map (using aerial photographs) are set to talus. Sand patches were identified from aerial photographs using field ground-truth data as a guide. For our purposes, an area is labeled as having "riparian" soil if it is adjacent to a stream channel and has low slope, or if wetland vegetation is present there in the 1997 Yosemite map. This distinction is important because of the routing of groundwater to riparian soils in this implementation of RHESSys.

Vegetation and Soil Parameters

Soil analyses at the locations of temporary weather stations within ICB (Figure 6.1) showed over 87% sand for everything except wetland soil. In the measured wetland, the top 10cm of soil was 71% sand, 10% silt, 6% clay, and 13% organic (Appendix D). At 1m depth, the wetland soil had nearly the same soil texture and percent organic matter (1.3%) as the forest soil. This is consistent with findings in a previous RHESSys study of the Merced Watershed which described the soils as sand or sandy loam (Saksa, 2015). We took this information into account in deciding how to parameterize the model soil.

Ranges for stomatal conductance were altered from commonly used RHESSys parameters based on field leaf porometer measurements (Appendix D.2). Snowmelt parameters (maximum snow energy deficit) were adjusted until the timing of the end of snowmelt-driven flow from the model matched observed snowmelt-driven flow.

We set rock outcrops to have a small soil depth and hydraulic conductivity, while talus has a high depth and hydraulic conductivity (although the individual rocks in a talus slope have low conductivity, the arrangement of boulders in a talus field make it highly permeable on a hillslope scale).

Weather Data Inputs

Precipitation and temperature data from the Yosemite Headquarters weather station (elevation 1225m) were used for initialization runs and calibration of the Upper Merced Watershed (www.ncdc.noaa.gov). Calibration using Illilouette Creek flow was only possible for 2011 through 2015, but Yosemite Headquarters climate data had a high number of missing data points during this time period (240 days) - we therefore used data from the Southern Entrance Yosemite weather station (elevation 1538m) to force the Illilouette Creek model

when simulating years beyond 2010 (www.ncdc.noaa.gov). Southern Entrance weather station data was also used to fill in data gaps in the Yosemite Headquarters data in 2005 and 2006, after adjusting for elevation. Southern Entrance weather data were not used as the primary weather data source for all years because there were too many periods of missing data. Locations of these long term weather stations are shown in Figure 6.1.

Streamflow Data

Daily streamflow data for 1915-2015 from the Happy Isles gage, which measures outflow from the UMW, was downloaded from nwis.waterdata.usgs.gov/.

Stream stage data for Illilouette Creek exists for 2011-2015 (collected and provided by the Yosemite Resources Management and Science Division). The stage is measured using a pressure sensor located under the Illilouette Falls bridge at the outlet of ICB. There is high uncertainty in the actual values of flow volume during high flows, since the stage-discharge relationship calibration is incomplete and no validation flow measurements have been taken during flood events. During the summer months, when Illilouette Creek flow measurements are most accurate, measured flow from ICB accounted for 29% of the flow at Happy Isles (recall that ICB covers 32% of the area of UMW).

This modeling project uses Happy Isles gage data for initial calibration, and this calibration is then refined by requiring that certain flow metrics captured by the Illilouette Creek data are accurately represented.

Model Initialization

Although remotely sensed products for leaf area index (LAI) exist, we do not have reliable measures of LAI for the pre-fire conditions. Because of this, we relied on the model's built-in vegetation growth processes to determine spatial variations in LAI. Before calibration, the model was initialized by running for 400 years - beginning with an unvegetated state - in order to allow vegetation to grow and carbon and nitrogen stores to develop in the soil. Following preliminary calibration, the model ran again until vegetation growth and decay reached an equilibrium. We compared the resulting LAI values to values estimated within forestry plots in the ICB (Collins et al., 2016) using field measurements of tree diameter, height, and species in allometric equations (John Battles, personal communication). We did not expect modeled and measured LAI to agree perfectly due to differences in spatial scale between the model and the field measurements, but the comparison allowed us to verify that initialized LAI values were within the ranges measured in the field. We altered parameters for conifer vegetation (including maximum LAI and specific leaf area) until the model gave plant heights and LAI values which were within the ranges measured at vegetation plots within ICB.

Calibration

RHESSys is generally calibrated using observed streamflow by varying a limited number of soil parameters which control the rate at which water travels from soil into the stream. For this project, it was deemed essential to capture snowpack dynamics accurately since fire-altered landscapes are predicted to greatly affect snow accumulation and melt rates. Therefore, in addition to calibrating soil properties we also calibrated the lapse rates which control temperature and precipitation across the watershed. Such a calibration is necessary because temperature and precipitation patterns in the Sierra Nevada are highly spatially variable, and accurate interpolation of these values is therefore challenging.

Initial calibration of lapse rates

In this implementation of the RHESSys model, precipitation and temperature vary with elevation via a constant lapse rate (LR). Precipitation increases with elevation via the equation

$$P_i = P_b * (1 + LR_P * (elev_i - elev_b))$$

where P_i and $elev_i$ are the precipitation(m) and elevation(m) at location i, respectively, P_b(m) and $elev_b$(m) are the precipitation and elevation at the base weather station, and $LR_P(\mathrm{m}^{-1})$ is the lapse rate of precipitation.

Temperature is given by

$$T_i = T_b - LR_T * (elev_i - elev_b)$$

where $T_i(^\circ\mathrm{C})$ is temperature at location i, $T_b(^\circ\mathrm{C})$ is temperature at the base weather station, $elev_i$ and $elev_b$ are the elvations at location i and the weather station (in meters), and $LR_T(^\circ\mathrm{C/m})$ is the lapse rate of temperature with elevation.

We calculated temperature and precipitation lapse rates between Yosemite Headquarters weather data and both our own temporary weather stations (Figure 6.1, Appendix D) and temperature sensors installed in other parts of the Upper Merced Watershed available from the University of Washington for 2001-2005 (Lundquist and Cayan, 2007). The temporary weather stations gave median lapse rates of 0.007°C/m for mean daily temperature and $0.00\mathrm{m}^{-1}$ for precipitation. These lapse rates were highly variable and were not constant throughout the year (precipitation lapse rate, for example, ranged from $-0.001\mathrm{m}^{-1}$ to $0.036\mathrm{m}^{-1}$). For the Upper Merced temperature data, median lapse rate for temperature was 0.005°C/m. Temperature lapse rates were strongest in the spring and summer (when temperature is important for controlling snow melt), and were as high as 0.02°C/m. We found similar seasonal trends and lapse rate values when comparing Yosemite headquarters weather to the higher elevation Southern Entrance station. We chose to hold lapse rates constant in time for simplicity, but to keep them similar to rates observed during the period of spring snowmelt rather than using an annual average. We used these calculated values to set the acceptable ranges for calibration.

Keeping all other parameters constant, we calibrated temperature and precipitation lapse rates independently, selecting potential lapse rates within a realistic range according to our calculated lapse rates.

We calibrated temperature lapse rate based on achieving the best match of the timing of snowmelt peaks in the observed hydrograph. Our final temperature lapse rate is 0.008°C/m.

Based on a preliminary analysis using Airborne Snow Observatory data (www.aso.com) we decided that we would capture snowfall patterns most realistically by setting the precipitation lapse rate to be 0 for elevations above 2800m (Brant, pers. comm.). We calibrated the precipitation lapse rate such that error in total annual streamflow was minimized. The final precipitation lapse rate (for elevations $\leq$ 2800m) is 0.00015/m. Precipitation at all elevations above 2800m was set to be equal to precipitation at 2800m.

Calibration of soil properties using streamflow

Some potential calibration data can be disinformative; for example, there is no possibility of the model capturing an observed snowmelt pulse caused by localized rainfall not captured by a weather station (Beven and Westerberg, 2011). Rather than insist on capturing storm flows with high accuracy, which is often not possible given the limited spatial coverage of observed weather data, we focused on matching summer low flows, total flow volumes, timing of the snowmelt pulse, and the timing of summer drawdown. These calibration steps, as well as information on the input data required for the calibrations, are shown in Figure 6.2.

Using a Monte Carlo calibration method, we explored the parameter space for five soil parameters: decay of hydraulic conductivity with depth (m), saturated hydraulic conductivity at the surface (K), soil depth (sd), the proportion of saturated soil water routed to groundwater (gw1), and the proportion of groundwater routed directly to streamflow (gw2). Fit was determined based on multiple criteria, including total percent error in streamflow, percent error in August streamflow, Pearson correlation coefficient (r^2) of both daily flow and mean monthly flow (the mean within each month taken over all years), Kling-Gupta Efficiency (KGE) of 3-day average streamflow, Nash-Sutcliffe Efficiency (NSE) of monthly average flow, and error in the timing of the streamflow center of mass (the day within each October-September water year when half of the water year's streamflow has passed).

NSE is a commonly used measure of the fit of data to observations which normalizes mean squared error (MSE) by the data's variance, but the NSE can lead to underestimating the variability of flows and is sensitive to large peak flows (Gupta et al., 2009). By contrast, KGE simultaneously optimizes the fit in terms of bias, ratio of modeled to observed variability, and the correlation coefficient (Gupta et al., 2009). For both NSE and KGE, a value of 1 is the maximum possible value and indicates a perfect fit to observed data.

Table 6.1 shows the ranges in m, K, depth (sd), gw1, and gw2 parameters for all soil types. The ranges for calibration were chosen based on previous modeling studies in this area as well as literature ranges for the types of soils found in ICB (Saksa, 2015). For each run in the Monte Carlo calibration, we randomly selected the coefficient for each parameter from a uniform distribution within these ranges.

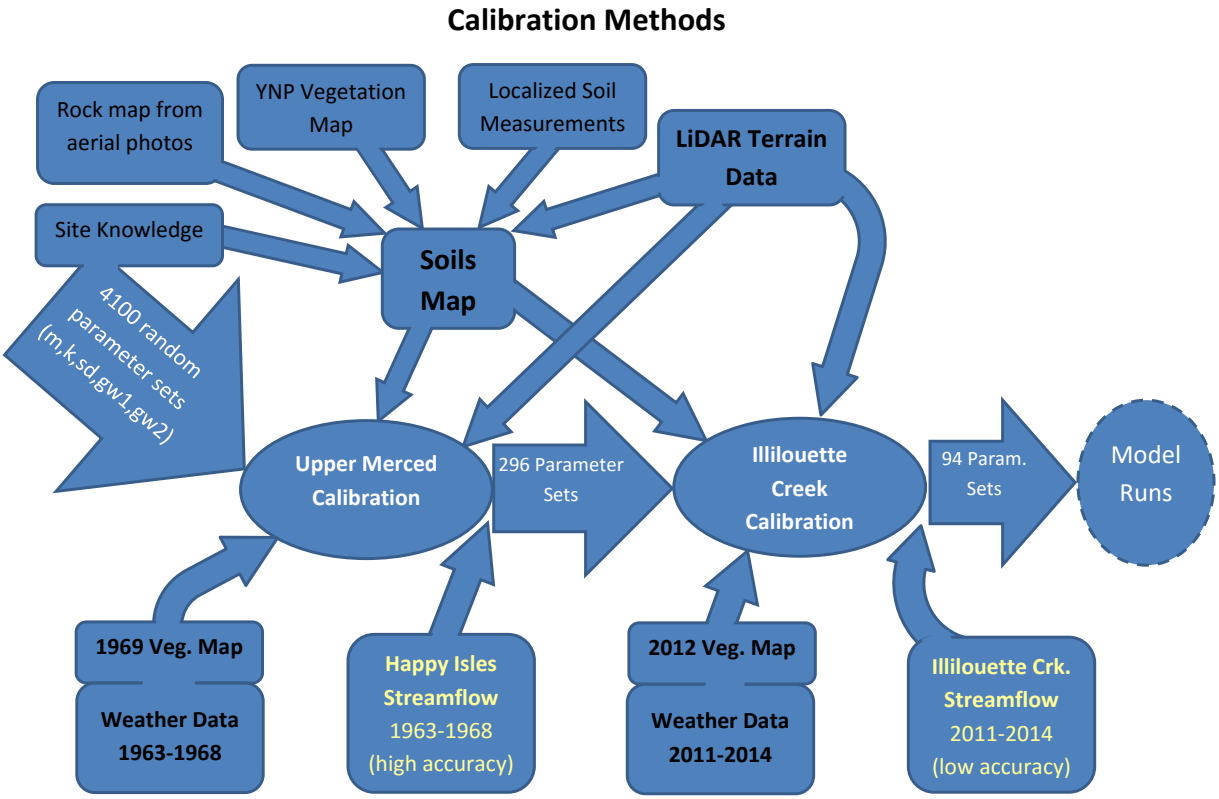

Figure 6.2: Flow chart of the methods for calibrating the RHESSys model. Input data are shown in black text, calibration steps in white text, and data used for the calibration in yellow. The calibration was done in two steps because our most high quality streamflow validation data is from the Happy Isles stream gage, which measures Upper Merced River streamflow, but our main area of interest is the Illilouette Creek sub-basin for which we do not have high-fidelity streamflow data.

I used years 1963-1968 for calibration to Happy Isles flow because this period did not experience any fires (which would complicate the calibration) and included a range of both relatively wet and relatively dry years with few missing data points for either streamflow or weather.

The best performing parameter sets from the Happy Isles calibration were then used in a calibration using Illilouette Creek flow only for 2011-2015. Given the limitations of the flow data available at Illilouette Creek, the purpose of this step was to exclude any parameter sets which did not accurately model the timing of flows and approximate low flow values. I removed year 2015 from the ICB calibration because flows during this extreme drought period were very low and dominated by peaks caused by individual storms. The model does not necessarily capture individual storms well due to the heterogeneous nature of precipitation in the Sierra Nevada, and thus the model was not expected to fit 2015 flow well.

After an initial calibration, the model was run again using the highest-performing calibrated set of soil parameters (using monthly KGE) for over 100 years until vegetation growth and decay reached equilibrium. Once the UMW calibration was complete, I initialized ICB separately, using the same calibrated parameter set after setting the soil carbon and nitrogen pools equal to the values from the UMW model following its initialization.

Rather than select only one parameter set from the calibrations, I kept all parameter sets that met certain criteria in terms of fitting the observed data. This facilitates tracking the sensitivity of the model results by comparing results under a range of realistic parameters. Using this range of results, prediction quantiles are estimated using the generalized likelihood uncertainty estimation (GLUE) method (Beven and Binley, 1992). GLUE accounts for the fact that different parameterizations may affect a model differently at different times in the hydrologic record. GLUE calculates the distribution of the likelihood of a modeled value by combining the likelihoods of models using many different parameter sets. In this way, GLUE incorporates the effects of autocorrelation between parameters and model nonlinearities implicitly.

Type	m(1/m H_2O)	K(m/d)	sd(m)	gw1	gw2
Sandy Loam Valleys	0.012-3.0	1-1000	0.25-12.5	0.0-0.25	0.0-1.0
Sandy Loam Slopes	0.012-3.0	1-1000	0.1-5	0.0-0.25	0.0-1.0
Riparian	0.009-2.25	0.8-800	0.5-25	0.0-0.05	0.0-1.0
Sand	0.012-3.0	1.5-1500	0.3-15	0.0-0.4	0.0-1.0
Solid Rock	0.012-3.0	0.00001-0.01	0.01-0.5	0.0-0.99	0.0-1.0
Talus	0.001-0.25	3-3000	0.6-30	0.0-0.8	0.0-1.0

Table 6.1: Ranges of possible values of the five calibrated parameters for each soil type.

Validation

Calibrations were validated both in terms of time series and spatial output. The time series validation uses fit metrics such as Nash-Sutcliffe Efficiency and total error for model output for the full period 1965-2015. For the spatial output, two qualitative checks were also performed:

I also compared modeled soil moisture to measured surface soil moisture (Chapter 4). The RHESSys model output for soil moisture, θ, gives the percent saturation of the soil. While θ includes the entire soil depth, our measured VWC values cover only the top 12cm. RHESSys model output is also aggregated to larger spatial scales than our manual measurements. Although these differences between modeled patch θ and measured surface VWC preclude a direct comparison for validation, there should still be a positive correlation between the two if RHESSys is successfully capturing large-scale spatial variability in soil moisture for the ICB. As a qualitative validation, I also verified that areas with especially high measured VWC were represented in the model as having above-average soil moisture.

To verify that the RHESSys model produced realistic timing of snowmelt, I qualitatively compared summer Landsat images to model output of percent snow cover. Because Landsat is only available on an eight day interval, and there is not always snow-free imagery available during the final stages of snowmelt, I could not compare the exact day of snowmelt completion, but I could verify that snow cover reached zero within the correct interval of 2-3 weeks.

Model Runs

RHESSys was used to evaluate the effects of fire-altered vegetation on the water balance via three separate model experiments. Figure 6.3 lists the vegetation maps, fire effects, and basin boundaries used for the paired runs in each experiment.

The first run, "UMW Historical", tests whether the model is accurately capturing the impact of fires on UMW by comparing modeled and observed streamflow from the Upper Merced River under burned and unburned conditions. If the model is accurately capturing the impact of fires on this watershed (and fires have a measurable effect), then we expect error to decrease when fires are included in the model. For the burned conditions, the run begins with the 1969 vegetation map and incorporates historical fire effects on vegetation and litter into the model over time as described below. For the unburned conditions the 1969 vegetation map stays unchanged for the entire model run and litter stores accumulate and decay without any disturbance. This run also serves to model changes to the water balance over time in response to repeated wildfires, both over time and across the spatial extent of the watershed.

The second run, "ICB Historical", compares burned and unburned conditions in the same way as before but only within the boundaries of ICB. The purpose of this run is to model the changes to the water balance that historical fires have caused over time.

The final model experiment, called "ICB Extremes", compares model results using the 1969 vegetation map to results using the 2012 vegetation map (which represents the largest deviation from 1969 vegetation cover). The ICB Extremes run does not include time-varying changes due to fire. Rather, it investigates the potential effect of the post-fire land cover on water balance over a range of weather conditions, rather than attempting to reconstruct historical timeseries of hydrologic variables.

For each model run, I calculated mean output as well as 95% confidence intervals (obtained from GLUE) for multiple hydrologic variables (streamflow, ET, etc.). I considered two model scenarios (i.e. burned vs unburned) to be significantly different if the 95% confidence intervals did not overlap. An alternate approach to defining statistical significance considers only the *change* between two model versions. For each parameter set, the unburned values are subtracted from the burned values, giving a set of 93 differences for which the mean and 95% confidence interval can be calculated. If the 95% confidence interval for changes includes zero, then there is no statistically significant change. It is important to note the distinction between these two measures of significance: If two *scenarios* are *statistically different*, this means that the range of all likely outcomes for the burned scenario is separate from the range of all likely outcomes for the unburned scenario. In contrast, if the *changes* from unburned to burned are *statistically significant*, this means that using any realistic model parameters it is likely that there is a non-zero change between the unburned and burned scenarios.

Incorporating Fire

In the UMW Historical and ICB Historical model runs, I incorporated historical fire data directly into the model in order to create as realistic as possible of a representation of the vegetation change over time (the "Burned" scenarios with "True Veg" in Figure 6.3). To represent the effects of fire within the RHESSys model, the following changes were imposed: for all fires, regardless of severity, all litter and dead wood is consumed within the fire perimeter. Additionally, in moderate severity burn areas 50 % of live plant carbon is consumed, and in high severity burn areas 100% of live plant carbon is consumed. In high severity burn areas, vegetation type post-fire may change according to our vegetation maps.

All vegetation changes due to fire were applied over one day in the model, rather than spreading them out over the days to months that an actual fire might burn. These methods are obviously an oversimplification of actual fire dynamics. For example, Collins et al. (2016) found that post-fire fuel loads were not well correlated with fire severity or time since fire, but rather depended on overstory canopy. The same study, however, noted a uniform reduction in surface fuels associated with the re-introduction of fire to the ICB (Collins et al., 2016). Although this modeling strategy does not represent detailed changes in litter, understory, and stand structure (all of which are important to hydrology but difficult to represent accurately based on available data), it captures the observed large-scale changes that affect interception, energy balance, and transpiration.

Fire perimeter data were obtained from a digital fire atlas (irma.nps.gov/Portal). The fire atlases are a best approximation of actual burn perimeters, but do not provide information

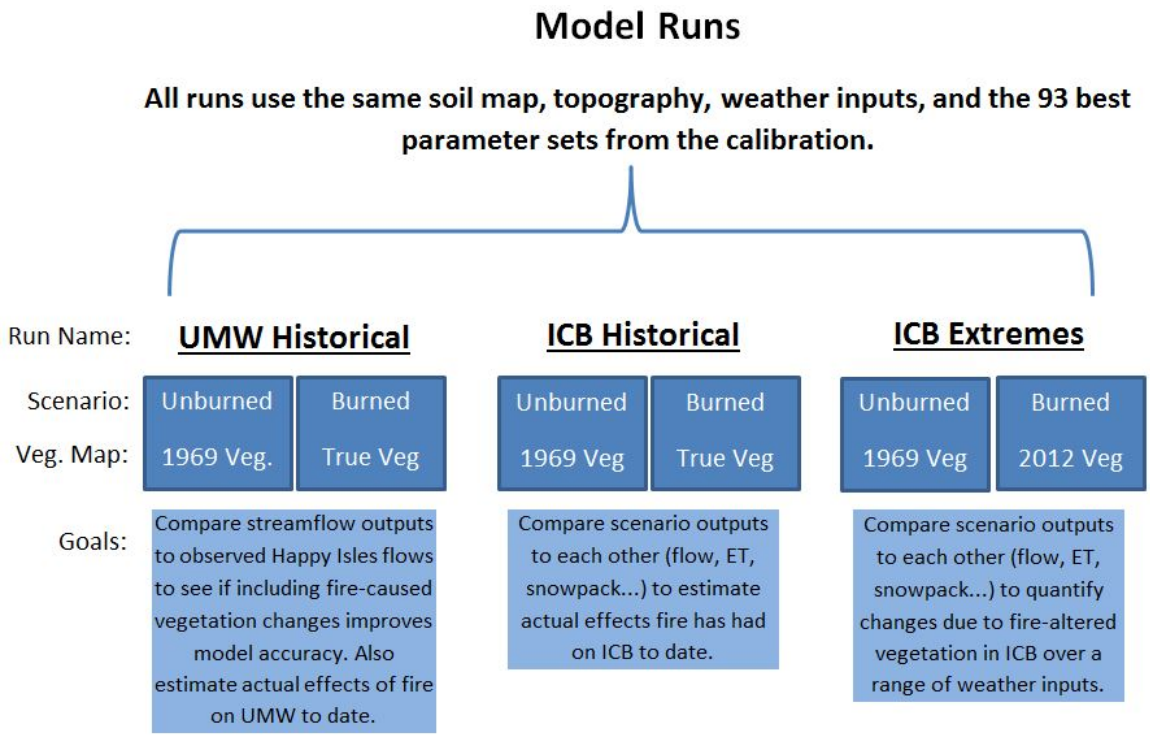

Figure 6.3: The three model runs use either the full Upper Merced River Watershed (UMW) or the Illilouette Creek Basin (ICB) which is one of its subbasins. The runs within each watershed either use the 1969 vegetation map (representing fire-suppressed conditions), the 2012 vegetation map (representing the present-day fire altered landscape), or True Veg (which incorporates fire-induced changes over time). All model experiments are run for the period 1965-2015.

on the spatial heterogeneity of burning within fire areas (Morgan et al., 2001). When possible, we used satellite-based estimates of fire severity to characterize heterogeneity within fire areas. For fires that occurred in 1984 or later (n = 20) we used a relative version of the differenced Normalized Burn Ratio (RdNBR), derived from Landsat Thematic Mapper images to divide the fire into severity classes (Miller and Thode, 2007). Fire severity data for fires prior to 1984 (n=12) was estimated using RdNDVI (see Chapter 4).

A preliminary study by Ian McGregor showed that high fire severity (as measured by Landsat) often did not predict where vegetation type would change, showing that we cannot rely solely on RdNBR severity maps to delimit areas of land cover change (Ian McGregor, pers. comm.). This may be partially due to different vegetation types not always behaving the same in terms of RdNBR, as well as the RdNBR maps being at a relatively coarse 30m resolution. It is also possible for fast vegetation regrowth following fire, or delayed mortality of fire-stressed trees, to cause inaccuracies in severity estimates based on remote sensing. In order to compensate for the observed discrepancies between high severity maps and maps

of stand-replacement, any 100m^2 pixel within a fire perimeter that experienced a change in vegetation type according to our vegetation maps was classified as high severity, regardless of RdNBR or RdNDVI. For areas that were classified as high severity using Landsat but showed no change in our vegetation maps, we assumed that the vegetation burned at high severity but then the same vegetation type grew back.

In summary, for each year which contained a fire over 100ha, we removed litter and carbon stores according to fire extent and severity. For high severity pixels, we set the new vegetation type to the vegetation from whichever map came soonest after the fire but was from imagery taken at least two years following the fire (for example, for fires in 1986 we used the 1997 vegetation map to determine what type of vegetation would regrow, rather than the 1987 map - see Figure 3.4c). We then allowed the vegetation to grow normally until either another fire burned through or the simulation ended.

The outputs evaluated from each model experiment include: streamflow volume and timing, evapotranspiration, subsurface water storage (unsaturated plus saturated stores), snowpack depth and timing, and climatic water deficit (PET-ET, a measure of how much water stress vegetation is experiencing). Whenever possible, values are divided by the watershed area in order to give a value in terms of water depth (mm) or a depth per unit time (mm/day or mm/year).

6.3 Results

Calibration

In the UMW calibration, 296 of the original 4100 randomly selected parameter sets were selected according to the criteria given in Table 6.2. These criteria were selected after testing many different measures of fit and finding those that consistently produced model results that appeared to match flows well and also captured qualities of the streamflow that were important to our research questions.

Measure of Fit	Criteria
3-day filtered flow KGE	>0.75
3-day filtered log of flow KGE	>0.5
monthly NSE	>0.85
total error in summer flows	<50%
error in total streamflow volume	<10%
mean error in February flow volume	<40%
mean error in the center of mass	<8 days

Table 6.2: Fit criteria for calibration to UMR flow.

We imposed additional criteria based on the calibration to the ICB data: mean error in center of mass <6 days, monthly correlation coefficient >0.85, total error in summer flows

<100% (proportional errors for summer are allowed to be large since mean summer flows are <1 mm/day in ICB. Summer ICB flow accounts for ≈ 30% of UMR's summer flow, but only 5% of UMR's annual flow), KGE of mean September flow >0.6, correlation coefficient of water year flow >0.3, and total error in September flow <50%. These criteria were selected by examining the distributions of errors for all calibration runs. We did not use any criteria, such as daily KGE, which require matching high flows well because of the uncertainty in the observed high flow data for Illilouette Creek. Based on these criteria, the 296 parameter sets were reduced to 93.

Validation

To verify the accuracy of the models, the unburned UMW model was compared to observed streamflow for water years 1966 through 2015, using a variety of measures of fit and all 93 of the final parameter sets. These measures of fit are given in Table 6.3.

Measure of Fit	Poorest	Best
r^2 of mean monthly streamflow	0.96	0.98
r^2 of daily flow time series	0.64	0.70
NSE of annual streamflow time series	0.88	0.91
NSE of mean monthly streamflow	0.89	0.94
NSE of year-to-year variation in August streamflow	0.28	0.58
NSE of log of daily streamflow time series	0.55	0.68
KGE of daily flow time series	0.56	0.65
KGE of log of daily streamflow time series	0.28	0.70
KGE of mean September flow time series	0.65	0.73
% Error in mean of annual max daily flow	61%	35%
Total error in summer flows (July-October)	70%	31%
Mean error in center of mass date	9.4 days	6.0 days

Table 6.3: Accuracy measures comparing unburned modeled streamflow for UMR to observed flow for water years 1966 through 2015. The poorest fit and best fit measures are shown across all 93 parameter sets.

Overall, the model produced slightly more variable runoff than the observed flow, but matched late summer flows and the timing of the snowmelt pulse well (Figure 6.4A). Daily observed and modeled flow are strongly correlated, although there are individual days with high error, and low flows tend to be overestimated (Figure 6.4B).

It is difficult to directly compare our soil moisture measurements to soil moisture given by RHESSys because of the different scales. Nevertheless, when we compared our manual soil moisture measurements (averaged within each patch) to θ values (soil's percent saturation) given by RHESSys there was a positive correlation (Pearson's correlation coefficient of 0.40-0.51 for June of 2015, depending on which parameter set used).

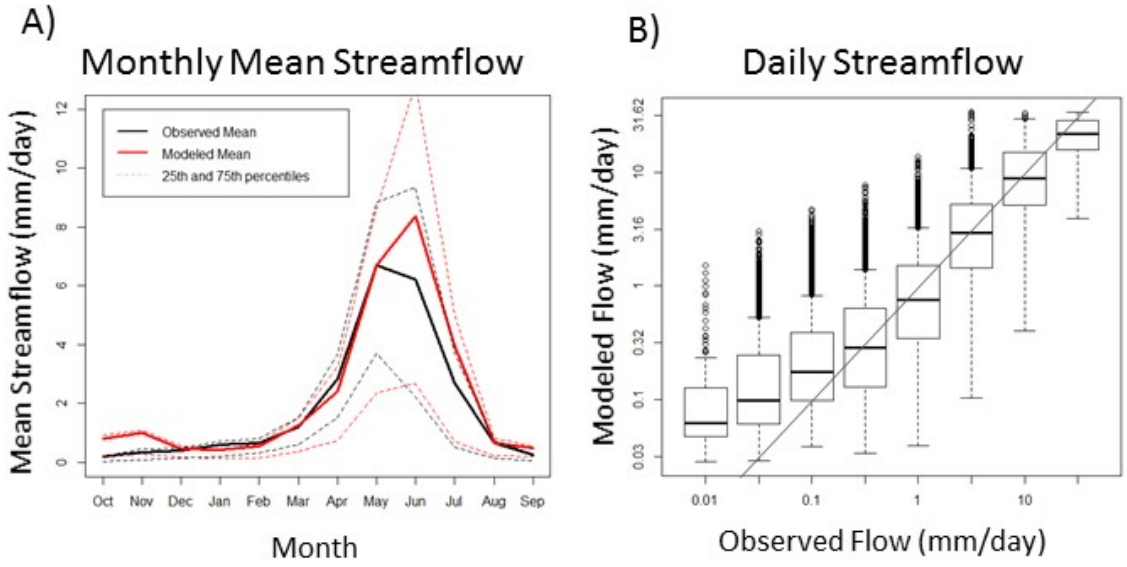

Figure 6.4: (A) Mean daily flow across all years within each month for both observed UMR flow (black) and modeled UMR flow (red). Dashed lines give the 25th and 75th percentiles of flow in each month across all years. The model results shown here are for the parameter set that had the best correlation with monthly mean streamflow. (B) Binned data showing daily modeled vs. observed streamflow on a log scale, compared to a 1:1 line. There is a strong correlation in daily flows but the lowest flows are overestimated. The model results shown here are for the parameter set that maximizes KGE of the log of daily streamflow.

Using a subset of five years to validate snow cover, I successfully verified that the final day of snowmelt occurred in the correct 2-week interval when compared to Landsat imagery.

Model Runs

All of the following results are averaged across 93 model runs (using the 93 different parameter sets described in the calibration results).

UMW Historical

The model ran from water years 1972 through 2015 after a six year initialization. In one version vegetation cover remained the same as in 1969, representing a fire-suppressed, or "unburned", scenario. The other version included fire activity and changing land cover beginning in 1974, the "burned" scenario (32 fires in UMW during this period). The largest fires occurred in 2001 and 2004 (over 2000ha each). There were also large fires (400ha-1600ha) in 1974, 1980, 1981, 1988, and 1991 (Figure 3.4c). If the model is accurately capturing the

Metric	Unburned Mean ± Standard Deviation	Burned Mean ± Standard Deviation
NSE of smoothed flow filtered by month	0.65 ± 0.02	**0.66** ± 0.02
NSE of daily flow	0.367 ± 0.031	**0.373** ± 0.031
KGE of daily flow	**0.603** ± 0.018	0.600 ± 0.017
NSE of mean monthly flow	0.918 ± 0.011	**0.922** ± 0.010
NSE of September flow	**0.360** ± 0.13	0.352 ± 0.13
Correlation (r^2), daily flow	0.788 ± 0.007	**0.789** ± 0.007
Correlation (r^2), mean monthly flow	0.970 ±0.004	**0.972** ± 0.004
Mean percent error in summer flow	57 ± 6	57 ± 6
Mean error in annual max flow (mm)	6.2 ± 1.0	6.2 ± 1.0

Table 6.4: Measures of fit for the burned and unburned scenarios in UMW for 1972-2015. Mean and standard deviation are measured for the 93 calibrated parameter sets. For each metric, the best fit is given in bold.

effects of fire, we would expect the burned model to match observed data better than the unburned model does.

Various metrics show a slight improvement in the model fit to observed data between the burned and unburned scenarios (Table 6.4).

The maximum increase in peak flow under the burned scenario (across all days and all calibrations) was 7.7mm, which is 16% of the maximum daily flow recorded during this period (47.1mm/day). In some years, the burned scenario produced lower peak flows than the unburned scenario, contrary to expectations.

There was no statistically significant difference in the total error in streamflow volume for the burned or unburned models at the UMW level (Figure 6.5). On average, the total water year flow modeled with fires was higher than that modeled without fires. For all but three years, the error in water year flow (observed flow subtracted from modeled flow) was greater in the burned scenario than the unburned scenario, though this difference was very small, not statistically significant, and likely driven by a positive bias in modeled annual streamflow for both model scenarios (less than 4% of annual flow).

Including fire in the watershed slightly decreased the error in center of mass timing in most years for most parameterizations (Figure 6.6). The only statistically significant improvement in timing ($p<0.05$) was in water year 2015, a drought year following 40 years of managed wildfire. In 2015, timing was improved by 4 days when fire was included (an error of 6 days vs. an error of 10 days when fire was not included).

In contrast to the differences in error, there were significant differences in total flow between the burned and unburned scenarios from 2001 onward (Figure 6.7A). The change from unburned to burned is significant in the first year following fire (1975), then there is less certainty, and after the 2001 fire the change is again statistically significant ($p<0.05$).

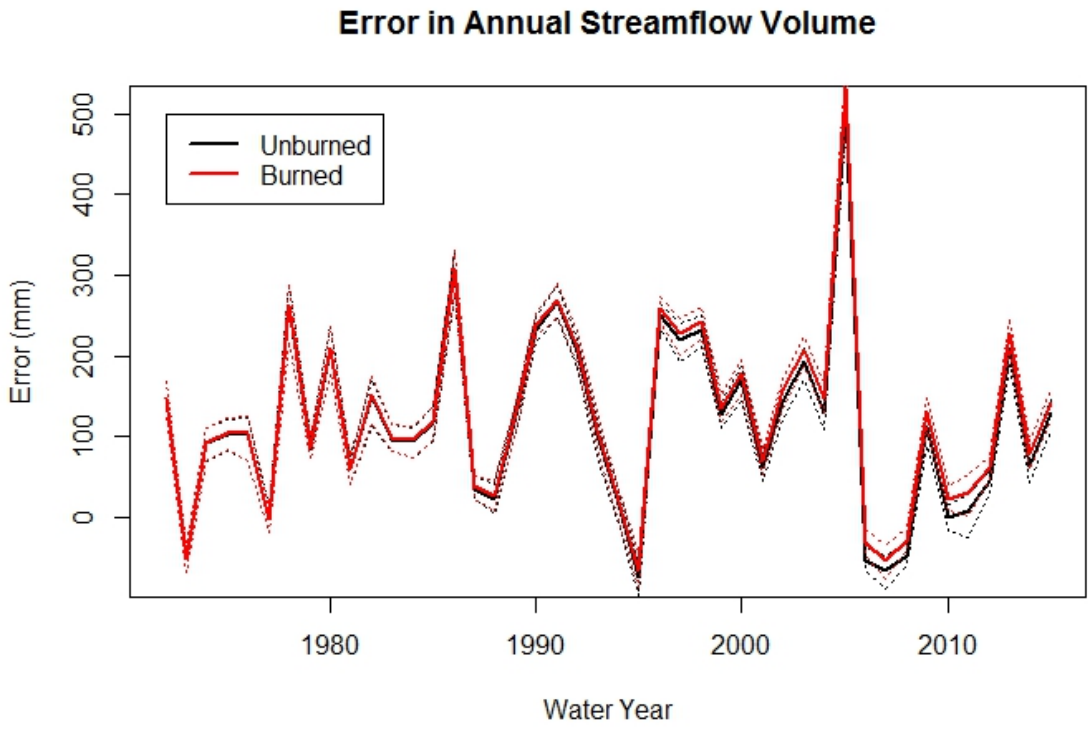

Figure 6.5: Error in total streamflow from UMR for each water year using the burned and unburned models. Dashed lines give 95% confidence intervals. Observed streamflow over this period ranged from 162mm/year to 1530 mm/year, with a mean of 695mm/year (1.9mm/day).

Climatic water deficit for UMW also decreased significantly for most years following 2001 (Figure 6.7B).

Summer water availability is largely driven by snowpack feeding streams and groundwater stores (Godsey et al., 2014). From October through March the model predicts more snow in the burned versus the unburned model for most years (Figure 6.8), but this increase is not spatially uniform (Figure 6.9). In April through July, in contrast, the model predicts less snow water equivalent (SWE) on average (Figure 6.8). This matches field observations of higher snowpack in burned areas of ICB compared to dense forest stands in February and March of 2016 (Appendix D). According to the model, spring snowpack changes are highly variable both between years and between patches. For example, in May 2015 (a drought year) most burned patches have either more snow or no change compared to the unburned scenario, while in 2011 (a fairly high precipitation year) many burned patches experience a decrease in snow cover compared to the unburned scenario (Figure 6.10).

Like snowpack, changes in soil moisture are spatially heterogeneous (Figure 6.11). Fire

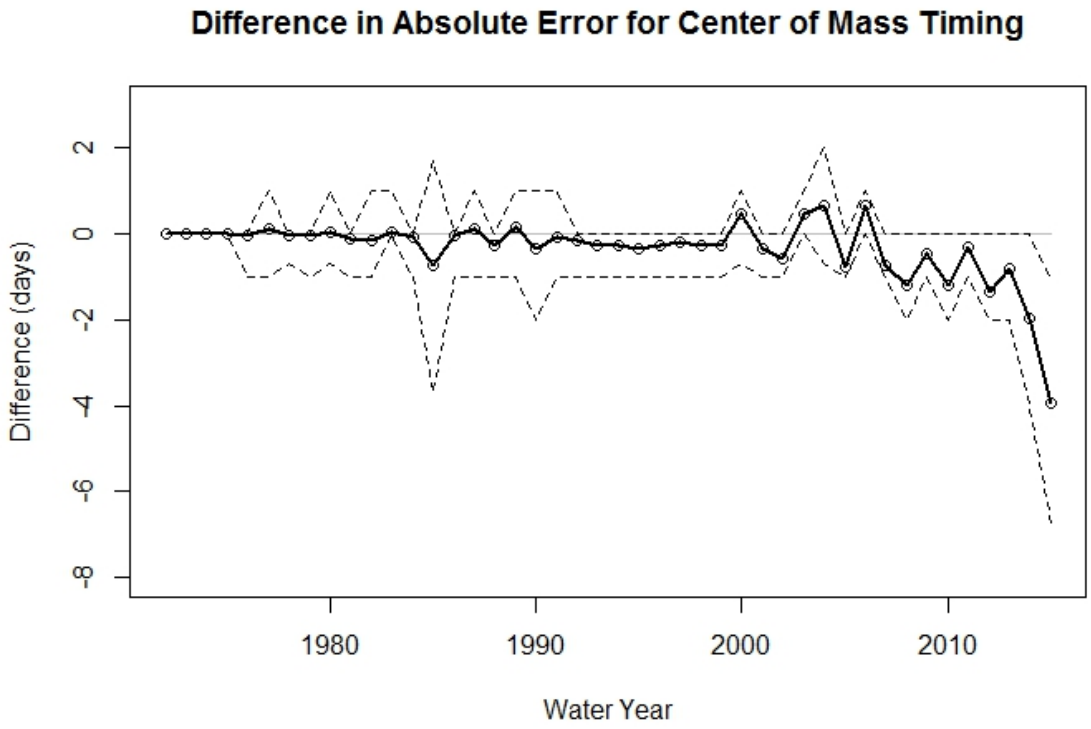

Figure 6.6: Change in absolute error in center of mass between the burned and unburned models for UMR. A negative value indicates that the burned model was closer to the true date of center of mass in the streamflow. Dashed lines give 95% confidence intervals.

changes summer 2015 volumetric water content in individual patches (θ, ranging from 0-1) from +0.75 to -0.76, depending on the patch.

The model predicts statistically significant increases in runoff ratio ($p<0.05$) from year 2001 onward (Figure 6.7C). By year 2015, runoff ratio is 4.3% higher than if fire suppression had continued, according to the model.

Annual transpiration for the whole UMW was significantly lower under burned conditions beginning in year 2001 (not shown). Annual evaporation was also lower on average in the burned model, but this difference was not statistically significant.

ICB Historical

In the following model runs, I compare model output for ICB from the burned scenario, which incorporates fire effects over time (21 fires in ICB from 1974 through 2004), to the unburned scenario in which vegetation cover is not altered by fire. This run is distinguished from the UMW historical run in that all results are reported at the scale of the ICB, where most of the vegetation change is concentrated.

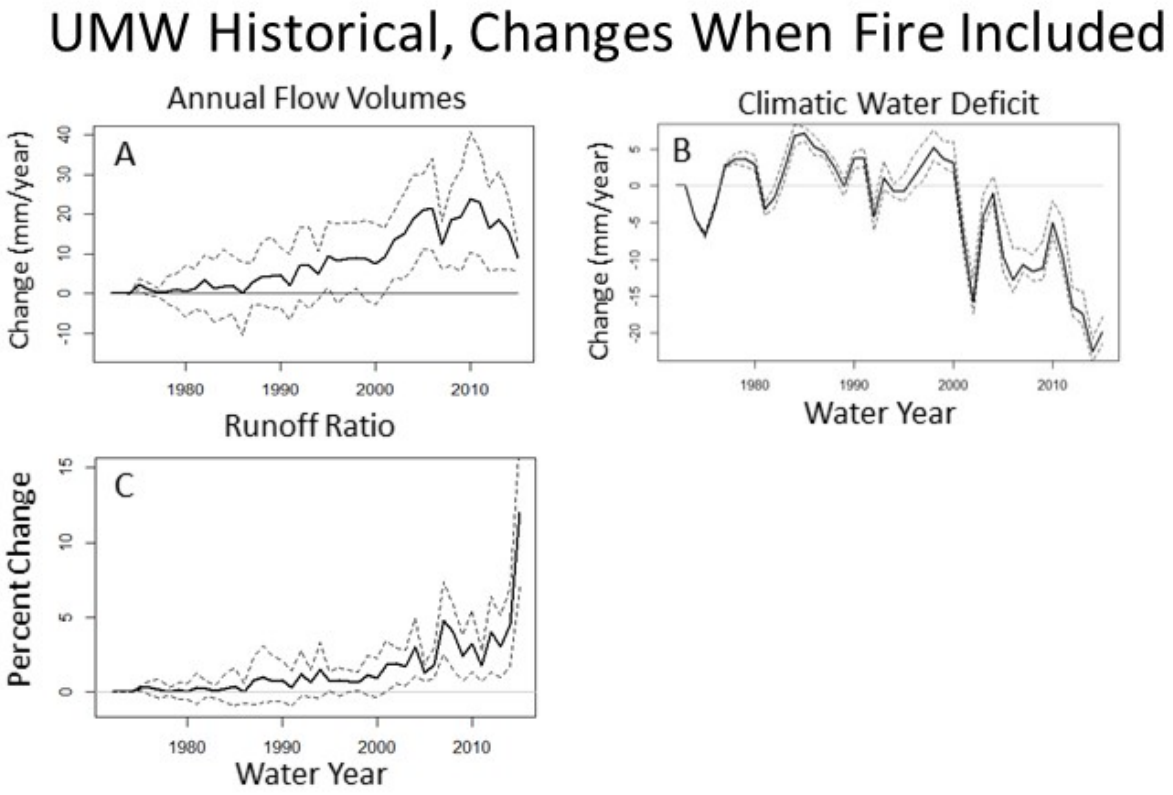

Figure 6.7: Results from the UMW historical run showing (A) change in total annual flow between unburned and burned scenarios, (B) change in annual total climatic water deficit, and (C) percent change in runoff ratio. Dashed lines give 95% confidence interval.

The models show sharp decreases in climatic water deficit following most fires, and a persistent decrease in climatic water deficit in the burned compared to the unburned scenario from 2001 onward (Figure 6.12E).

Soil evaporation was highly variable between model calibrations, and there was no significant difference between the ranges of soil evaporation in the burned and unburned models. Looking at the change in burned and unburned models using the same parameters, however, suggests that soil evaporation effects of fire varied over time; Initially soil evaporation decreased and then after 2012 there was a significant increase (Figure 6.12A). Annual transpiration was lower in burned compared to unburned models once fires began in 1974; this difference was statistically significant ($p<0.05$) for 2005-2006 and 2009-2011 (Figure 6.13), while the change in transpiration was statistically significant beginning in 1991 (Figure 6.12B).

Subsurface water storage in the ICB was highly sensitive to the parameter sets used. However, looking only at the change from unburned to burned using the same parameter sets shows a clear upward trend in this change (Figure 6.12D). This increase reaches the 95%

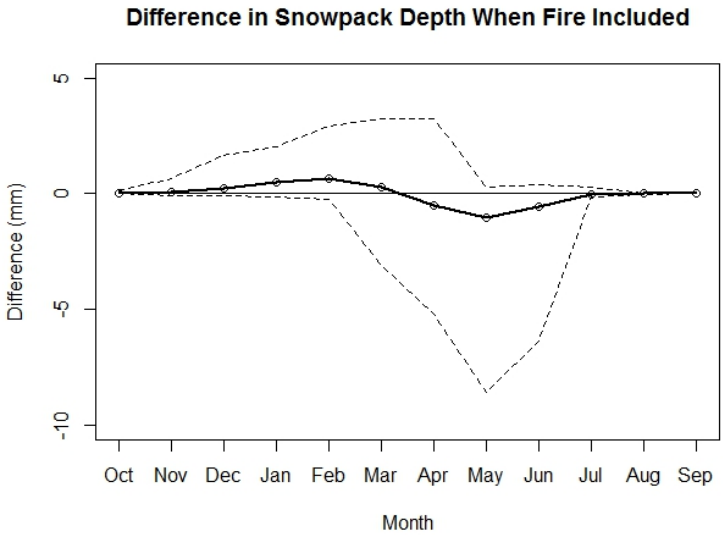

Figure 6.8: Mean change in monthly mean snowpack in UMW due to fires (a positive value means deeper snowpack using the burned model than in the unburned model). Dashed lines shown the range of the middle 95% of differences across all years (for 95% of years, or 47 out of the 50 years, the difference in snowpack was between these two lines).

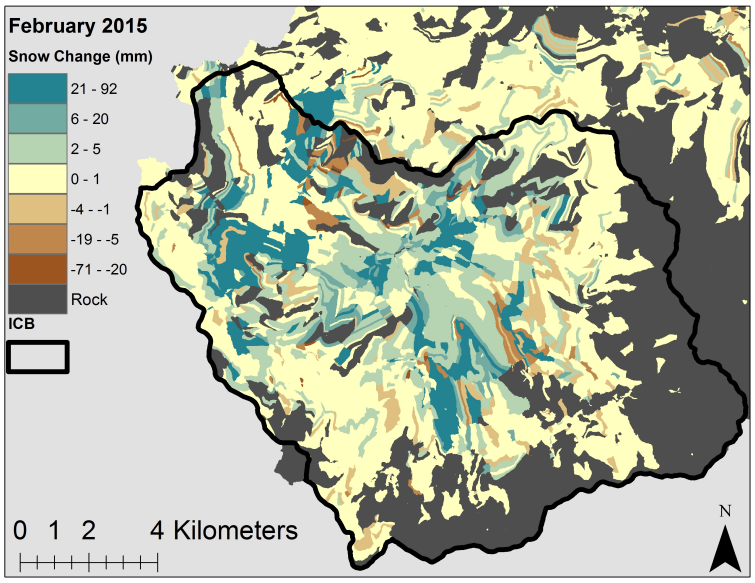

Figure 6.9: Map of change in snow depth for February 2015 when historical fires are included in the model, showing the entire ICB and a portion of the rest of the UMW. Most patches within ICB have increased snowpack in the burned scenario. The portion of UMW that is not shown consists mostly of exposed bedrock which is not affected by burning.

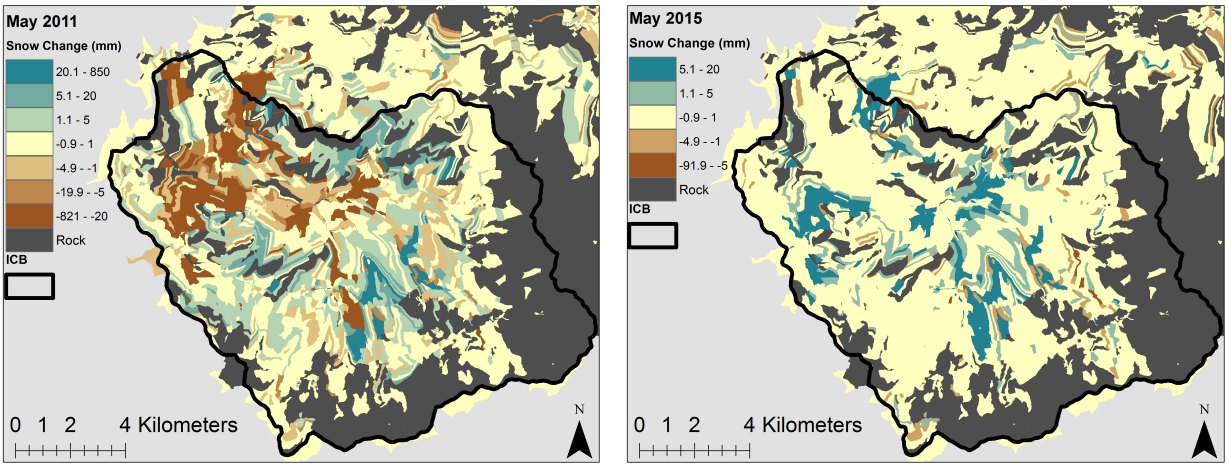

Figure 6.10: Maps of change in snow depth for May of 2011 and 2015 when historical fires are included in the model compared to the unburned model scenario. The winter of 2011 had higher snowfall than 2015 and was also four years closer to a large fire that burned much of the Western portion of ICB in 2004. There are many more patches that experience a decrease in snow due to fire in 2011 compared to 2015.

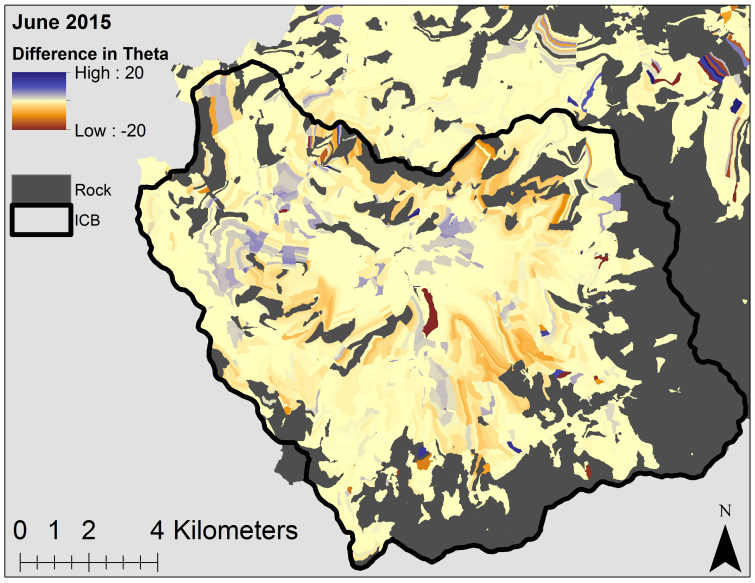

Figure 6.11: Modeled change in June 2015 soil moisture due to fire between the burned and unburned scenarios, measured using theta (θ), the percent saturation. Blue areas show patches where there is more soil moisture when fires are included in the model, and red areas show patches where soil moisture decreases with fire.

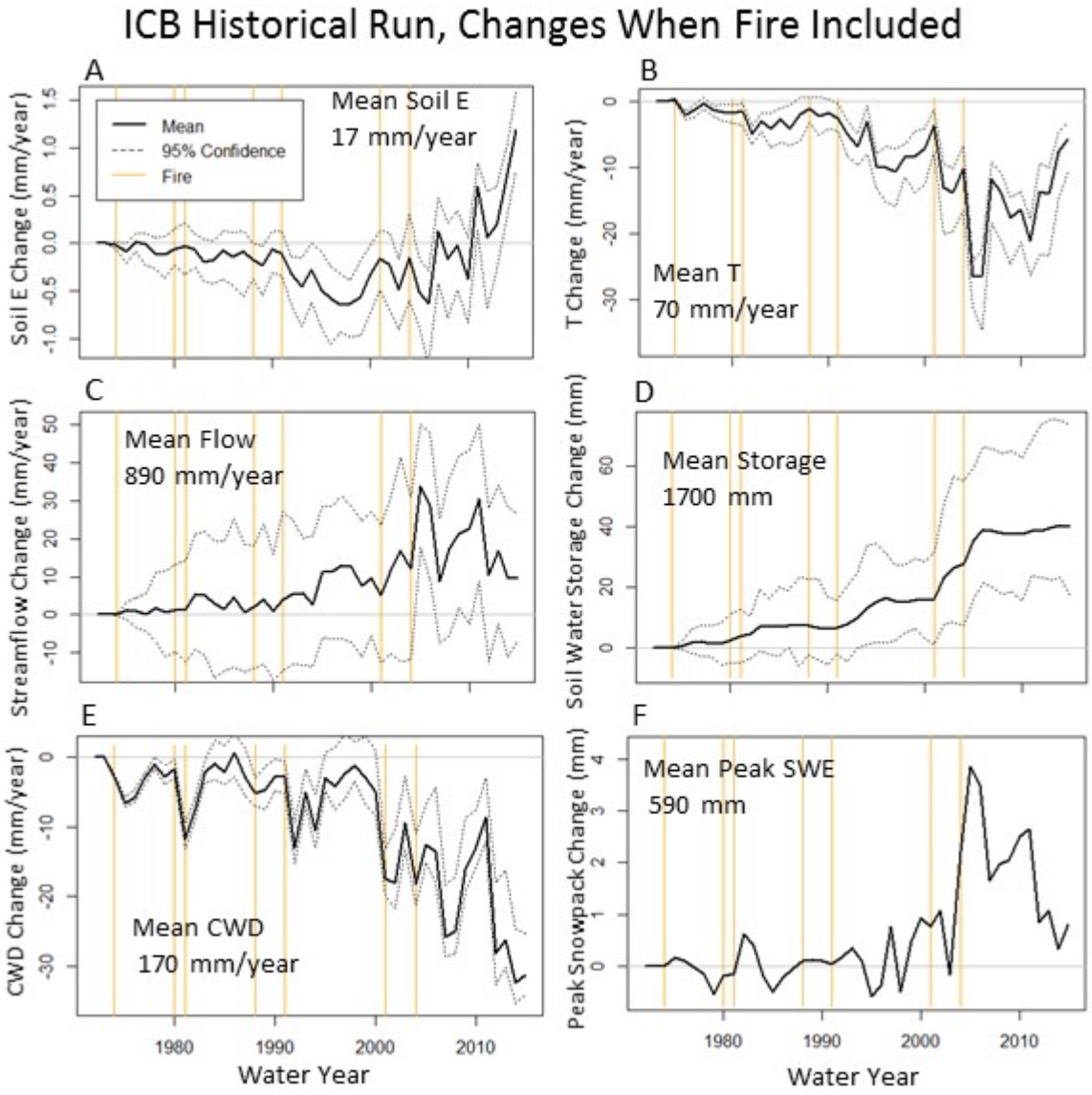

Figure 6.12: When historical fires are included in the ICB model: (A) Soil evaporation initially decreases but eventually increases, (B) transpiration steadily decreases, (C) streamflow has a non-significant increase, (D) mean soil water storage increases, (E) climatic water deficit (CWD) decreases, and (F) peak snow water equivalent (SWE) generally increases over time but is lower in some years. Dashed lines show the 95% confidence interval estimated using the ensemble of 93 different model parameterizations. Vertical lines show the years of the largest fires. Mean values from the unburned model for each variable are given for reference.

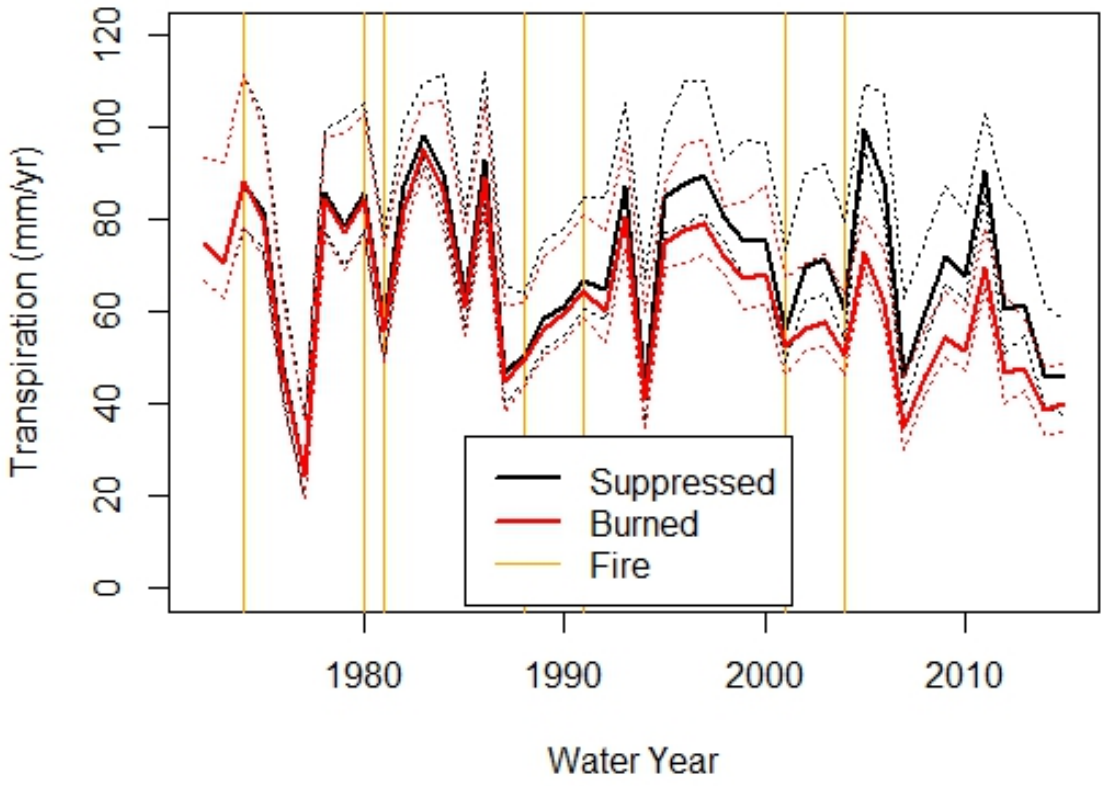

Figure 6.13: Annual total transpiration for the ICB under burned and unburned scenarios for water years 1972-2015. Dashed lines show the 95% confidence interval estimated using the ensemble of 93 different model parameterizations. The two model outputs are identical prior to the first fire, in 1974. Although mean transpiration is always lower in the burned scenario than the unburned scenario, the confidence intervals overlap for most years, especially prior to 2004. Vertical lines show the seven largest fire years.

confidence level in 1994 and remains highly significant through the end of the study period.

On average, total streamflow was higher in the burned models compared to the unburned models, but this difference only surpassed the 95% confidence interval for the years 2005-2007 and 2011 (Figure 6.12C). Peak snowpack depth generally increased over time and the increase due to fire history persisted from 2004 onward (Figure 6.12F).

Viewing output from individual hillslopes helps to better understand how fire was affecting the landscape at smaller scales. Figure 6.14 shows an example time series from a hillslope which burned three times: in 1974, 1988, and 2001. The 2001 fire had the largest high severity patches. After the first fire, snowpack initially increased but within four years vegetation regrowth had caused snowpack to decrease compared to the unburned scenario. After 12 years there was almost no difference in snowpack between burned and unburned scenarios for this hillslope. The 2001 fire led to an increase in snowpack that lasted through 2015. The effect of the fires on soil water storage was highly variable in time but in the first year following the smaller fires in 1974 and 1988 there were increases in groundwater storage (0.2% and 6.8% respectively) followed by decreases as vegetation regrew. After the 2001 fire, groundwater storage initially increased 11.2% and then generally stayed higher than the unburned scenario. In the drought years of 2012-2015 soil water storage was still higher compared to the unburned scenario due to the 2001 fire. The effect on evapotranspiration was also highly variable in time, but evapotranspiration decreased by 30% and 83% following the 1988 and 2001 fires, respectively. The outflow from groundwater in this hillslope increased following each fire, and remained consistently higher than the unburned scenario following the high severity 2001 fire. These results should not necessarily be interpreted as typical, but they give an example of how a hillslope can respond to fires over time.

ICB Extremes

In this experiment, the model ran from 1965 through 2015 holding the vegetation map constant in order to capture the effects of these vegetation changes under a range of climatic variability. There are two different scenarios: One with the 1969 (fire suppressed) vegetation map, and the other with a 2012 vegetation map representing the conditions following 38 years of repeated fires. For both scenarios, I verified that the groundwater and vegetation was in a steady state before the fifty year simulation began by checking for multi-year trends that would indicate a landscape in transition.

In all monthly time series plots, a solid black line denotes the average across all years and all runs, while dashed lines indicate the 95% confidence interval calculated using the 97.5 and 2.5 percentiles of all model runs using our set of acceptable parameter sets.

Snowpack reaches a higher peak depth under 2012 vegetation but also melts faster, as shown by lower mean snowpack in April-June in Figure 6.15A (only one line is shown because the varying soil parameters do not affect snowpack). The increase in February (the month with the largest mean increase), is 2mm of SWE on average, which translates to an additional 300,000m^3 of water stored in ICB in February. There is a much greater difference in subsurface water storage between the vegetation scenarios, with mean storage across all

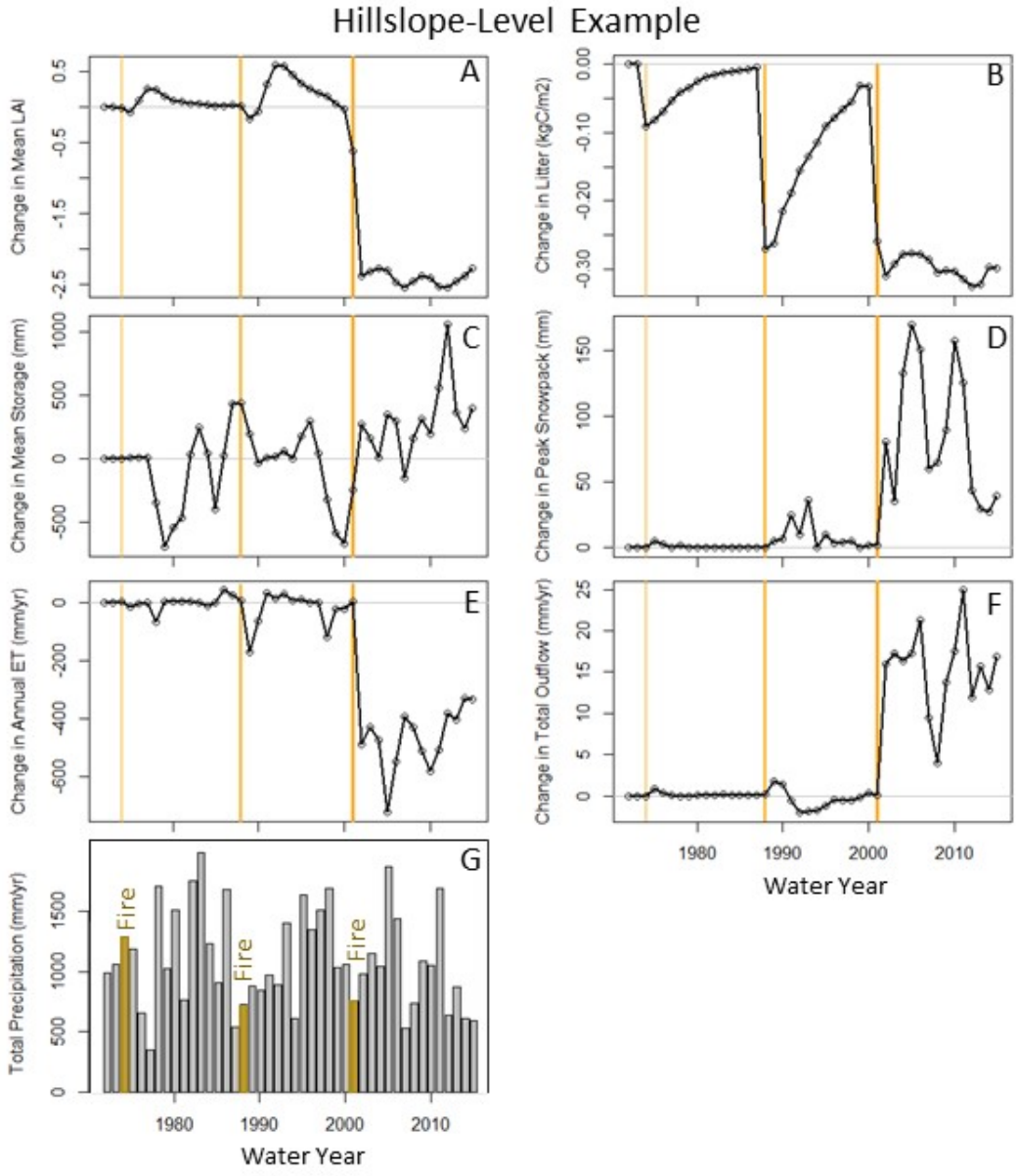

Figure 6.14: Model output for an individual hillslope from water years 1972-2015 showing precipitation totals for the ICB (G) as well as the change from unburned conditions for (A) LAI, (B) litter (Initial litter change after each fire is proportional to total area burned), (C) soil water storage, (D) snowpack, (E) total evapotranspiration, and (F) total groundwater outflow. This hillslope within ICB burned in 1974, 1988, and 2001, shown using vertical lines with widths relative to mean severity over this hillslope. The 2001 fire was high severity in this area, while the other two fires were moderate severity.

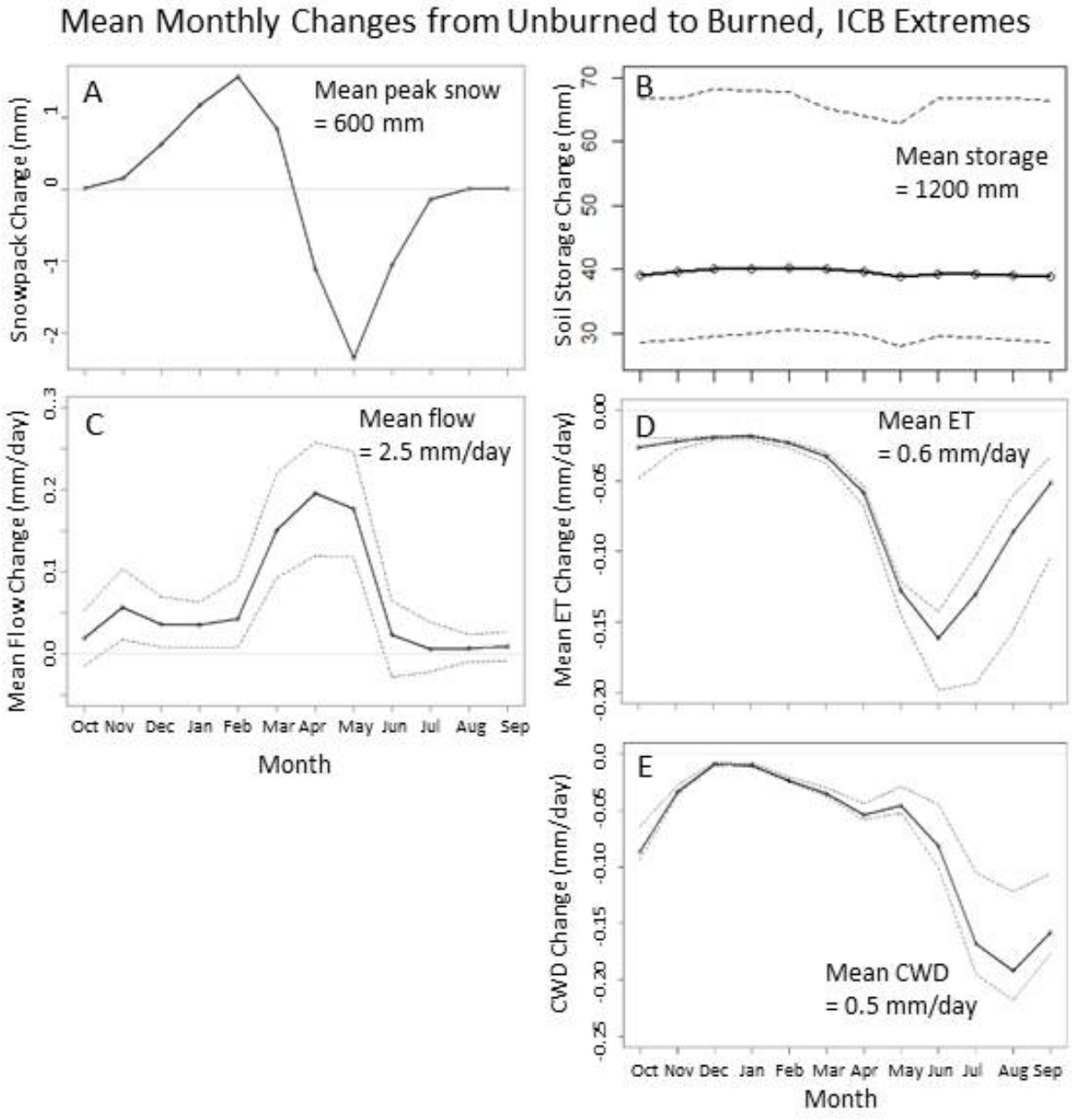

Figure 6.15: Difference in mean monthly values within ICB between model runs using 1969 and 2012 vegetation maps. Positive numbers indicate that the value is higher under 2012 vegetation compared to 1969 vegetation. All plots show the mean change and 95% confidence interval (averaged over 50 years). Changes are shown for (A) snowpack water content, (B) subsurface water storage, (C) streamflow, (D) evapotranspiration (ET), (E) climatic water deficit (CWD). Mean values for each variable in the unburned scenario are given on the plots for context.

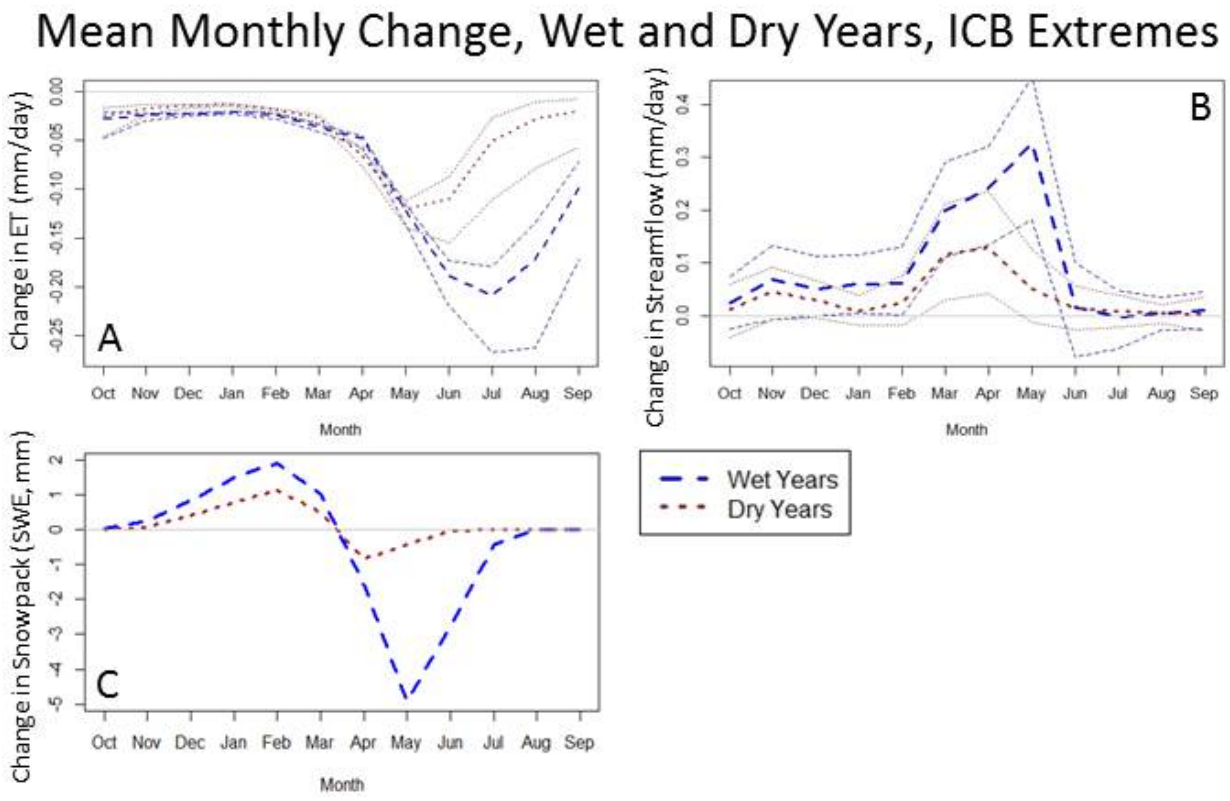

Figure 6.16: Difference in mean monthly values between model runs using 1969 and 2012 vegetation maps for the top 33% wettest years (blue dashed line) and the bottom 33% driest years (red dotted line) in terms of total water year precipitation. Thin lines show the range of values about the mean. (A) Evapotranspiration is lower under 2012 vegetation, with a greater difference in wet years. (B) Streamflow is usually higher under 2012 vegetation, with the greatest increase occuring in May for wet years and April for dry years. (C) On average, winter snowpack increases while spring snowpack decreases under 2012 vegetation. The spring decrease is much stronger in wet years.

years being 30-70mm higher under 2012 vegetation, compared to a mean storage of 1,700mm (Figure 6.15B).

Modeled streamflow is usually higher under 2012 vegetation than 1969 vegetation in all months, and for all tested model parameterizations the mean flow is higher during the winter and during the high snowmelt months of April and May using the burned scenario (Figure 6.15C). The largest May flow increases compared to unburned conditions occur during the years with the highest precipitation (Figure 6.16B), and there is a correspondingly strong decrease in May snowpack in wet years (Figure 6.16C). In dry years, mean summer flows still stay slightly higher using the burned vegetation map compared to the unburned vegetation.

On average, evapotranspiration (ET) is lower under 2012 (burned) vegetation compared

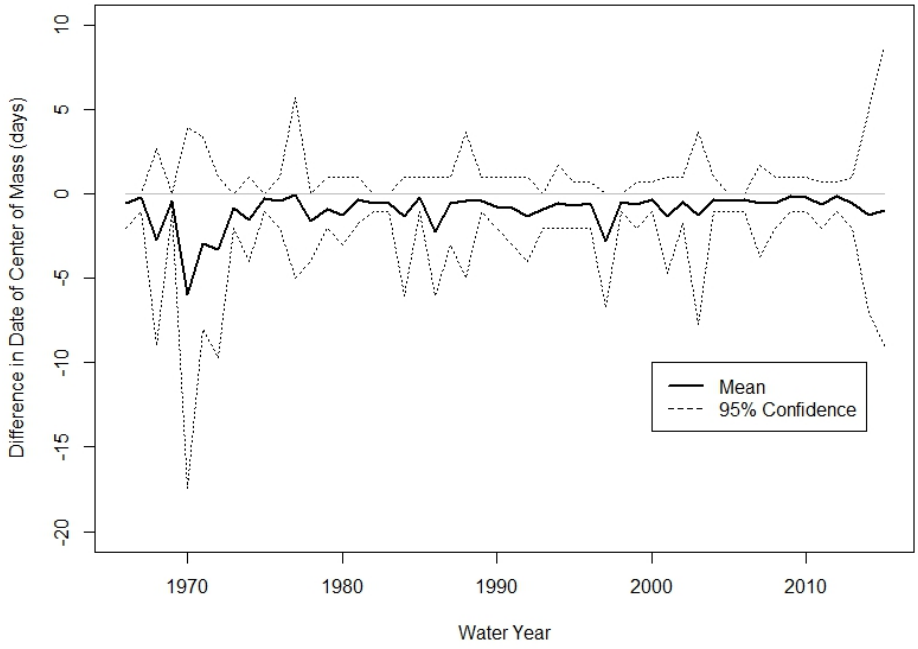

Figure 6.17: Change in annual center of mass of streamflow timing when using 2012 vegetation map versus 1969 vegetation map. Negative values mean that the 2012 vegetation map gives earlier center of mass.

to 1969 (unburned) vegetation, which has higher basin-averaged LAI (Figure 6.15D). The biggest differences occur during the peak growing months, which is largely driven by strong seasonal trends in transpiration. Evaporation from soil is generally higher under 2012 vegetation, but evaporation from the canopy and transpiration are lower (not shown). In relatively dry years, the influence of burned vegetation on ET is less than in wet years, especially in the late summer months of July-September (Figure 6.16A).

The center of mass of streamflow is sometimes later and sometimes earlier under the 2012 vegetation. On average, however, the center of mass moves earlier, likely due to earlier snowmelt (Figure 6.17). This difference can be as high as 19 days earlier. The model confidence intervals widen noticeably during the drought years at the end of the time series.

All model parameterizations predict that mean monthly climatic water deficit is lower under the burned, 2012 vegetation than under fire suppressed vegetation, meaning that vegetation should be less water stressed in the burned scenario (Figure 6.15E). The greatest reduction in water deficit occurs in August.

6.4 Discussion

Although hydrologic models solve many of the problems that plague field studies, they come with their own difficulties. The main difficulty lies in obtaining model parameterizations that reflect the actual processes in the watershed (Seibert and McDonnell, 2002). In this study, we combined qualitative and quantitative information in order to create a model which matches observations while capturing realistic processes. We calibrated the model using multiple criteria in terms of the fit to streamflow data (e.g. matching timing as well as magnitude of flows) and incorporating soft data into the model design (e.g. using maps of vegetation cover and measured soil moisture to help determine the spatial resolution desired for our model, comparing modeled snow cover to Landsat imagery, and constraining soil parameters to within realistic ranges based on our field measurements). This approach may result in slightly lower model accuracy than if we had aimed solely to maximize a given measure of fit to the streamflow data, but it allows us to obtain a model that captures a range of realistic processes (Seibert and McDonnell, 2002).

Modeled annual transpiration ranged from 60 to 180mm for the UMW (note that this represents an average over the full watershed, including unvegetated surfaces), which is lower than the amounts calculated in Christensen et al. (2008) for the same watershed, which ranged from approximately 250-550 mm. These differences may be related to our different methods of estimating precipitation, our different temperature lapse rates (we used 0.008°C/m versus 0.0064°C/m in Christensen et al. (2008)) and/or the use of different vegetation maps. Transpiration from a different mixed conifer forest in the Sierra Nevada was measured at ≈760 mm/year (Bales et al., 2011). This is within the range of our model, in which conifer patches transpired at rates between 500 and 1400 mm/yr. Actual evapotranspiration has been shown to be very sensitive to soil parameterization in spatial models, but the interannual variability in ET is less sensitive to soil parameterization (Lundquist and Loheide, 2011). This means that, even if our actual rates of evapotranspiration may not be highly accurate in an absolute sense, we can have more confidence in trends of how evapotranspiration changes in response to changes in weather and land cover drivers.

Lundquist and Cayan (2007) found that temperature patterns in the Sierra Nevada are highly spatially and temporally variable. Our use of a simple temperature lapse rate therefore is a source of error. The fact that RHESSys takes slope and aspect into account in calculating energy balances partially corrects for this issue. Lundquist's cold air pooling model also predicts much pooling within the Upper Merced Watershed (Katherine Wilkin, personal communication), which could strongly affect snow accumulation and melt rates. I plan to incorporate cold air pooling in future work with RHESSys in this watershed.

Including fire in the model for the UMW did not always reduce model error compared to runs using 1969 vegetation maps throughout the model run. This was unexpected, since the burned scenario should be closer to the true land cover dynamics in the study watersheds, but is not necessarily problematic. The differences in total streamflow between the historical and unburned runs were very small, likely due to the large proportion of UMW and ICB that consists of exposed bedrock and therefore is not susceptible to change from wildfire, as

well as compensation of increased evaporation for transpiration losses (Neary et al., 2005; Wine and Cadol, 2016). Some measures of model accuracy, especially those that incorporate timing of streamflow such as monthly flow correlation and date of center of mass, showed slightly higher model accuracy when fire was included (although this increase in accuracy was not statistically significant). It is expected that streamflow timing would be altered by fire due to vegetation cover's effects on snowpack (Godsey et al., 2014).

The duration of an individual fire's effect on the water balance has a wide range, and depends greatly on post-fire vegetation. For example, peak snowpack was only affected for a few years following the first two fires in the hillslope depicted in Figure 6.14, but the third fire led to a long-term LAI shift which altered snowpack for at least 14 years. This example hillslope also shows how different parts of the water balance may behave very differently from each other, as demonstrated by the very different shapes of the time series in Figure 6.14.

Fires have been shown to strongly affect peak flows (Seibert et al., 2010; Wine and Cadol, 2016). This model does not predict large increases in peak flows due to fire, which suggests that the existing fire regime is not resulting in the unwanted effect of extreme flooding seen in many studies of high severity fires (e.g. Helvey (1980); Moody and Martin (2001)). However, factors such as ash clogging of soil pores or fire-induced soil hydrophobicity are not represented in the model.

Although streamflow changes did not have high statistical significance in most years, other portions of the water balance showed distinct changes. There were significant differences in annual transpiration beginning after year 2001, which had one of the two largest fires in the UMW (7% of ICB area burned at high severity in 2001). Groundwater storage began to increase significantly even earlier, in the 1990s. Unsaturated storage continually increases as transpiration decreases in the model, as would be expected (He et al., 2013). The decrease in soil evaporation following fire during most of the study period is curious. This may be due to post-fire regrowth shading soil.

Including fire in the models nearly always led to an increase in peak snowpack, likely due to decreased interception (Lundberg and Halldin, 2001). Spring snowpack was often decreased in the burned scenario (Figure 6.8), likely due to increased radiation reducing snowpack in the spring (Lundquist et al., 2013). The effect of fire on spring snowpack, however, was highly variable. In the drought year of 2015, fires caused an increase in snowpack through May, whereas four years earlier May snowpack was reduced due to fire (Figure 6.10). These differences may be partially due to plant growth during those four years (in which there were no large fires), or it could be that warmer temperatures in the early spring of 2015 led to a change in the energy balance which caused snow under canopies to melt faster than in open areas (Lundquist et al., 2013).

Streamflow does not seem to increase significantly in most years. Instead, it appears that much of the extra water from reduced transpiration and increased snowpack is staying as soil moisture rather than generating streamflow or being immediately used by plants. The change in storage due to fire appears to increase over time until it levels out around 2006 (Figure 6.12D), despite streamflow beginning to drop back toward fire-suppressed levels during the

last few years of the simulation (Figure 6.12C). This extra water storage could help sustain the watershed during drought years. In fact, modeled decreases in climatic water deficit are greatest during the 2012-2015 drought, even though there had not been any major fires in ICB since 2004 (Figure 6.12E). Decreasing climatic water deficit in the ICB suggests that vegetation should be less water stressed than if fire suppression had continued. This fits with the reduced tree mortality in ICB compared to nearby watersheds during the drought summers of 2014-2015 (Chapter 5) and other studies showing decreases in drought stress and increases in soil moisture following fire (Ursino and Rulli, 2011; van Mantgem et al., 2016). These results also show the importance of looking at long term impacts of fires, rather than only the first few years post-fire which are the most commonly studied.

6.5 Conclusion

According to the model results, the fire history in the Upper Merced has led to increased groundwater stores, decreased evapotranspiration, decreased climatic water deficit, and slightly higher streamflow at an annual level compared to fire suppressed conditions. As expected, we also found increased peak snowpacks (up to 1% higher, or 2×10^6 m^3 of additional SWE) and runoff ratio (up to 15% in low flow years), as well as decreased climatic water deficit in response to the watershed's fire regime. Summer low flows were not strongly affected by fire, but there was a very slight increase in the average low flows for June-August. At the patch level, response of the landscape to fire can be highly variable. These results show that managed wildfire is capable of providing desirable outcomes in terms of water resources at the watershed scale, and that highly localized factors can affect the small scale results.

While most studies of fire and hydrology focus on the immediate post-fire effects, this project explores the long-term implications of a frequent mixed severity fire regime. Hydrologic responses varied over time due to both fire-induced vegetation changes and variations in the weather. Overall, however, the long-term effect of fires in the ICB and UMW appear to include increased subsurface water storage, deeper peak snowpack, and reduced transpiration demands. All of these changes are vital to sustaining a snow-dominated watershed such as ICB and UMW through long, dry summers, especially in the face of drought.

Chapter 7

Conclusion

7.1 Summary of Findings

The hypotheses tested in this dissertation were mainly upheld:

1. Hypothesis: Runoff ratio (Ratio of annual streamflow to annual precipitation) has increased significantly in the watershed containing the ICB since ending fire suppression in 1972, but not in nearby unburned watersheds.

   Result: Runoff ratio for the Upper Merced River did not change significantly over the period of record, but the control watersheds experienced a decrease in runoff ratio (Chapter 5). Although UMW runoff ratio did not increase as we hypothesized, its stability compared to the control watersheds' decreasing runoff ratios suggests an increase in flow compared to what would be expected under unburned conditions.

2. Hypothesis: Vegetation and moisture changes are positively correlated, and thus satellite observations of vegetation can be used to map areas throughout the basin with high soil moisture storage. Specifically, I hypothesize that the presence of dense meadow vegetation is indicative of higher summer soil moisture levels compared to other vegetation types.

   Result: Vegetation type was a strong predictor of soil moisture, and dense meadows had higher summer soil moisture than other vegetation types; although areas that had transitioned from forest to dense meadow had much higher mean soil moisture than unchanged forests, soil moisture was highest in areas that had been dense meadow since before 1969 (Chapter 4).

3. Hypothesis: Remote sensing will show that forest cover has significantly declined, while percent cover of grasslands, and meadows has increased, since the reintroduction of wildfire to the ICB.

Result: This hypothesis was upheld: conifer cover decreased by 21km^2 (24%), shrublands increased by 4km^2 (35%), sparse meadow area increased by 17km^2 (199%) and dense meadows increased by 1km^2 (161%) (Chapter 3).

4. Hypothesis: Remote sensing data of drought-related tree mortality will show that the ICB has lower incidences of such mortality compared to nearby, unburned watersheds.

   Result: There were fewer drought-killed trees per forested acre in the ICB than in control watersheds, sometimes by a factor of 50 (Chapter 5).

5. Hypothesis: A distributed hydrologic model of the ICB will (a) demonstrate a closer match to observed streamflow when parameterized with observed changes in vegetation cover compared to simulations with unaltered vegetation, and (b) show increases in soil moisture, decreased evapotranspiration, and earlier snowmelt in burned areas.

   Result: (a) For some measures of model fit (e.g. correlation of daily and monthly flow and timing of streamflow center of mass) the model better matched observed streamflow when fire effects were included, while for others (e.g. error in annual flow and NSE of September flow) including fire led to a worse fit (Chapter 6). None of these differences were statistically significant. (b) On average, the model showed increased soil water storage and decreases in evapotranspiration, as well as a deeper peak snowpack but earlier complete melting. These results were variable in both space and time (Chapter 6).

Although there is much uncertainty, evidence from multiple sources suggests that restoring a natural fire regime to the Illilouette Basin has affected its hydrological state: field measurements and models of soil moisture show that many burned areas are likely to have higher soil moisture than dense unburned forests (Chapters 4,5, and 6), runoff ratio since 1973 is generally higher from the Upper Merced River than would be expected compared to control watersheds (Chapter 5) and compared to modeled fire-suppressed conditions (Chapter 6), and drought-related tree mortality is low in the ICB compared to nearby unburned watersheds (Chapter 5).

Both RHESSys (a distributed hydrologic model, Chapter 6) and the random forest model (a statistical model, Chapter 4) showed that burned areas sometimes contained higher moisture levels and sometimes lower, compared to what conditions would have been under continued, successful fire suppression. There is noticeable overlap between the two models as far as the direction of change in soil moisture, especially in areas where the random forest model predicts wetter soils (Figure 7.1). There was a very small positive correlation between patch θ from RHESSys and the mean surface VWC modeled within each patch using the random forest model (correlation coefficient = 0.09-0.15 for June 2015).

RHESSys modeled a decrease in climatic water deficit and an increase in soil water storage during the current drought compared to the values that would have existed under fire suppression. The statistical model trained on our field measurements also suggested that many areas experienced increased soil moisture under the fire-altered landscape compared

to a fire-suppressed landscape (Chapter 4). The aerial surveys of drought mortality from Chapter 5 show that trees appear to be less drought stressed in burned areas than in unburned areas, which is expected given an increase in soil moisture.

7.2 General Observations

The Illilouette Creek Basin is not the only place that fire is being shown to positively affect forest resilience. In low elevation Sierra Nevada forests, van Mantgem et al. (2016) found that fire likely increases forest resistance to drought, though prescribed burns alone may not provide sufficient reduction of vegetation density to recreate the natural resilience of fire-adapted, drought-tolerant forests. In Montana, Larson et al. (2013) found that repeated fires helped maintain the resilience of ponderosa pine forests which had been transitioning to an alternate forest type under fire suppression. These findings demonstrate both the potential usefulness of fire as a tool for managing forest health and the fact that prescribed burns may not provide all of the benefits that managed wildfires can.

This study of the ICB has shown very promising results in terms of the drought resilience and diversity of the landscape. It is important to note, however, that there are some limitations in trying to generalize results from ICB. The main limitation is that all of the fieldwork presented here was conducted during a historic drought. This means we do not have hydrologic field data representing an average year. These drought measurements may ultimately prove to be more useful than wet year measurements would be, however, since they likely provide a good proxy for normal conditions under some future climate scenarios. A second particularity to note in the ICB is that precipitation levels were relatively high in 1972 when the managed wildfire policy was instated (Graumlich, 1993). This high moisture may have helped keep the first fires in the ICB in the 1970s from becoming too big or too high severity, despite the heavy fuel loads that were present for these initial managed wildfires.

Of course, managed wildfire is not appropriate everywhere, and there are large risks associated with allowing fires to burn through forests (especially when initially implementing a managed wildfire program in an area with high fuel loads due to years of suppression). However, fire has been a part of California's natural landscapes for millenia, and will continue to shape the landscape even in the face of suppression efforts. In order to coexist with this natural process, we need a variety of strategies, and managed wildfire can provide great benefits in the correct situations.

7.3 Future Work

There is still much to be learned in terms of the specific processes affecting snowpack and soil moisture retention in this watershed, and how they can be related to other watersheds. Three weather stations installed in July of 2015 are already providing insights into the effects of burned vegetation patches on the Illilouette Basin's microclimates (Appendix D).

For example, in the spring of 2016 snow persisted longest in burned areas, likely due to warmer nighttime temperatures in unburned areas (Figures D.2 and D.3). Differences in water balance between burned and unburned sites may provide important hydrologic refugia under the warmer future temperatures predicted due to climate change (Keppel et al., 2012). Once more data is available from these stations, we will have a stronger understanding of the water and energy balance changes that this landscape is experiencing.

I plan to further investigate the effects of topography, weather, and vegetation patterns on how fire has affected the ICB. This will involve both a study of the factors that control what type of vegetation establishes following high severity fires, as well as a RHESSys study of hydrologic response as a function of topographic and vegetation cover conditions.

Future work with the Stephens Lab at UC Berkeley will expand this study to include Sugarloaf Basin in Kings Canyon National Park. Sugarloaf Basin is the only other watershed in California with a long-term managed wildfire program, and we aim to determine how its response to a restored fire regime mirrors, or differs from, the ICB's response. Comparing these two watersheds will provide needed insight into the variability and predictability of hydrologic response to fire regime changes across different regions of the Sierra Nevada.

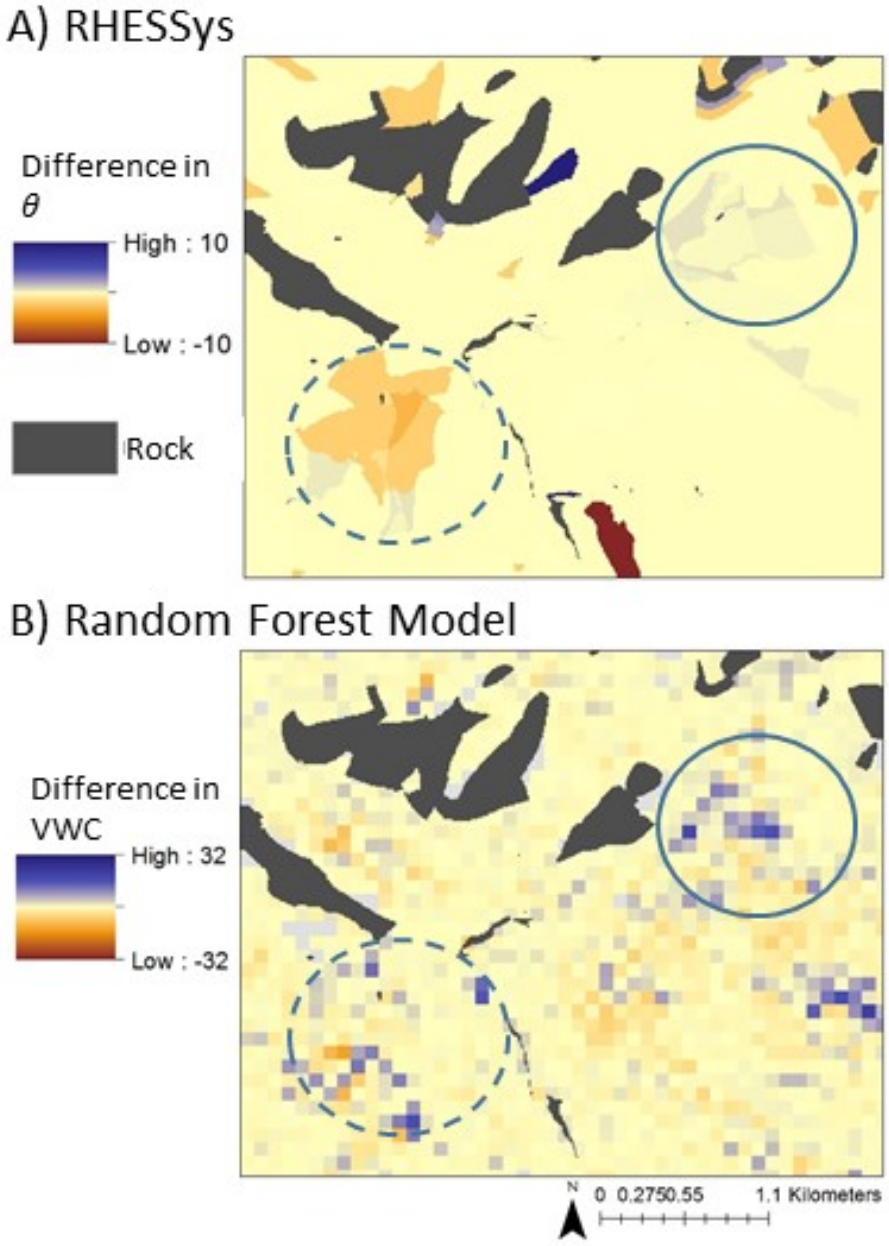

Figure 7.1: Modeled differences in soil moisture between burned and unburned scenarios for August 2015 in an area of the ICB with both increases and decreases in soil moisture due to fire. RHESSys (A) predicts patch-level moisture across the full soil depth, and the random forest statistical model (B) predicts surface soil moisture on a 10m grid. The solid circle shows an area where both models predict an increase in moisture due to fire, while the dashed circle denotes an area where both models show a mix of increasing and decreasing moisture.

Bibliography

Agee, J. K. and Skinner, C. N. (2005). Basic principles of forest fuel reduction treatments. Forest Ecology and Management, 211(1):83–96.

Allen, C. D., Macalady, A. K., Chenchouni, H., Bachelet, D., McDowell, N., Vennetier, M., Kitzberger, T., Rigling, A., Breshears, D. D., Hogg, E. H. T., Gonzalez, P., Fensham, R., Zhang, Z., Castro, J., Demidova, N., Lim, J.-H., Allard, G., Running, S. W., Semerci, A., and Cobb, N. (2010). A global overview of drought and heat-induced tree mortality reveals emerging climate change risks for forests. Forest Ecology and Management, 259(4):660–684.

Alvarez, O., Guo, Q., Klinger, R. C., Li, W., and Doherty, P. (2014). Comparison of elevation and remote sensing derived products as auxiliary data for climate surface interpolation. International Journal of Climatology, 34(7):2258–2268.

Andreadis, K. M., Storck, P., and Lettenmaier, D. P. (2009). Modeling snow accumulation and ablation processes in forested environments. Water Resources Research, 45(5):n/a–n/a. W05429.

Araya, Y. N., Silvertown, J., Gowing, D. J., McConway, K. J., Peter Linder, H., and Midgley, G. (2011). A fundamental, eco-hydrological basis for niche segregation in plant communities. New Phytologist, 189(1):253–258.

Baker, W. L. (1994). Restoration of landscape structure altered by fire suppression. Conservation Biology, 8(3):763–769.

Bales, R. C., Hopmans, J. W., O'Geen, A. T., Meadows, M., Hartsough, P. C., Kirchner, P., Hunsaker, C. T., and Beaudette, D. (2011). Soil moisture response to snowmelt and rainfall in a Sierra Nevada mixed-conifer forest. Vadose Zone Journal, 10(3):786–799.

Barnett, T., Malone, R., Pennell, W., Stammer, D., Semtner, B., and Washington, W. (2004). The effects of climate change on water resources in the west: Introduction and overview. Climatic Change, 62(1):1–11.

Bart, R. R., Tague, C. L., and Moritz, M. A. (2016). Effect of tree-to-shrub type conversion in lower montane forests of the Sierra Nevada (USA) on streamflow. PLOS ONE, 11(8):e0161805.

Benson, L., Kashgarian, M., Rye, R., Lund, S., Paillet, F., Smoot, J., Kester, C., Mensing, S., Meko, D., and Lindström, S. (2002). Holocene multidecadal and multicentennial droughts affecting northern California and Nevada. Quaternary Science Reviews, 21(4):659–682.

Beven, K. and Binley, A. (1992). The future of distributed models: Model calibration and uncertainty prediction. Hydrological Processes, 6(3):279–298.

Beven, K. and Westerberg, I. (2011). On red herrings and real herrings: disinformation and information in hydrological inference. Hydrological Processes, 25(10):1676–1680.

Bird, R. B., Bird, D. W., Codding, B. F., Parker, C. H., and Jones, J. H. (2008). The fire stick farming hypothesis: Australian Aboriginal foraging strategies, biodiversity, and anthropogenic fire mosaics. Proceedings of the National Academy of Sciences, 105(39):14796–14801.

Blaschke, T., Hay, G. J., Kelly, M., Lang, S., Hofmann, P., Addink, E., Feitosa, R. Q., van der Meer, F., van der Werff, H., van Coillie, F., et al. (2014). Geographic object-based image analysis–towards a new paradigm. ISPRS Journal of Photogrammetry and Remote Sensing, 87:180–191.

Boisramé, G. F. S., Thompson, S. E., Collins, B. M., and Stephens, S. L. (2016). Managed wildfire effects on forest resilience and water in the Sierra Nevada. Ecosystems, pages 1–16.

Bréda, N., Granier, A., Barataud, F., and Moyne, C. (1995). Soil water dynamics in an oak stand. Plant and Soil, 172(1):17–27.

Brown, A. E., Zhang, L., McMahon, T. A., Western, A. W., and Vertessy, R. A. (2005). A review of paired catchment studies for determining changes in water yield resulting from alterations in vegetation. Journal of Hydrology, 310(14):28–61.

Burkle, L. A., Myers, J. A., and Belote, R. T. (2015). Wildfire disturbance and productivity as drivers of plant species diversity across spatial scales. Ecosphere, 6(10):1–14.

Campbell Scientific (2015). HS2. www.campbellsci.com/hs2.

Caridade, C., Marçal, A. R., and Mendonça, T. (2008). The use of texture for image classification of black & white air photographs. International Journal of Remote Sensing, 29(2):593–607.

Christensen, L., Tague, C. L., and Baron, J. S. (2008). Spatial patterns of simulated transpiration response to climate variability in a snow dominated mountain ecosystem. Hydrological Processes, 22(18):3576–3588.

Clark, J. (2007). Models for ecological data. Princeton University Press, Princeton.

Coleman, T. W., Heath, Z., Cluck, D., Flowers, R., Hanavan, R., and Graves, G. (2015). Multiregional accuracy assessment of aerial detection survey data. Technical report, USDA Forest Service, Forest Health and Protection, available from http://foresthealth.fs.usda.gov/portal.

Collins, B., Everett, R., and Stephens, S. (2011). Impacts of fire exclusion and recent managed fire on forest structure in old growth Sierra Nevada mixed-conifer forests. Ecosphere, 2(4):1–14. art51.

Collins, B., Kelly, M., van Wagtendonk, J., and Stephens, S. (2007). Spatial patterns of large natural fires in Sierra Nevada wilderness areas. Landscape Ecology, 22(4):545–557.

Collins, B., Miller, J., Thode, A., Kelly, M., van Wagtendonk, J., and Stephens, S. (2009). Interactions among wildland fires in a long-established Sierra Nevada natural fire area. Ecosystems, 12:114–128.

Collins, B. and Skinner, C. (2014). Fire and Fuels in Science synthesis to promote resilience of social-economic systems in the Sierra Nevada and southern Cascade range. General Technical Report PSW-GTR-247. Technical report, U.S. Department of Agriculture, Forest Service, Pacific Southwest Research Station, Albany, CA.

Collins, B. M., Lydersen, J. M., Fry, D. L., Wilkin, K., Moody, T., and Stephens, S. L. (2016). Variability in vegetation and surface fuels across mixed-conifer-dominated landscapes with over 40 years of natural fire. Forest Ecology and Management, 381:74 – 83.

Collins, B. M. and Stephens, S. L. (2007). Managing natural wildfires in Sierra Nevada wilderness areas. Frontiers in Ecology and the Environment, 5(10):523–527.

Collins, B. M. and Stephens, S. L. (2010). Stand-replacing patches within a 'mixed severity' fire regime: quantitative characterization using recent fires in a long-established natural fire area. Landscape Ecology, 25(6):927–939.

Congalton, R. G. and Green, K. (2008). Assessing the accuracy of remotely sensed data: principles and practices. CRC press.

Crist, E. P. and Cicone, R. C. (1984). A physically-based transformation of thematic mapper data—the TM Tasseled Cap. Geoscience and Remote Sensing, IEEE Transactions on, 22(3):256–263.

Curry, R. R. (1969). Holocene climatic and glacial history of the central Sierra Nevada, California. Geological Society of America Special Papers, 123:1–48.

Cushman, S. A., McGarigal, K., and Neel, M. C. (2008). Parsimony in landscape metrics: strength, universality, and consistency. Ecological indicators, 8(5):691–703.

Cuthbertson, A., Lynn, E., Anderson, M., and Redmond, K. (2014). Estimating historical California precipitation phase trends using gridded precipitation, precipitation phase, and elevation data: Memorandum report. Technical report, Department of Water Resources.

Czikowsky, M. J. and Fitzjarrald, D. R. (2004). Evidence of seasonal changes in evapotranspiration in Eastern U.S. hydrological records. Journal of Hydrometeorology, 5:974–988.

Dawson, T. E., Burgess, S. S. O., Tu, K. P., Oliveira, R. S., Santiago, L. S., Fisher, J. B., Simonin, K. A., and Ambrose, A. R. (2007). Nighttime transpiration in woody plants from contrasting ecosystems. Tree Physiology, 27(4):561–575.

Department of Water Resources (2008). Managing an uncertain future: Climate change adaptation strategies for California's water. Technical report, State of California Resources Agency, www.water.ca.gov/climatechange/docs/ClimateChangeWhitePaper.pdf.

Dettinger, M. D. and Anderson, M. L. (2015). Storage in California's reservoirs and snowpack in this time of drought. San Francisco Estuary and Watershed Science, 13(2).

Dettinger, M. D., Cayan, D. R., Meyer, M. K., and Jeton, A. E. (2004). Simulated hydrologic responses to climate variations and change in the Merced, Carson, and American River basins, Sierra Nevada, California, 19002099. Climatic Change, 62(1-3):283–317.

Dettinger, M. D., Ralph, F. M., Das, T., Neiman, P. J., and Cayan, D. R. (2011). Atmospheric rivers, floods and the water resources of California. Water, 3(2):445–478.

D'Odorico, P., Laio, F., and Ridolfi, L. (2006). A probabilistic analysis of fire-induced tree-grass coexistence in savannas. The American Naturalist, 167(3):E79–E87.

Donato, D. C., Fontaine, J. B., Robinson, W. D., Kauffman, J. B., and Law, B. E. (2009). Vegetation response to a short interval between high-severity wildfires in a mixed-evergreen forest. Journal of Ecology, 97(1):142–154.

Dorner, B., Lertzman, K., and Fall, J. (2002). Landscape pattern in topographically complex landscapes: issues and techniques for analysis. Landscape Ecology, 17(8):729–743.

Duan, Q., Schaake, J., Andrassian, V., Franks, S., Goteti, G., Gupta, H., Gusev, Y., Habets, F., Hall, A., Hay, L., Hogue, T., Huang, M., Leavesley, G., Liang, X., Nasonova, O., Noilhan, J., Oudin, L., Sorooshian, S., Wagener, T., and Wood, E. (2006). Model parameter estimation experiment (MOPEX): An overview of science strategy and major results from the second and third workshops. Journal of Hydrology, 320(12):3 – 17.

Ellis, C. R., Pomeroy, J. W., and Link, T. E. (2013). Modeling increases in snowmelt yield and desynchronization resulting from forest gap-thinning treatments in a northern mountain headwater basin. Water Resources Research, 49(2):936–949.

Farm Service Agency and USDA (2015). NAIP imagery. http://www.fsa.usda.gov/programs-and-services/aerial-photography/imagery-programs/naip-imagery/index.

Farr, T. G., Rosen, P. A., Caro, E., Crippen, R., Duren, R., Hensley, S., Kobrick, M., Paller, M., Rodriguez, E., Roth, L., Seal, D., Shaffer, S., Shimada, J., Umland, J., Werner, M., Oskin, M., Burbank, D., and Alsdorf, D. (2007). The shuttle radar topography mission. Reviews of Geophysics, 45(2):n/a–n/a.

Federer, C. A. (1973). Forest transpiration greatly speeds streamflow recession. Water Resources Research, 9(6):1599–1604.

Fernandes, P. M. and Botelho, H. S. (2003). A review of prescribed burning effectiveness in fire hazard reduction. International Journal of wildland fire, 12(2):117–128.

Finney, M. A., McHugh, C. W., Grenfell, I. C., Riley, K. L., and Short, K. C. (2011). A simulation of probabilistic wildfire risk components for the continental United States. Stochastic Environmental Research and Risk Assessment, 25:973–1000.

Fisher, J. B., DeBiase, T. A., Qi, Y., Xu, M., and Goldstein, A. H. (2005). Evapotranspiration models compared on a Sierra Nevada forest ecosystem. Environmental Modelling & Software, 20(6):783–796.

Fites-Kaufman, J. A., Rundel, P., Stephenson, N., and Weixelman, D. A. (2007). Montane and subalpine vegetation of the Sierra Nevada and Cascade ranges. Terrestrial Vegetation of California. University of California Press, Berkeley, pages 456–501.

Fowells, H. A. (1965). Silvics of forest trees of the United States. Agriculture Handbook US Department of Agriculture, 271.

Godsey, S. E., Kirchner, J. W., and Tague, C. L. (2014). Effects of changes in winter snowpacks on summer low flows: case studies in the Sierra Nevada, California, USA. Hydrological Processes, 28(19):5048–5064.

Goulden, M., Anderson, R., Bales, R., Kelly, A., Meadows, M., and Winston, G. (2012). Evapotranspiration along an elevation gradient in California's Sierra Nevada. Journal of Geophysical Research: Biogeosciences (2005–2012), 117(G3).

Goulden, M. L. and Bales, R. C. (2014). Mountain runoff vulnerability to increased evapotranspiration with vegetation expansion. Proceedings of the National Academy of Sciences, 111(39):14071–14075.

Grant, G. E., Tague, C. L., and Allen, C. D. (2013). Watering the forest for the trees: an emerging priority for managing water in forest landscapes. Frontiers in Ecology and the Environment, 11(6):314–321.

Graumlich, L. J. (1993). A 1000-year record of temperature and precipitation in the Sierra Nevada. Quaternary Research, 39(2):249 – 255.

Griffin, D. and Anchukaitis, K. J. (2014). How unusual is the 2012 - 2014 California drought? Geophysical Research Letters, 41(24):9017–9023. 2014GL062433.

Grmping, U. (2009). Variable importance assessment in regression: Linear regression versus random forest. The American Statistician, 63(4):308–319.

Gunderson, L. H. (2000). Ecological resilience–in theory and application. Annual review of ecology and systematics, 31:425–439.

Gupta, H. V., Kling, H., Yilmaz, K. K., and Martinez, G. F. (2009). Decomposition of the mean squared error and NSE performance criteria: Implications for improving hydrological modelling. Journal of Hydrology, 377(12):80–91.

Gupta, H. V., Perrin, C., Kumar, R., Bloschl, G., Clark5, M., Montanari, A., and Andreassian, V. (2013). Large-sample hydrology: a need to balance depth with breadth. Hydrology and Earth System Sciences Discussions, 10:9147–9189.

Gutman, G. and Ignatov, A. (2010). The derivation of the green vegetation fraction from NOAA/AVHRR data for use in numerical weather prediction models. International Journal of Remote Sensing, 19(8):1533–1543.

He, L., Ivanov, V. Y., Bohrer, G., Thomsen, J. E., Vogel, C. S., and Moghaddam, M. (2013). Temporal dynamics of soil moisture in a northern temperate mixed successional forest after a prescribed intermediate disturbance. Agricultural and Forest Meteorology, 180(0):22 – 33.

Helms, J. A. and Ratliff, R. D. (1987). Germination and establishment of pinus contorta var. murrayana (pinaceae) in mountain meadows of Yosemite National Park, California. Madroño, 34(2):77–90.

Helvey, J. (1980). Effects of a north central Washington wildfire on runoff and sediment production. Water Resources Bulletin.

Hessburg, P. F., Agee, J. K., and Franklin, J. F. (2005a). Dry forests and wildland fires of the inland Northwest USA: Contrasting the landscape ecology of the pre-settlement and modern eras. Forest Ecology and Management, 211(12):117–139.

Hessburg, P. F., Agee, J. K., and Franklin, J. F. (2005b). Dry forests and wildland fires of the inland Northwest USA: Contrasting the landscape ecology of the pre-settlement and modern eras. Forest Ecology and Management, 211(12):117–139.

Hessburg, P. F., Churchill, D. J., Larson, A. J., Haugo, R. D., Miller, C., Spies, T. A., North, M. P., Povak, N. A., Belote, R. T., Singleton, P. H., Gaines, W. L., Keane, R. E., Aplet, G. H., Stephens, S. L., Morgan, P., Bisson, P. A., Rieman, B. E., Salter, R. B., and Reeves, G. H. (2015). Restoring fire-prone Inland Pacific landscapes: seven core principles. Landscape Ecology, 30(10):1805–1835.

Hicke, J. A., Meddens, A. J., and Kolden, C. A. (2016). Recent tree mortality in the western United States from bark beetles and forest fires. Forest Science, 62(2):141–153.

Hicks, B. J., Beschta, R. L., and Harr, R. D. (1991). Long-term changes in streamflow following logging in western Oregon and associated fisheries implications. JAWRA Journal of the American Water Resources Association, 27(2):217–226.

Holling, C. and Meffe, G. K. (1996). Command and control and the pathology of natural resource management. Conservation Biology, 10(2):328–337.

Holling, C. S. (2001). Understanding the complexity of economic, ecological, and social systems. Ecosystems, 4(5):390–405.

Johnson, E. A. and Miyanishi, K. (2010). Disturbance and succession. In Johnson, E. A. and Miyanishi, K., editors, Plant disturbance ecology: the process and the response, chapter 1, pages 1–10. Academic Press, Burlington, MA.

Jones, B. E., Rickman, T. H., Vazquez, A., Sado, Y., and Tate, K. W. (2005). Removal of encroaching conifers to regenerate degraded aspen stands in the Sierra Nevada. Restoration Ecology, 13(2):373–379.

Kane, V. R., Lutz, J. A., Alina Cansler, C., Povak, N. A., Churchill, D. J., Smith, D. F., Kane, J. T., and North, M. P. (2015). Water balance and topography predict fire and forest structure patterns. Forest Ecology and Management, 338(0):1–13.

Kane, V. R., Lutz, J. A., Roberts, S. L., Smith, D. F., McGaughey, R. J., Povak, N. A., and Brooks, M. L. (2013). Landscape-scale effects of fire severity on mixed-conifer and red fir forest structure in Yosemite National Park. Forest Ecology and Management, 287:17–31.

Kane, V. R., North, M. P., Lutz, J. A., Churchill, D. J., Roberts, S. L., Smith, D. F., McGaughey, R. J., Kane, J. T., and Brooks, M. L. (2014). Assessing fire effects on forest spatial structure using a fusion of Landsat and airborne LiDAR data in Yosemite National Park. Remote Sensing of Environment, 151:89–101.

Katul, G. G., Oren, R., Manzoni, S., Higgins, C., and Parlange, M. B. (2012). Evapotranspiration: A process driving mass transport and energy exchange in the soil-plant-atmosphere-climate system. Reviews of Geophysics, 50(3):RG3002.

Keane, R. E., Cary, G. J., Davies, I. D., Flannigan, M. D., Gardner, R. H., Lavorel, S., Lenihan, J. M., Li, C., and Rupp, T. S. (2004). A classification of landscape fire succession models: spatial simulations of fire and vegetation dynamics. Ecological Modelling, 179(1):3–27.

Kelly, M., Tuxen, K. A., and Stralberg, D. (2011). Mapping changes to vegetation pattern in a restoring wetland: Finding pattern metrics that are consistent across spatial scale and time. Ecological Indicators, 11(2):263 – 273.

Keppel, G., Van Niel, K. P., Wardell-Johnson, G. W., Yates, C. J., Byrne, M., Mucina, L., Schut, A. G. T., Hopper, S. D., and Franklin, S. E. (2012). Refugia: identifying and understanding safe havens for biodiversity under climate change. Global Ecology and Biogeography, 21(4):393–404.

LANDFIRE (2012a). Biophysical setting layer, LANDFIRE 1.3.0. http://landfire.cr.usgs.gov/viewer/.

LANDFIRE (2012b). Existing vegetation type layer, LANDFIRE 1.3.0. http://landfire.cr.usgs.gov/viewer/.

Lane, P., Feikema, P., Sherwin, C., Peel, M., and Freebairn, A. (2010). Modelling the long term water yield impact of wildfire and other forest disturbance in eucalypt forests. Environmental Modelling & Software, 25(4):467–478.

Larson, A. J., Belote, R. T., Cansler, C. A., Parks, S. A., and Dietz, M. S. (2013). Latent resilience in ponderosa pine forest: effects of resumed frequent fire. Ecological Applications, 23(6):1243–1249.

Lauvaux, C. A., Skinner, C. N., and Taylor, A. H. (2016). High severity fire and mixed conifer forest-chaparral dynamics in the southern Cascade range, USA. Forest Ecology and Management, 363:74–85.

Legates, D. R. and McCabe, G. J. (1999). Evaluating the use of goodness-of-fit measures in hydrologic and hydroclimatic model validation. Water Resources Research, 35(1):233–241.

Li, H. and Wu, J. (2004). Use and misuse of landscape indices. Landscape Ecology, 19(4):389–399.

Liaw, A. and Wiener, M. (2015). Breiman and Cutler's random forests for classification and regression. R Package RandomForest.

Loheide, S. P. and Gorelick, S. M. (2005). A local-scale, high-resolution evapotranspiration mapping algorithm (ETMA) with hydroecological applications at riparian meadow restoration sites. Remote Sensing of Environment, 98(2):182–200.

Lundberg, A. and Halldin, S. (2001). Snow interception evaporation. Review of measurement techniques, processes, and models. Theoretical and Applied Climatology, 70(1-4):117–133. WOS:000172271800010.

Lundquist, J. D. and Cayan, D. R. (2007). Surface temperature patterns in complex terrain: Daily variations and long-term change in the central Sierra Nevada, California. Journal of Geophysical Research: Atmospheres, 112(D11):D11124.

Lundquist, J. D., Dickerson-Lange, S. E., Lutz, J. A., and Cristea, N. C. (2013). Lower forest density enhances snow retention in regions with warmer winters: A global framework developed from plot-scale observations and modeling. Water Resources Research, 49(10):6356–6370.

Lundquist, J. D. and Loheide, S. P. (2011). How evaporative water losses vary between wet and dry water years as a function of elevation in the Sierra Nevada, California, and critical factors for modeling. Water Resources Research, 47(3):W00H09.

Ma, S., Concilio, A., Oakley, B., North, M., and Chen, J. (2010). Spatial variability in microclimate in a mixed-conifer forest before and after thinning and burning treatments. Forest Ecology and Management, 259(5):904–915.

Mast, M. A. and Clow, D. W. (2008). Effects of 2003 wildfires on stream chemistry in Glacier National Park, Montana. Hydrological Processes, 22(26):5013–5023.

Maurer, E., Stewart, I., Bonfils, C., Duffy, P., and Cayan, D. (2007). Detection, attribution, and sensitivity of trends toward earlier streamflow in the Sierra Nevada. Journal of Geophysical Research: Atmospheres, 112(D11).

Mayor, A. G., Bautista, S., Llovet, J., and Bellot, J. (2007). Post-fire hydrological and erosional responses of a Mediterranean landscape: Seven years of catchment-scale dynamics. CATENA, 71(1):68–75.

McGarigal, K., Cushman, S., and Ene, E. (2012). FRAGSTATS v4: Spatial pattern analysis program for categorical and continuous maps. computer software program produced by the authors at the University of Massachusetts, Amherst. www.umass.edu/landeco/research/fragstats/fragstats.html.

Millar, C. I., Stephenson, N. L., and Stephens, S. L. (2007). Climate change and forests of the future: managing in the face of uncertainty. Ecological Applications, 17(8):2145–2151.

Milledge, D. G., Warburton, J., N. Lane, S., and J. Stevens, C. (2013). Testing the influence of topography and material properties on catchment-scale soil moisture patterns using remotely sensed vegetation patterns in a humid temperate catchment, northern Britain. Hydrological Processes, 27(8):1223–1237.

Miller, C. and Urban, D. L. (2000a). Connectivity of forest fuels and surface fire regimes. Landscape Ecology, 15:145–154.

Miller, C. and Urban, D. L. (2000b). Modeling the effects of fire management alternatives on Sierra Nevada mixed-conifer forests. Ecological Applications, 10(1):85–94.

Miller, D. A. and White, R. A. (1998). A conterminous United States multilayer soil characteristics dataset for regional climate and hydrology modeling. Earth Interactions, 2(2):1–26.

Miller, J., Collins, B., Lutz, J., Stephens, S., van Wagtendonk, J., and Yasuda, D. (2012a). Differences in wildfires among ecoregions and land management agencies in the Sierra Nevada region. Ecosphere, 3(9):1–20.

Miller, J. and Safford, H. (2012). Trends in wildfire severity 1984-2010 in the Sierra Nevada, Modoc Plateau and southern Cascades, California, USA. Fire Ecology, 8:41–57.

Miller, J., Safford, H., Crimmins, M., and Thode, A. (2009). Quantitative evidence for increasing forest fire severity in the Sierra Nevada and southern Cascade Mountains, California and Nevada, USA. Ecosystems, 12:16–32.

Miller, J. D., Collins, B. M., Lutz, J. A., Stephens, S. L., van Wagtendonk, J. W., and Yasuda, D. A. (2012b). Differences in wildfires among ecoregions and land management agencies in the Sierra Nevada region, California, USA. Ecosphere, 3(9):art80.

Miller, J. D. and Thode, A. E. (2007). Quantifying burn severity in a heterogeneous landscape with a relative version of the delta normalized burn ratio (dNBR). Remote Sensing of Environment, 109(1):66 – 80.

Moody, J. A. and Martin, D. A. (2001). Post-fire, rainfall intensity–peak discharge relations for three mountainous watersheds in the western USA. Hydrological Processes, 15(15):2981–2993.

Moore, J. (2015). Aerial detection survey - April 15th-17th, 2015. Technical report, United States Department of Agriculture. Forest Service.

Morgan, J. L., Gergel, S. E., and Coops, N. C. (2010). Aerial photography: a rapidly evolving tool for ecological management. BioScience, 60(1):47–59.

Morgan, P., Hardy, C. C., Swetnam, T. W., Rollins, M. G., and Long, D. G. (2001). Mapping fire regimes across time and space: understanding coarse and fine-scale fire patterns. International Journal of Wildland Fire, 10(4):329–342.

Mori, A. S. (2011). Ecosystem management based on natural disturbances: hierarchical context and non-equilibrium paradigm. Journal of Applied Ecology, 48(2):280–292.

Mountford, J. and Chapman, J. (1993). Water regime requirements of British wetland vegetation: Using the moisture classification of Ellenberg and Londo. Journal of Environmental Management, 38(4):275 – 288.

Musick, H. and Pelletier, R. E. (1988). Response to soil moisture of spectral indexes derived from bidirectional reflectance in thematic mapper wavebands. Remote Sensing of Environment, 25(2):167 – 184.

Neary, D., Ryan, K. C., and DeBano, L. F. (2005). Wildland fire in ecosystems: Effects of fire on soil and water. Technical report, United States Department of Agriculture. Forest Service.

Norman, S. P. and Taylor, A. H. (2005). Pine forest expansion along a forest-meadow ecotone in northeastern California, USA. Forest Ecology and Management, 215(1):51–68.

North, M., Innes, J., and Zald, H. (2007). Comparison of thinning and prescribed fire restoration treatments to Sierran mixed-conifer historic conditions. Canadian Journal of Forest Research, 37(2):331–342.

North, M. P., Stephens, S. L., Collins, B. M., Agee, J. K., Aplet, G. H., Franklin, J. F., and Fule, P. Z. (2015). Reform forest fire management. Science, 349:1280–1281.

Oregon State University (2004). PRISM climate group. http://prism.oregonstate.edu.

Parks, S. A., Miller, C., Nelson, C. R., and Holden, Z. A. (2014). Previous fires moderate burn severity of subsequent wildland fires in two large western US wilderness areas. Ecosystems, 17:29–42.

Parsons, D. J. and DeBenedetti, S. H. (1979). Impact of fire suppression on a mixed-conifer forest. Forest Ecology and Management, 2:21–33.

Pausas, J. G. (2006). Simulating Mediterranean landscape pattern and vegetation dynamics under different fire regimes. Plant Ecology, 187(2):249–259.

Pausas, J. G. and Lloret, F. (2007). Spatial and temporal patterns of plant functional types under simulated fire regimes. International Journal of Wildland Fire, 16(4):484–492.

Perry, D. A., Hessburg, P. F., Skinner, C. N., Spies, T. A., Stephens, S. L., Taylor, A. H., Franklin, J. F., McComb, B., and Riegel, G. (2011). The ecology of mixed severity fire regimes in Washington, Oregon, and Northern California. Forest Ecology and Management, 262(5):703 – 717.

Perry, T. D. and Jones, J. A. (2016). Summer streamflow deficits from regenerating douglas-fir forest in the Pacific Northwest, USA. Ecohydrology, pages n/a–n/a. ECO-16-0049.R1.

Peterson, G. D. (2002). Contagious disturbance, ecological memory, and the emergence of landscape pattern. Ecosystems, 5(4):329–338.

Pierson, F. B., Robichaud, P. R., and Spaeth, K. E. (2001). Spatial and temporal effects of wildfire on the hydrology of a steep rangeland watershed. Hydrological Processes, 15(15):2905–2916.

Ponisio, L. C., Wilkin, K., M'Gonigle, L. K., Kulhanek, K., Cook, L., Thorp, R., Griswold, T., and Kremen, C. (2016). Pyrodiversity begets plantpollinator community diversity. Global Change Biology, pages n/a–n/a.

Rambo, T. and North, M. (2009). Canopy microclimate response to pattern and density of thinning in a Sierra Nevada forest. Forest Ecology and Management, 257(2):435–442.

Ratliff, R. D. (1985). Meadows in the Sierra Nevada of California: state of knowledge. Technical report, Pacific Southwest Forest and Range Experiment Station, Forest Service, U.S. Department of Agriculture.

Rollins, M. G. (2009). LANDFIRE: a nationally consistent vegetation, wildland fire, and fuel assessment. International Journal of Wildland Fire, 18(3):235–249.

Romme, W. H. (1982). Fire and landscape diversity in subalpine forests of Yellowstone National Park. Ecological Monographs, 52(2):199–221.

Royce, E. B. and Barbour, M. G. (2001). Mediterranean climate effects. I. conifer water use across a Sierra Nevada ecotone. American Journal of Botany, 88(5):911–918.

Rutter, A. J., Kershaw, K. A., Robins, P. C., and Morton, A. J. (1972). A predictive model of rainfall interception in forests, 1. Derivation of the model from observations in a plantation of Corsican pine. Agricultural Meteorology, 9(0):367 – 384.

Rutter, A. J., Morton, A. J., and Robins, P. C. (1975). A predictive model of rainfall interception in forests. II. generalization of the model and comparison with observations in some coniferous and hardwood stands. Journal of Applied Ecology, 12(1):pp. 367–380.

Saksa, P. (2015). Forest management, wildfire, and climate impacts on the hydrology of Sierra Nevada mixed-conifer watersheds. PhD thesis, UC Merced: Environmental Systems, https://escholarship.org/uc/item/90w5r5qs.

Scheller, R. M., Mladenoff, D. J., Crow, T. R., and Sickley, T. A. (2005). Simulating the effects of fire reintroduction versus continued fire absence on forest composition and landscape structure in the Boundary Waters Canoe Area, Northern Minnesota, USA. Ecosystems, 8(4):396–411.

Schlesinger, W. H. and Jasechko, S. (2014). Transpiration in the global water cycle. Agricultural and Forest Meteorology, 189–190:115 – 117.

Scholl, A. E. and Taylor, A. H. (2010). Fire regimes, forest change, and self-organization in an old-growth mixed-conifer forest, Yosemite National Park, USA. Ecological Applications, 20(2):362–380.

Schwartz, M. D., Ahas, R., and Aasa, A. (2006). Onset of spring starting earlier across the northern hemisphere. Global Change Biology, 12(2):343–351.

Seibert, J. and McDonnell, J. J. (2002). On the dialog between experimentalist and modeler in catchment hydrology: Use of soft data for multicriteria model calibration. Water Resources Research, 38(11):1241.

Seibert, J., McDonnell, J. J., and Woodsmith, R. D. (2010). Effects of wildfire on catchment runoff response: a modelling approach to detect changes in snow-dominated forested catchments. Hydrology research, 41(5).

Seiferling, I., Proulx, R., and Wirth, C. (2014). Disentangling the environmental-heterogeneityspecies-diversity relationship along a gradient of human footprint. Ecology, 95(8):2084–2095.

Sellin, A. (1999). Does pre-dawn water potential reflect conditions of equilibrium in plant and soil water status? Acta Oecologica, 20(1):51 – 59.

Silva, J. S., Vaz, P., Moreira, F., Catry, F., and Rego, F. C. (2011). Wildfires as a major driver of landscape dynamics in three fire-prone areas of Portugal. Landscape and Urban Planning, 101(4):349–358.

Sivapalan, M., Blöschl, G., Zhang, L., and Vertessy, R. (2003). Downward approach to hydrological prediction. Hydrological Processes, 17(11):2101–2111.

Sörensen, R., Zinko, U., and Seibert, J. (2006). On the calculation of the topographic wetness index: evaluation of different methods based on field observations. Hydrology and Earth System Sciences Discussions, 10(1):101–112.

Soulard, C. E. (2015). Sierra Nevada ecoregion summary. Technical report, USGS.

Sousa, W. P. (1984). The role of disturbance in natural communities. Annual Review of Ecology and Systematics, 15:353–391.

Stephens, S. L., Lydersen, J. M., Collins, B. M., Fry, D. L., and Meyer, M. D. (2015). Historical and current landscape-scale ponderosa pine and mixed conifer forest structure in the Southern Sierra Nevada. Ecosphere, 6(5):art79.

Stephens, S. L., Martin, R. E., and Clinton, N. E. (2007). Prehistoric fire area and emissions from California's forests, woodlands, shrublands, and grasslands. Forest Ecology and Management, 251(3):205–216.

Stephens, S. L. and Moghaddas, J. J. (2005). Experimental fuel treatment impacts on forest structure, potential fire behavior, and predicted tree mortality in a California mixed conifer forest. Forest Ecology and Management, 215(1):21–36.

Stephens, S. L., Moghaddas, J. J., Edminster, C., Fiedler, C. E., Haase, S., Harrington, M., Keeley, J. E., Knapp, E. E., McIver, J. D., Metlen, K., Skinner, C. N., and Youngblood, A. (2009). Fire treatment effects on vegetation structure, fuels, and potential fire severity in western U.S. forests. Ecological Applications, 19(2):305–320.

Stine, S. et al. (1994). Extreme and persistent drought in California and Patagonia during mediaeval time. Nature, 369(6481):546–549.

Stuart, J. D. and Sawyer, J. O. (2001). Trees and shrubs of California, volume 62. Univ of California Press.

Sugihara, N. G., Van Wagtendonk, J. W., Fites-Kaufman, J., Shaffer, K. E., and Thode, A. E. (2006). Fire in California's Ecosystems. University of California Press.

Sujono, J., Shikasho, S., and Hiramatsu, K. (2004). A comparison of techniques for hydrograph recession analysis. Hydrological Processes, 18(3):403–413.

Swanson, F., Jones, J., Wallin, D., and Cissel, J. (1994). Natural variabilityimplications for ecosystem management. ME Jensen and PS Bourgeron, editors, 2:80–94.

Swetnam, T. W. and Baisan, C. H. (2003). Tree-ring reconstructions of fire and climate history in the Sierra Nevada and southwestern United States. In Fire and climatic change in temperate ecosystems of the western Americas, pages 158–195. Springer.

Tague, C. and Band, L. (2004). RHESSys: Regional hydro-ecologic simulation system–an object-oriented approach to spatially distributed modeling of carbon, water, and nutrient cycling. Earth Interactions, 8(1).

Tague, C. and Dugger, A. L. (2010). Ecohydrology and climate change in the mountains of the western USA - a review of research and opportunities. Geography Compass, 4(11):1648–1663.

Tague, C. and Peng, H. (2013). The sensitivity of forest water use to the timing of precipitation and snowmelt recharge in the California Sierra: Implications for a warming climate. Journal of Geophysical Research: Biogeosciences, 118(2):875–887.

Tallaksen, L. (1995). A review of baseflow recession analysis. Journal of Hydrology, 165(14):349 – 370.

Taylor, A. H., Vandervlugt, A. M., Maxwell, R. S., Beaty, R. M., Airey, C., and Skinner, C. N. (2014). Changes in forest structure, fuels and potential fire behaviour since 1873 in the Lake Tahoe Basin, USA. Applied Vegetation Science, 17:17–31.

Thode, A. (2005). Quantifying the fire regime attributes of severity and spatial complexity using field and imagery data. PhD thesis, Davis, CA: University of California.

Tian, F., Li, H., and Sivapalan, M. (2012). Model diagnostic analysis of seasonal switching of runoff generation mechanisms in the Blue River basin, Oklahoma. Journal of Hydrology, 418419(0):136 – 149. ¡ce:title¿The Distributed Model Intercomparison Project (DMIP) - Phase 2 Experiments in the Oklahoma Region, USA¡/ce:title¿.

Todd, S. W. and Hoffer, R. M. (1998). Responses of spectral indices to variations in vegetation cover and soil background. Photogrammetric engineering and remote sensing, 64:915–922.

Turner, M. G. (1989). Landscape ecology: The effect of pattern on process. Annual Review of Ecology and Systematics, 20:171–197.

University of Montana (2015). Wilderness.net.

Ursino, N. and Rulli, M. C. (2011). Hydrological minimal model for fire regime assessment in a mediterranean ecosystem. Water Resources Research, 47(11):n/a–n/a.

U.S. Congress (1964). The wilderness act: Public law 88-577 (16 u.s. c. 1131-1136). http://wilderness.nps.gov/document/wildernessAct.pdf.

USDA-FS (2011). Region five ecological restoration: Leadership intent. March 2011. U.S. Forest Service, Pacific Southwest Region.

USGS (2015). The national map: 3D Elevation Program (3DEP). http://nationalmap.gov/3DEP/index.html.

van Mantgem, P. J., Caprio, A. C., Stephenson, N. L., and Das, A. J. (2016). Does prescribed fire promote resistance to drought in low elevation forests of the Sierra Nevada, California, USA? Fire Ecology, 12(1):13–25.

van Wagtendonk, J., van Wagtendonk, K., and Thode, A. (2012). Factors associated with the severity of intersecting fires in Yosemite National Park, California, USA. Fire Ecology, 8:11–31.

van Wagtendonk, J. W. (2007). The history and evolution of wildland fire use. Fire Ecology, 3:3–17.

Vieira, D., Fernndez, C., Vega, J., and Keizer, J. (2015). Does soil burn severity affect the post-fire runoff and interrill erosion response? a review based on meta-analysis of field rainfall simulation data. Journal of Hydrology, 523:452 – 464.

Voepel, H., Ruddell, B., Schumer, R., Troch, P. A., Brooks, P. D., Neal, A., Durcik, M., and Sivapalan, M. (2011). Quantifying the role of climate and landscape characteristics on hydrologic partitioning and vegetation response. Water Resources Research, 47(10):n/a–n/a.

Webb, A. A. and Jarrett, B. W. (2013). Hydrological response to wildfire, integrated logging and dry mixed species eucalypt forest regeneration: The Yambulla experiment. Forest Ecology and Management, 306:107–117.

Weisman, R. (1977). The effect of evapotranspiration on streamflow recession. Hydrological Sciences Bulletin, 22(3):371–377.

Weiss, A. (2001). Topographic position and landforms analysis. In Poster presentation, ESRI User Conference, San Diego, CA, pages 200–200.

Westerling, A. and Bryant, B. (2008). Climate change and wildfire in California. Climatic Change, 87(1):231–249.

Westerling, A., Hidalgo, H., Canay, D., and Swetnam, T. (2006). Warming and earlier spring increase western US forest wildfire activity. Science, 313:940–943.

Western, A. W., Blschl, G., and Grayson, R. B. (1998). Geostatistical characterisation of soil moisture patterns in the Tarrawarra catchment. Journal of Hydrology, 205(142):20–37.

Western, A. W., Grayson, R. B., Blschl, G., Willgoose, G. R., and McMahon, T. A. (1999). Observed spatial organization of soil moisture and its relation to terrain indices. Water Resources Research, 35(3):797–810.

Wilkin, K. (2016). California forest and shrubland ecosystem changes in relation to fire, fuel hazard, and climate change. PhD thesis, University of California at Berkeley.

Wine, M. L. and Cadol, D. (2016). Hydrologic effects of large southwestern USA wildfires significantly increase regional water supply: fact or fiction? Environmental Research Letters, 11(8).

Woodhouse, C. A., Meko, D. M., MacDonald, G. M., Stahle, D. W., and Cook, E. R. (2010). A 1,200-year perspective of 21st century drought in southwestern North America. Proceedings of the National Academy of Sciences, 107(50):21283–21288.

Wu, J. (2004). Effects of changing scale on landscape pattern analysis: scaling relations. Landscape Ecology, 19(2):125–138.

Ye, S., Yaeger, M., Coopersmith, E., Cheng, L., and Sivapalan, M. (2012). Exploring the physical controls of regional patterns of flow duration curves–part 2: Role of seasonality, the regime curve, and associated process controls. Hydrology and Earth System Sciences, 16(11):4447–4465.

Zald, H. S., Gray, A. N., North, M., and Kern, R. A. (2008). Initial tree regeneration responses to fire and thinning treatments in a Sierra Nevada mixed-conifer forest, USA. Forest Ecology and Management, 256(1):168–179.

Zegre, N., Skaugset, A. E., Som, N. A., McDonnell, J. J., and Ganio, L. M. (2010). In lieu of the paired catchment approach: Hydrologic model change detection at the catchment scale. Water Resources Research, 46(11):n/a–n/a.

Zhang, L., Dawes, W. R., and Walker, G. R. (2001). Response of mean annual evapotranspiration to vegetation changes at catchment scale. Water Resources Research, 37(3):701–708.

Zinke, P. J. (1967). Forest interception studies in the United States. Forest Hydrology. Oxford, UK: Pergamon Press.

Appendix A

Supporting Information for Chapter 3

A.1 Confusion Matrices

This supplemental material shows confusion matrices both for individual years and for transitions from one year to another.

	True Category					
Mapped	Conifer	Shrub	Sparse	Dense	Total Count	Reliability
Conifer	395	8	4	1	408	0.9681
Shrub	0	45	6	0	51	0.8823
Sparse	3	5	32	0	40	0.8000
Dense	1	0	0	9	10	0.9000
Total Count	338	59	34	3	509	

Table A.1: Confusion Matrix for map created using 1969 black and white aerial imagery. Overall accuracy: 94.5%.

	True Category					
Mapped	Conifer	Shrub	Sparse	Dense	Total Count	Reliability
Conifer	316	10	21	0	347	0.9107
Shrub	1	32	2	0	35	0.9143
Sparse	9	4	97	0	110	0.8818
Dense	1	0	1	8	10	0.8000
Total Count	327	46	121	8	502	

Table A.2: Confusion Matrix for map created using 1997 NAPP imagery. Overall accuracy: 90.2%.

	Reference Data														
Classified Data	MXC MXC	SHR SHR	BRG BRG	MDW MDW	MXC SHR	MXC BRG	MXC MDW	SHR MXC	SHR BRG	BRG MXC	BRG SHR	MDW MXC	Row Sum	User Acc.
MXC-MXC	287	3	2	0	4	16	2	1	0	0	0	0	315	0.91
SHR-SHR	0	47	0	0	2	0	0	0	0	0	0	0	49	0.96
BRG-BRG	0	2	42	0	0	1	0	0	1	0	0	0	46	0.91
MDW-MDW	0	0	0	11	0	0	0	0	0	0	0	0	11	1.00
MXC-SHR	11	9	0	0	74	3	1	0	0	0	1	0	99	0.75
MXC-BRG	9	2	7	0	6	80	0	0	1	0	0	0	105	0.76
MXC-MDW	2	0	0	0	1	0	37	0	0	0	0	0	40	0.93
SHR-MXC	2	13	0	0	1	0	0	29	2	0	0	0	47	0.62
SHR-BRG	2	3	4	0	0	4	0	0	32	0	0	0	45	0.71
BRG-MXC	6	1	8	0	0	0	0	1	1	21	2	0	40	0.53
BRG-SHR	0	2	3	0	0	0	0	0	0	1	1	0	7	0.14
MDW-MXC	6	0	0	1	0	0	0	0	0	0	0	3	10	0.30

Table A.3: This table shows the number of points verified for every type of vegetation transition found in our maps for 1969-2012 (that occurred in $> 0.1\%$ of the landscape). The vegetation types are mixed conifer (MXC), shrub (SHR), sparse meadow (BRG), and dense meadow (MDW). Reading along the diagonal gives the number of points that were classified correctly. The user's accuracy column gives the proportion of verification points that were classified correctly using the vegetation maps.

A.2 Varying Resolution Analysis Details

		% Area of Largest Patch				Shannon's Even. Index
Resolution(m)	Year	Conifer	Shrub	Sparse	Meadow	Whole Watershed
5	1969	76.0	0.7	0.2	0.1	0.45
30	1969	77.8	0.7	0.1	0.1	0.45
90	1969	77.2	0.7	0.2	0.1	0.45
500	1969	78.6	1.7	1.9	0.2	0.47
5	1987	69.5	0.8	1.2	0.0	0.53
30	1987	70.4	1.2	1.2	0.0	0.53
90	1987	71.0	1.3	1.0	0.0	0.53
500	1987	73.5	1.0	1.4	0.2	0.53
5	1997	57.9	1.2	3.0	0.1	0.60
30	1997	59.5	1.2	3.0	0.1	0.60
90	1997	57.7	1.2	2.9	0.1	0.60
500	1997	64.3	2.0	4.0	0.3	0.60
5	2005	57.2	2.3	2.9	0.3	0.66
30	2005	57.9	2.5	3.0	0.3	0.66
90	2005	57.5	3.0	3.1	0.3	0.66
500	2005	61.5	3.2	4.4	0.5	0.67
5	2012	45.2	2.6	1.5	0.2	0.70
30	2012	47.9	2.6	1.3	0.2	0.70
90	2012	47.6	2.6	2.9	0.2	0.70
500	2012	48.5	1.7	6.3	0.2	0.68

Table A.4: This table gives the % of the total landscape area covered by the largest patch of each vegetation type. It also gives the Shannon's evenness index for the whole watershed. An evenness index of 1 would mean that all vegetation types were equally represented in the landscape; higher evenness means more landscape diversity.

A.3 Changes in Area from Year to Year

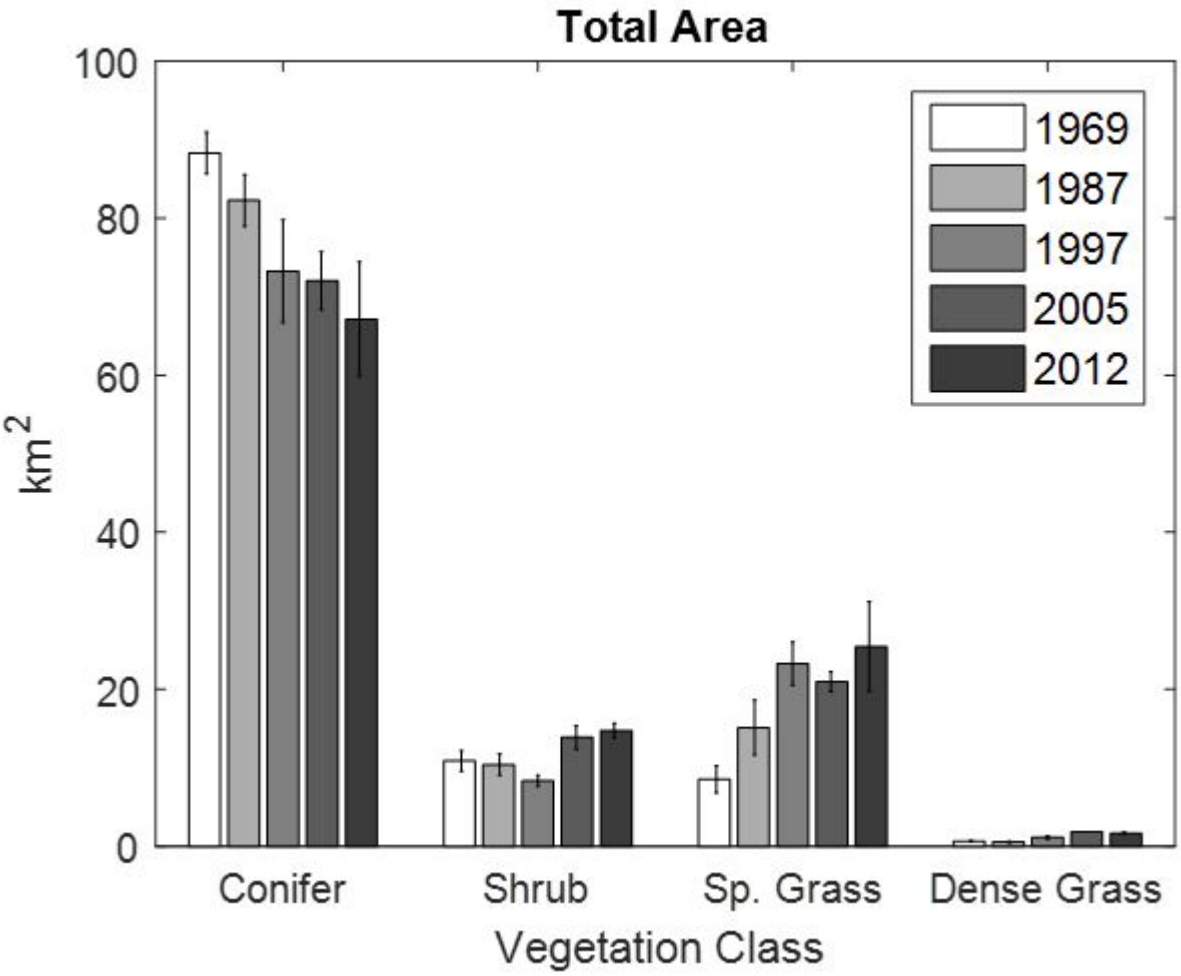

Figure A.1: Total area covered by each vegetation class in each year. Error bars represent the level of uncertainty in the vegetation mapping. For example, if conifers were mapped with 90% accuracy, then the error bars for conifer would show ±10% of the area calculated. Aspen is not included due to difficulty identifying aspen in the black and white 1969 images making quantification of change in area highly uncertain. While we have high confidence that the area covered by each vegetation type is different in 1969 compared to 2012 (the ranges covered by the error bars do not overlap), certain transitions from one mapped year to the next are smaller than our range of uncertainty (e.g. the change in conifer cover from 1997 to 2005 is insignificant compared to our level of accuracy).

Appendix B

Supporting Information for Chapter 4

This appendix presents details of the leaf water potential measurements used to relate surface VWC to root-zone soil saturation.

Figure B.1 shows a stronger relationship between PSI and surface soil water content in the pre-dawn measurements compared to those in the afternoon. Certain species separate well in the afternoon measurements: *Pinus jeffreyi* has relatively low afternoon leaf water potentials, indicating that they are not losing much water to transpiration. The *Salix* species, on the other hand, all have high afternoon leaf water potentials, suggesting high levels of transpiration.

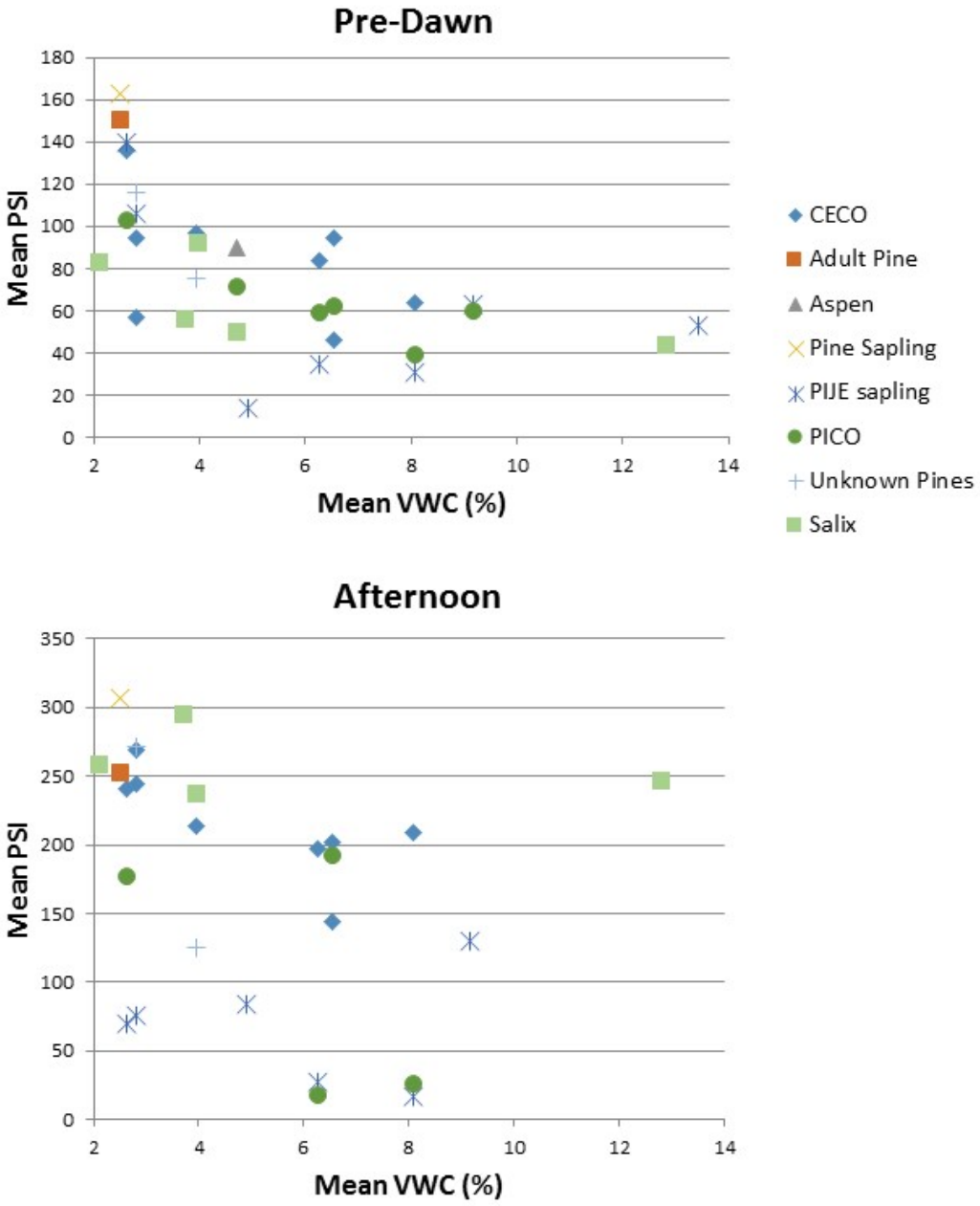

Figure B.1: Leaf water potentials measured just before dawn and during mid-day, plotted agains surface soil water content (VWC). Each point on the plot represents the average of measurements in a given species taken at the same time of the same day, in the same location. The species are whiethorn ceanothus (CECO, *Ceanothus cordulatus*), aspen (*Populus tremuloides*), Jeffrey pine (PIJE, *Pinus jeffreyi*), lodgepole pine (PICO, *Pinus contorta*, willow (*Salix*), and unidentified pines that are likely either CECO or PIJE.

Appendix C

Supporting Information for Chapter 5

C.1 Supplementary Maps and Tables

This supplementary material includes details of the study areas which were not deemed necessary for overall comprehension, but may be of interest for those wishing to gain a deeper understanding of our methods. The map The map in Figure C.1 shows the locations of control watersheds used for our analysis of drought-related tree mortality. We have also included a table which details the range of physical variables captured by our soil moisture measurement campaign compared to the range within the watershed as a whole (Table C.1).

Variable	Min	Max	Mean	Median
Slope (Degrees) All	0	79	13	12
Slope (Degrees) Measured	0	31	8	7
Aspect (Degrees) All	-1	360	190	215
Aspect (Degrees) Measured	-1	360	184	217
Elevation (m) All	1890	2490	2270	2291
Elevation (m) Measured	1893	2487	2203	2192
Dist from River (m) All	0	681	128	102
Dist from River (m) Measured	0	436	83	67
TPI All	-63	201	-1	-2
TPI Measured	-38	55	-6	-7
TWI All	0	17	3	3
TWI Measured	0	15	4	4
Upslope Area (m^2) All	0	374126	344	6
Upslope Area (m^2) Measured	0	51417	1081	21
Times Burned All	0	5	1	1
Times Burned Measured	0	4	2	2
Years Since Fire All	5	101	32	14
Years Since Fire Measured	10	101	19	13
RdNBR All	0	3857	253	172
RdNBR Measured	0	1129	390	339
Severity All	0	4	2	2
Severity Measured	0	4	3	3

Table C.1: Range of physical variables for the watershed, labeled "All", and for the soil moisture measurement locations, labeled "Measured", as well as the mean and median. The watershed ("All") variables are only calculated for the area between 1890m and 2490m in elevation, since this is the elevation range in which all known fires have burned in ICB, and the range of elevations we were able to access for measurements. These variables include slope (degrees), aspect (degrees from North, -1 indicates a horizontal surface), elevation (m), distance from nearest stream (m), Topographic Position Index (TPI, negative values indicate valley bottoms, positive values indicate ridge tops, and 0 is flat), Topographic Wetness Index (TWI, higher values have low slope and a large contributing area), upslope area (m^2 upslope of measurement), times burned in the record (going back to approximately 1930), Years since most recent fire (if no fire on record, marked as 101), Relative Difference Normalized Burn Ratio (RdNBR, higher values correspond to higher fire severity), and fire severity as a number from 0 = unburned to 4 = high severity. Note that many steep areas are both prohibitively difficult to access for measurements and are mainly rock, therefore they have few fires and do not store much soil moisture. This results in our measurement sites not always covering the full range of variability in physical characteristics, though the measured span does include the median watershed value for every variable.

Figure C.1: Map of all watersheds used in Table 5.3, along with 2015 tree mortality, elevation, and fire perimeters. Although this dataset includes all mortality without regard to source, most mortality in this region at these dates is likely related to drought conditions. For simplicity, only fires in the past 20 years are included.

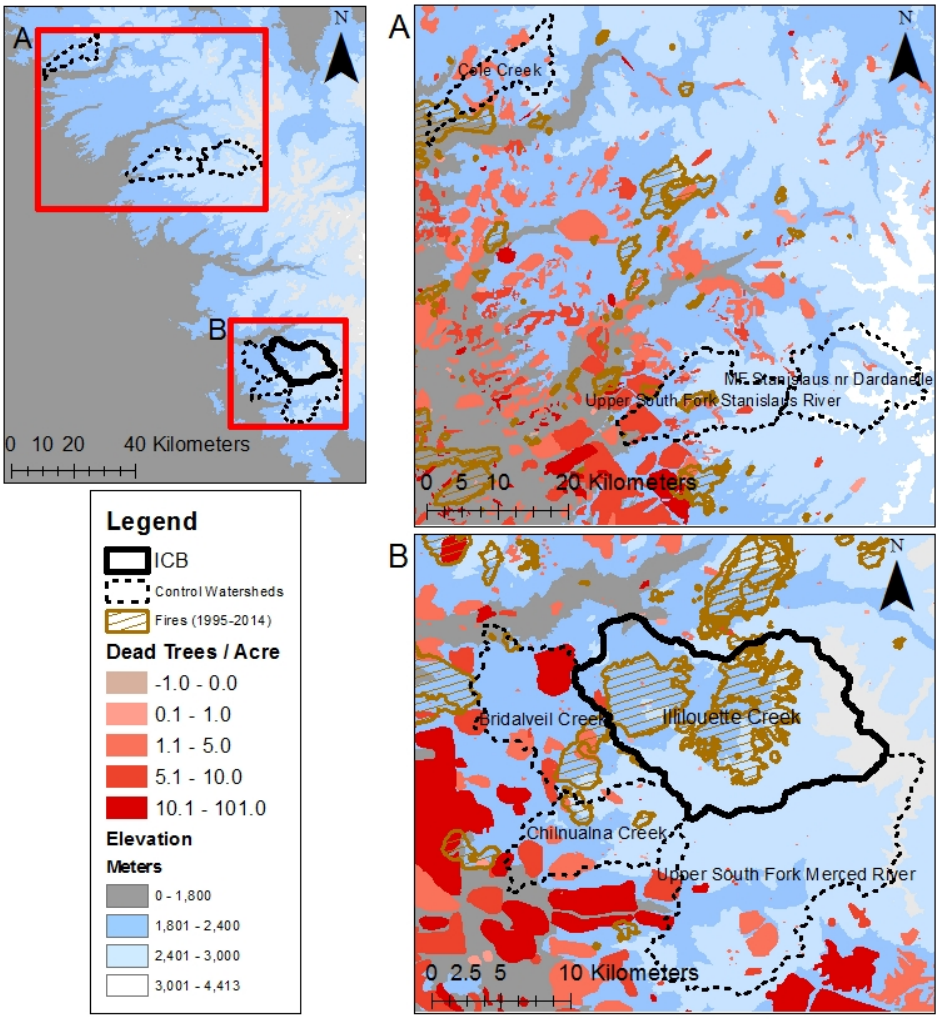

Appendix D

Supporting Information for Chapter 6

D.1 Temporary Weather Station Observations in Illilouette Creek Basin

Three temporary weather stations installed in July 2015 monitor temperature, relative humidity, soil moisture, soil temperature, wind speed, and solar radiation in the ICB. All three stations are within an area that has burned twice, most recently in 2004. One station is in a low severity burn area with an intact, mature, mixed conifer canopy. The other two stations are in nearby burned areas with no mature trees within at least 25m. One of these stations is dominated by shrubs, and the other is in a wet meadow dominated by grasses. These stations are within 200m of each other. Measurements are recorded every 10 minutes using a Campbell Scientific CR1000 datalogger (www.campbellsci.com).

All three stations are located in the southwest region of Illilouette Creek Basin, at an elevation of approximately 2100m. They are located uphill of the nearest trails and are over 3km from the nearest road, and therefore should not be affected by human infrastructure.

TDR probes were installed at three depths ranging from 12cm to 100cm at each weather station in order to capture subsurface water storage dynamics. Soil from three depths within each of the pits dug for these installations was analyzed by the UC Davis Analytical Laboratory for soil texture and percent organic matter (anlab.ucdavis.edu). Only the surface (top 10 cm) wet meadow soil sample contained over 10% organic matter. All other soil samples consisted of over 87% sand particles, even the deeper wet meadow soils.

Each station has associated time lapse cameras which capture snow depth four times each day during the winter. I also visited the weather stations in February and March 2016 to take manual measurements of snow depth (using a 3m folding snow depth probe from snowmetrics.com.) and density (calculated by weighing known volumes of snow at multiple depths). In March, snow depth was measured on 100m grids centered on each weather station, and snow density was measured in one pit near each weather station. Snow water equivalent (SWE) was highest in the wet meadow site and lowest in the forested site (Figure D.1). In fact, most of the forested area immediately surrounding the forest weather station

had bare earth in March, while the other sites were entirely covered with snow except for isolated tree wells.

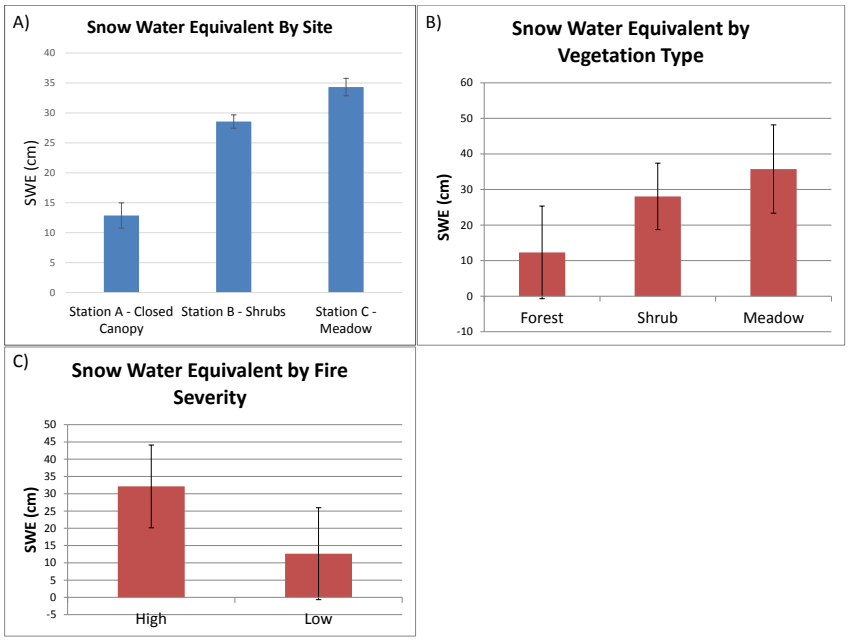

Figure D.1: Snow water equivalent (SWE) measured in March 2016. All three plots were created using the same data, but the data are grouped either by weather station site (A), by dominant vegetation type covering the measurement point (B), or by fire severity of the measurement point (C). Error bars in (A) give the standard error of the mean, while (B) and (C) show the standard deviation in order to gain a better understanding of the data variability.

Temperatures vary between each station, with the forested site being warmest on average. This higher temperature is mainly driven by warmer nighttime temperatures in the forested site compared to the open areas (Figure D.2).

This increased nighttime temperature in the forested site may be leading to much earlier snowmelt under the dense canopy compared to the open areas (Figure D.3).

These snowpack differences, among other effects, lead to very different soil moisture responses in terms of both magnitude and timing (Figure D.4).

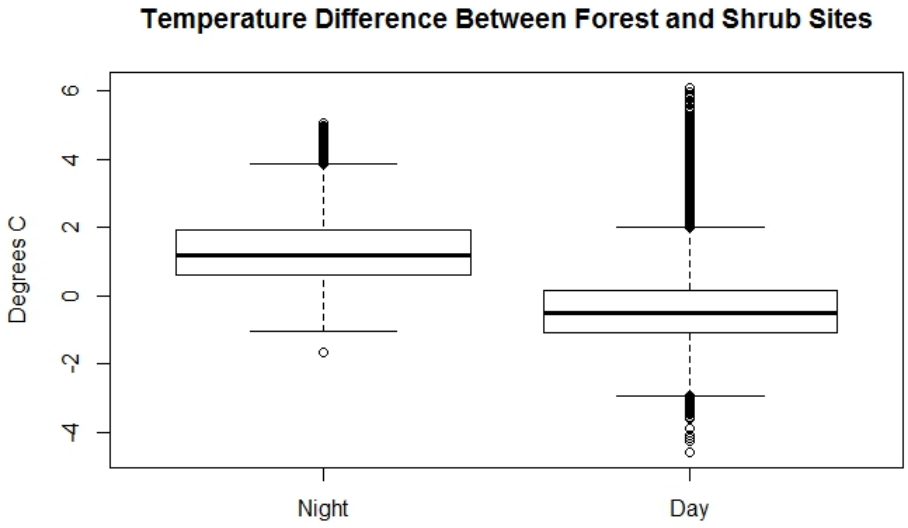

Figure D.2: Difference in temperature in the forested site compared to the shrub-dominated site. At night, it is warmer in the forest on average, whereas mean daytime temperature is higher in the shrubs.

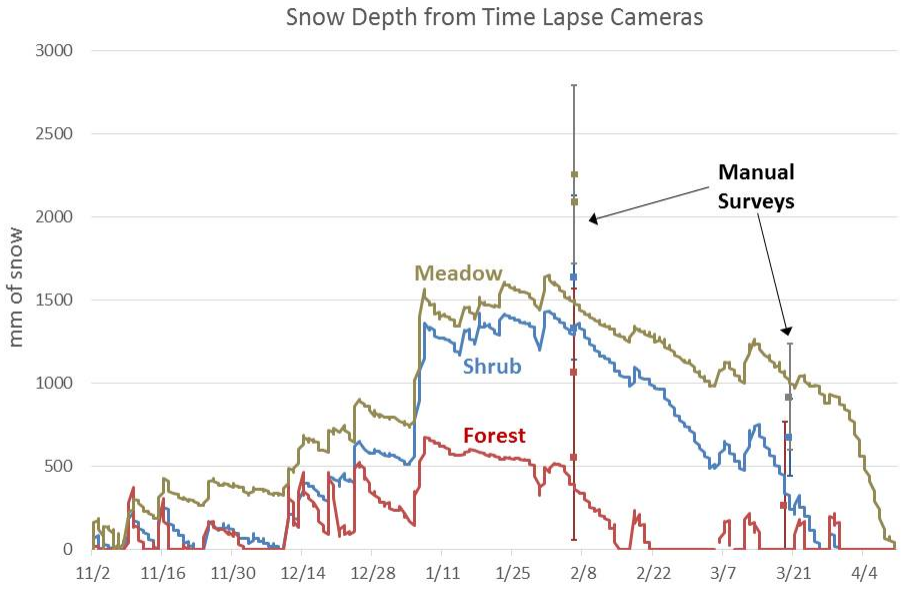

Figure D.3: Snow depth over time at each weather station.

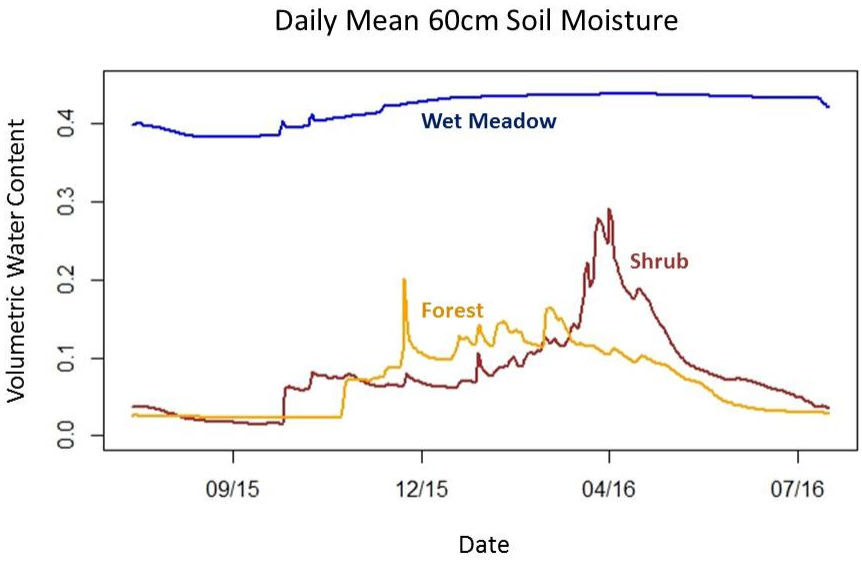

Figure D.4: Soil moisture measured at 60cm depth at each weather station.

D.2 Measurements of Leaf Stomatal Conductance

Stomatal conductance in terms of mmol of gas per m^2 per second was measured in multiple locations within ICB in May and June 2014 using a Model SC-1 steady state diffusion porometer from Decagon Devices. For each species in each location, we took at least three separate measurements on different leaves. Measured leaves were in full sun, since these leaves are likely to have open stomata in order to conduct photosynthesis. Plants were selected that were growing in relatively moist areas in order to avoid the effects of water limitation on stomatal conductance. Results are given in Table D.1.

Species	Mean ($mmol/m^2s$)	Min ($mmol/m^2s$)	Max ($mmol/m^2s$)
White fir	82.6	43.5	146.4
Jeffery Pine	118.8	58.1	167.5
Fir Sapling	169.7	100.1	241.2
Sedge	329.0	46.6	798.8
Lodgepole	357.1	246.6	436.6
Lupine	385.5	75.0	758.6
Aspen	403.8	29.4	677.2
Ceanothus	486.5	16.3	1012.5
Willow (riparian)	707.3	311.4	1270.0
Willow (dryland)	759.3	179.5	1150.3

Table D.1: Mean, minimum, and maximum stomatal conductance measured on representative species. For willow (*Salix*) species the results are divided between plants growing in riparian zones and those growing in upslope, dryland areas.

Appendix E

Poems Inspired Along the Way

E.1 Haikus

A drought year is not
the only time scientists
should be listened to.

Is streamflow changing?
Natural Variation
Makes this question hard.

Field measures, models,
Please give me the same numbers.
It works on paper.

Fire, plants, water.
Each one affects the other.
A fragile balance.

I can't feel my toes.
Socks haven't been dry for days.
But I got data.

E.2 All Dry on the Western Front

Written in 2013

It is summer in December

Grass is brown, the sky is blue.
It is summer in December
And we don't know what to do.

On the East Coast it's all buried
In a blanket cold and white.
Here our skis are hitting gravel
Were that all, we'd be all right

But snow banks wont be granting loans
Once real summer rolls around
And the farmers take a crack at
Growing crops in bone dry ground.

Reservoirs are sprouting ghost towns
While the hills nearby are bare.
If levels stay below the norm
Well, we'll have to learn to share.

Fish are fighting versus farmers,
Or at least thats what they say.
What's the water gonna go to?
Flushing toilets? Growing hay?

All the Californians dreaming
Of horizons growing dark;
Trying to ignore this prospect:
Dry hills lit with just one spark.

True, we all did choose to live here;
Raise our cattle, dig our pools.
But I'm sure we'll think of something,
We poor desert-dwelling fools.

It is summer in December
Grass is brown, the sky is blue
It is summer in December
And we don't know what to do

E.3 Fire and Water

It's often been shown that right after strong fire
The rivers nearby may start flowing much higher.

But what if you change the whole fire regime?
The many small flares, they may act as a team,
To form a new balance 'tween growth and decay
Which makes water flow in a whole diffrent way.

Instead of evaporate some sticks around
What trees to not drink may stay down in the ground.
Wait 'til late in summer to enter the stream,
When thoughts of a rainstorm may feel like a dream.

And what if this new equilibrium proves
To alter the way that a water drop moves
And help make the mountains resistant to drought?
Then that gives the "let it burn" backers more clout.

I do not think that it's much exaggeration
To say this could save our state from dehydration.